Determination of Kinetics of Char Reactivity with Carbon Dioxide Using Thermogravimetry and the Distributed Activation Energy Model

A dissertation submitted to the Faculty of Engineering and the Built Environment, University of the Witwatersrand, Johannesburg, in fulfilment of the requirements for the degree of Master of Science in Engineering.

Thinesh Vittee

Johannesburg, 2012

Declaration

I declare that this dissertation is my own unaided work, unless otherwise stated and acknowledged. It is being submitted for the degree of Master of Science in Engineering to the University of the Witwatersrand, Johannesburg. It has not been submitted before for any degree or examination to any other university.

Signed: .....(Signature of candidate) on this ..... day of....., year .....

Abstract

A particular field of interest in the development and understanding of current coal-based fuel and energy production is the determination of reaction kinetics of various materials. A more efficient and accurate method would improve the design and operation of current technology used in fuel and energy production.

An established DAEM-based algorithm was further developed to determine the reaction behaviour of materials reacting in CO_2 by means of incorporating the Random Pore Model (RPM). A method for modifying the algorithm to accurately use any other reaction model (for both isothermal and non-isothermal cases) was developed. It was found that the multiple reaction approach characteristic to the DAEM resulted in far more accurate reaction behaviour predictions than conventional methods that presuppose a single overall reaction.

The novelty in this research was the determination of multiple reactions occurring in RPM systems. Despite specifying multiple reactions, a single RPM structural parameter (φ=*12.2*) was still suitable, and produced accurate data fits. Charred Coal-CO_2 reactivity data was processed with the algorithm and activation energy values of E_1=261.7kJ/mol, E_2=246.4kJ/mol and E_3=227.6kJ/mol were found. Grouped pre-exponential factor values were found to be A_1^*=1.60E+07$s^{-1}.m^{-1}$, A_2^*=2.08E+06$s^{-1}.m^{-1}$ and A_3^*=2.75E+06$s^{-1}.m^{-1}$. The corresponding mass fractions were $f_{0,1}$=0.31, $f_{0,2}$=0.32, $f_{0,3}$=0.37. These proved to predict the reaction behaviour better than the conventional single reaction approach which found activation energy and grouped pre-exponential factor of E=254.5kJ/mol and A^*=1.0E+07 $s^{-1}.m^{-1}$ respectively.

The algorithm was then used to compare reactivities of plain South African coal char and of the South African coal-pinewood blend char in CO_2. This particular combination was found to exhibit improved reactivity as compared to the plain coal. The coal-pine blend was found to have a lower structural parameter value (φ=*11.7*) compared to plain coal char. The change in the structural parameter value suggests structural changes as a result of the biomass addition, which improved reactivity.

The findings show that the algorithm can be successfully adapted to process RPM (and other reaction model) data and produce accurate and reliable results. The biomass-blend results indicate the potential benefits of co-feeding the two feedstocks commercially; this must however be investigated further.

Acknowledgements

I wish to thank the following people for their contribution to my work:

• My supervisors, Dr. S. Kauchali and Prof. N. Wagner for the support, guidance and advice. Dr. S. Kauchali for help with all aspects of coding, interpretation of results and support in this work and Prof. N. Wagner for support in obtaining the required equipment and materials

• Fadeela Saloojee for research suggestions, TGA training and assistance with coding, and Qasim Fakir who preceded Fadeela Saloojee in this research field and helped us both

• Sasol Corporate Graduate Services for helping to fund this research through the Post Graduate Bursary Programme, and to my Sasol Mentor Celo Mausse for offering advice and support

• My Parents, my brother and my fiancée, Anisha, for encouragement, support, motivation and for affording me the opportunity to complete this research

Table of Contents

List of Figures

List of Tables

Nomenclature

A, (PE) – pre-exponential factor (s^{-1})

A^* - Grouped pre-exponential Factor ($s^{-1}.m^{-1}$)

E – Activation energy ($J.mol^{-1}$)

err – relative error (–)

e, exp – exponential constant (e≈2.718)

f – fraction of material (–)

k – reaction constant (–)

L – Overlapping length (m)

M – mass, total (kg)

m – component mass (kg)

m(E) – mass density function ($kg.mol.kJ^{-1}$)

P – pressure (Pa)

P_A – Partial Pressure of component A (–)

R – ideal gas constant ($J.mol^{-1}K^{-1}$)

R^2 – r-squared, "coefficient of correlation" (–)

r – reaction rate ($mol.s^{-1}.K^{-1}$)

S – surface area (m)

T – temperature (K)

T_f – Temperature at an equivalent (fixed) conversion(K)

TGA – Thermo-gravimetric analyser

t – time (sec)

u – dummy variable (–)

V – volatile mass (kg)

w – inert mass (kg)

X, x – fractional conversion (–)

$\hat{Y}_i$ - model-predicted dependent variable value (–)

Y_i - observed (experimental) dependent variable value (–)

$\bar{Y}$ - mean of the experimental values. (–)

Script

$_i$ or $_n$ – indicates reaction number, or component number

$_t$ – indicates time-dependent property

$_v$ – indicates property of volatile matter

$_0$ – indicates initial state

Greek Letters

α – fractional conversion (–)

β(or B) – heating rate ($K.s^{-1}$)

ε – voidage (–)

θ – Modified RPM structural parameter (–)

φ – RPM structural parameter (–)

Ψ – $\exp\left[-A(E)\int_0^t \exp((-E)/RT)dt\right]$ (–) or $\exp\left[-A(E)/\beta\int_{T_0}^{T_f}\exp((-E)/RT)dT\right]$

Chapter 1: Introduction

Fossil fuels are currently the world's primary energy source. Coal is one of the more abundant low-cost fossil fuels, but the high carbon to hydrogen ratio results in high production of CO_2 which, given the concern over global warming, is an unfavourable trait of the use of this fuel (Irfan et al., 2011). While much emphasis is being placed on the development of renewable energy, it is widely accepted that current fossil fuel utilisation must be optimized. Fossil fuel utilisation must become as clean and as efficient as possible, so as to maintain the steady supply of affordable energy for as long as possible, until viable large-scale alternatives are found. Coal is currently either combusted or gasified. The former process is usually used in electricity production. The latter process is used to extract the gaseous volatile components in the coal, as well as produce synthesis gas, both of which are used to produce gaseous and liquid fuels, among other things.

Due to global warming concerns, much emphasis has been placed on increasing the thermal efficiency of coal use (WCI, n.d.). The report notes that while efficiency gains (up to 45%) are being achieved in coal combustion processes, gasification processes used for electricity production (integrated gasification combined cycle, or IGCC) are more efficient. IGCC has been found to reach nearly 50% thermal efficiency and simultaneously remove 95-99% of SOx and NOx components in the effluent. Other coal gasification applications noted in the report include coal liquefaction. An example of this process is the Sasol (Fischer-Tropsch) Process for converting coal to fuels and other organic components via indirect coal liquefaction. This application is important since it offers a viable substitute for processing crude oil to fuel, and offers the opportunity to better control effluent (WCI, n.d.). Hence, it is vital that this process be thoroughly understood.

The entire thermal conversion process can be classed into drying, devolatilisation (collectively known as pyrolysis) and gasification (Kirubakaran et al., 2009). Also, the distinction between an inert and reactive environment must be made. In an inert environment (e.g. nitrogen gas), the process is known as pyrolysis, while in a reactive environment, it is known as gasification (gasification environments are usually made up of steam or CO_2, or a combination of the two). Drying is done to reduce moisture content which would otherwise reduce efficiencies and functionality of the gasification process. Pyrolysis produces a char, which is then gasified in the reactive environment.

In a laboratory environment, fundamental studies are often conducted using instruments other than an actual gasifier or boiler. A common tool is a thermo-gravimetric analyser (TGA). TGA's record mass-loss data as a function of temperature (non-isothermal) or as a function of time (isothermal). The chemical process to be studied is determined by the choice of gas used i.e. inert gasses (typically nitrogen/argon) will result in pyrolysis while reactive gasses (typically air/oxygen) will result in combustion/gasification (Kirubakaran et al., 2009). The validity of using thermo-gravimetric analysis as a tool for kinetics determination has been comprehensively studied for combustion and gasification reactivity (Feng and Bhatia, 2002). The study involved the extent to which chemisorption dynamics detract from the validity of the steady state assumption made when using TGA data to determine reaction kinetics. It was shown that for chars undergoing CO_2 gasification, the assumption is valid for almost all common TGA conditions, provided the specific surface

area of the material being studied does not exceed 312m^2/g; most materials fall well within this boundary.

One particular aspect of the gasification process which is being considered in this research is the determination of the kinetics of the reactions occurring when chars are gasified. A comprehensive review of the many factors affecting the kinetics of gasification in CO_2 is covered in Irfan et. al. (2011). The review thoroughly documents work based on model-specific methods for determining the desired kinetic parameters. It shows that many researchers have proposed reaction mechanisms and successfully shown that experimental data can be fitted to produce these parameters. The drawback is that the parameters found are heavily dependent on the conditions and materials used in the experiments and hence have little relevance elsewhere. These methods will be referred to as "model-dependent methods' and will be elaborated upon in Chapter 2. A different type of solution method exists which does not depend on the reaction model to determine the kinetic parameters. A collection of these methods is given by Starink (2003) and are commonly known as model-free isoconversion methods. While the model-dependent methods are based mainly on the Langmuir-Hinshelwood model, the isoconversion methods are based on the premise that reaction rate is a product of two functions; one depending solely on temperature, and the other depending solely on the fraction transformed. The temperature function is usually expressed as an Arrhenius type dependency, in which the pre-exponential factor (*A*) and activation energy (*E*) are the desired kinetic parameters. Almost all isoconversion methods make an approximation to the "temperature integral" (an integral term present in the derivation of all isoconversion methods) and then find *E*, without needing a reaction model. A reaction model is further required to find *A*. The results are however presented as a range rather than discrete values since the solution method requires the parameters to be determined at specified conversions. Starink (2003) refers to a separate form of model-free isoconversion methods which does not approximate the temperature integral, but rather use more complex numerical algorithms to calculate the value of the integral in order to determine the activation energy, and consequently, the other kinetic parameters. These will be referred to as "algorithmic methods". These methods have been deemed too complex compared to the regular isoconversion methods and supposedly do not produce results which are considerably more accurate than those of the regular isoconversion methods.

However, a recent algorithm based on the Distributed Activation Energy Model (DAEM) has been developed to determine the pyrolysis kinetics of complex solid fuels (Scott et al., 2006). It has inadvertently been found to be model-independent when determining the activation energy of a particular substance. The algorithm provides a way of inverting the DAEM which results in the determination of discreet mass-fraction values which accurately identify the activation energy and pre-exponential factor for each parallel step participating in the thermal decomposition of the fuel. This algorithmic method is arguably less complex than those referred to by Starink (2003) and simultaneously more accurate than regular isoconversion methods in that it gives discreet values of the desired kinetic parameters for each reaction taking place. Current research has focussed on adapting Scott's algorithm to O_2 reactivity in a combustion process, with apparent success (Saloojee, 2011). This research will therefore focus on extending this method to CO_2 reactivity.

This research is important since the understanding of the elementary processes occurring within a complex system such as a commercial gasifier is vital to its design. Work by the Commonwealth Scientific and Industrial Research Organisation (CSIRO) has shown the use

of the elementary Arrhenius kinetics and the use of the random pore model, among many other fundamental principles to generate a complete model of an entrained flow gasifier (Hla et al., 2011). It was shown that the use of these and other fundamentals could accurately simulate the behaviour of various coal species in an entrained flow gasifier

Great emphasis has also been placed on improving current fuel and energy production schemes before moving toward completely renewable technologies. One proposed means of achieving this, with particular focus on coal gasification, is to blend biomass into the conventional coal feed. Bio-energy will be the most significant renewable energy source in the next few decades, until solar- or wind power production offers an economically attractive large scale alternative (Sipila, 1993). Biomass is classified as any agricultural and forestry residues, by-products from processing of biological materials, wood, as well as organic parts of municipal and sludge wastes (Kumar et al., 2009). Studies on the CO_2 reactivity in gasification of biomass and of coal-biomass blends have shown that the mineral content of the biomass had catalytic effects; the activation energies reported were lowered compared to those of coals, implying that biomass is a viable fuel source (Zhu et al., 2008; Vamvuka et al., 2011). These findings present the opportunity to investigate the effects of blending biomass with coals in a South African context in the gasification process. The kinetics can be found using the DAEM-based algorithm and then compared to determine whether the addition of biomass proves synergistic.

This research offers many benefits for industry. A quicker, more detailed means of acquiring intrinsic gasification kinetics of any solid fuel will greatly aid the design and modelling of new gasification schemes and as well as the optimisation of current gasification schemes. The inclusion of biomass is beneficial because the material is carbon neutral and replaces a portion of the fossil fuel used. The catalytic effects also imply less energy usage for the same production rates which results in lower running costs.

Following this introduction, is a detailed review of the literature in this research area. The chapter that follows the literature review outlines the approach that will be taken in this research to further develop the algorithm and conduct physical experimentation. Then, using the defined research methodology, the steps taken to develop, modify and use the algorithm are presented. The fifth chapter illustrates the applicability of the algorithm to experimental data, and assesses the effects of blending biomass and coal. Finally, the findings are summarised and recommendations for future research are presented.

Chapter 2: Literature Review

2.1. Introduction

This review outlines and compares various methods used to find reaction kinetics as well as the different applications of the methods to different situations. The reaction being studied in this research is presented, and is followed by an explanation of kinetics determination methods other than DAEM, which do not necessarily produce Arrhenius-type kinetics results. Then, the development of the DAEM and the algorithms based on this model are presented, including the algorithm that will be closely studied and modified in this research. The kinetics determination review is followed by a review of the study of biomass co-gasification and its effects on reactivity.

2.2. The Boudouard Reaction

The Boudouard reaction is the name given to the reversible reaction between carbon and CO_2 to produce carbon monoxide (CO). A key issue which must be addressed before elaborating on the research in this particular field is the issue of reactive environment selection, i.e. why has CO_2 been selected over steam. According to Irfan et. al. (2011), the char-CO_2 reaction is used primarily to test (and most likely compare) the reactivities of various chars derived from various parent coals (as well as other materials such as biomass). This reaction is used because it is relatively slow and is thus easier to measure, but is still similar to the char-steam reaction. Cakal et. al. (2007) cited in Irfan et. al. (2011), states that at a laboratory level the slower reaction rate and lower temperature allow for better control and data analysis. The CO_2-char reaction better known as the Boudouard reaction is given in equation 2-1:

$$C + CO_2 \leftrightarrow 2CO \qquad \Delta H = 159.7 kJ/mol \tag{2-1}$$

2.3. Early Methods for Kinetics Determination

As Irfan et al. (2011) suggests, the study of CO_2-char gasification kinetics has been a key research topic for many years. Over the past 60 years, various methods have been proposed and used, with varying degrees of success. These methods can be classed into three broad categories: Model-dependent methods; Isoconversion methods; and algorithmic methods.

2.3.1. Langmuir-Hinshelwood Based Methods

Irfan et. al. (2011) presents reaction mechanisms and corresponding reaction rate expressions proposed by several researchers. There are models proposed which take into account the inhibiting effects of the presence of CO, and others which do not. Particular attention is paid to the model proposed by Hurt (2002) cited in Irfan et. al. (2011). This model proposes a combined combustion/gasification mechanism involving 8 reactions, 2 of which

are reversible, resulting in a total of 10 reactions. Based on this reaction model, several researchers have proposed an overall Langmuir-Hinshelwood (L-H) type reaction rate expression. An example of these expressions is equation 2-2 given by Műhlen et. al. (1985) cited in Irfan et. al. (2011):

$$R_{C-Gas} = \frac{k_{13}P_{CO_2} + k_{20}P_{CO_2}^2 + k_{21}P_{H_2O} + k_{23}P_{H_2O}^2 + k_{24}P_{H_2O}P_{H_2} + k_{16}P_{H_2}}{1 + k_{14}P_{CO_2} + k_{15}P_{co} + k_{22}P_{H_2O} + k_{17}P_{H_2}} \quad \textbf{2-2}$$

It is evident that while this approach (i.e. using an L-H type expression and a reaction model to fit experimental data to in order to determine kinetics) may be beneficial in the sense that it accounts for the effects of the presence of the product gas, and that it accounts for adsorption, desorption, and other mechanistic considerations, the method is cumbersome. Finding such a large number of parameters numerically can be difficult, as well as a source of error. Therefore, even though the use of L-H type expressions for determination of intrinsic kinetics of C-CO_2 reaction has been validated by several researchers according to Irfan et. al. (2011), there is sufficient motivation to investigate the use of Arrhenius-type methods and their accuracy.

2.3.2. Isoconversion Methods

The force-fitting of non-isothermal data to different reaction models results in widely varying Arrhenius parameters; the only way is to extract parameters in a way that is independent of reaction model (Vyazovkin, 1997). A particularly effective and simple branch of these methods are the isoconversion methods, which are mostly Arrhenius-type methods. A comprehensive review of various isoconversion methods was conducted, which defines an isoconversion method as follows: An isoconversion method involves the activation energy analysis being conducted by determining the temperatures at which an equivalent stage of conversion is reached for different heating rates (Starink, 2003). Starink (2003) explains that most of this branch of research hinges on the assumption that the reaction rate is a production of two functions; one solely a function of conversion (α), and the other solely a function of temperature (*T*), as shown in equation 2-3:

$$\frac{d\alpha}{dt} = f(\alpha)k(T) \quad \textbf{2-3}$$

The temperature-dependent function usually follows an Arrhenius-type dependency, as shown in equation 2-4:

$$k(T) = Ae^{-E/RT} \quad \textbf{2-4}$$

From this, it can then be noted that the primary parameters are the pre-exponential factor *A*, the activation energy *E* and the reaction function *f(α)*. These parameters are known as the

kinetic triplet. For non-isothermal experiments in particular, the determination of these 3 parameters is an interlinked problem, meaning that the deviation of one of these parameters significantly affects the others. This implies that it is important to start any thermal analysis of this sort by determining one of these parameters (usually the activation energy) with high accuracy. Starink (2003) goes on to present and compare a host of different isoconversion methods. Two types of isoconversion methods are presented, named “type A” and “type B”. Type A methods involve substituting equation 2-4 into equation 2-3 and taking the logarithm. This type A equation is given in equation 2-5:

$$\ln\left(\frac{d\alpha}{dT}\beta\right) = {}^{E}/_{RT} - \ln f(\alpha) \qquad \textbf{2-5}$$

Then, if the heating rate is known, the gradient of the straight line generated from plotting $\boldsymbol{\ln\left(d\alpha/dT.\beta\right)}$ vs. $\boldsymbol{1\ /\ T}$ will give the activation energy. The y-intercept will give the f(α). This line can therefore be plotted at different temperatures for an equivalent conversion over the full conversion range, yielding a range of activation energy and reaction function values. A known reaction function will in turn yield the pre-exponential factor values (note however that no reaction model is needed for the determination of *E*, making it a model-free method). Type B methods essentially adopt the same approach; except that the differential term is now separated, the variables grouped, and an integration step is incorporated, as shown in equations 2-6 and 2-7:

$$\int_0^{\alpha} \frac{d\alpha}{f(\alpha)} = \frac{A}{\beta}\int_0^{T_f} \exp\left(-\frac{E}{RT}\right) dT \qquad \textbf{2-6}$$

$$\int_0^{\alpha} \frac{d\alpha}{f(\alpha)} = \frac{AE}{\beta R}\int_{y_f}^{\infty} \frac{\exp\left(-y\right)}{y^2} dy \qquad \textbf{2-7}$$

Where $y = E/RT$ and T_f is the temperature at an equivalent (fixed) conversion rate. Note too that β is the heating rate. The integral term with the y-substitution is known as $\mathrm{p(y)}$.

The right hand side integral is commonly referred to as the “temperature integral” and most, if not all type B methods are defined by their unique numeric approximation of this integral. Starink (2003) presents and compares the accuracy of these methods, but also acknowledges other methods for determining activation energy, such as the work of Serra et. al. (1998) and Vyazovkin (1997). These methods do not use approximations of the temperature integral, resulting in mathematically complex, non-linear expressions.

2.3.3. Algorithmic Methods

The Non-Parametric Kinetics method (NPK) (Serra., 1998) uses equation 2-3 as a basis for the analysis. This analysis expresses equation 2-3 in a three-dimensional space as a surface, with elements generated from mass-loss and temperature data collected during

experimentation. Then, a mathematical algorithm call “single value decomposition” (SVD) is used to separate the elements of the matrix generated into 2 vectors, each representing one of the two functions expressed in equation 2-3. The method involves complex matrix algebra, which would rely substantially on the use of computer calculation. The benefit however is that no assumption is made about the kinetic model or temperature dependence of the rate constant in determining the vectors which represent each of the two functions. The activation energy, pre-exponential factor and reaction order can then be determined by fitting a kinetic model to the vectors. Vyazovkin (1997) proposes a method using equation 2-6, where the right-hand side is called g(α), and the temperature integral is called $I(E,T)$; this form is given in equation 2-8:

$$g(\alpha) = \int_0^{\alpha} \frac{d\alpha}{f(\alpha)} = \frac{A}{\beta} I(E,T) \qquad \textbf{2-8}$$

Then, for a given conversion, at different heating rates, the following algorithm is proposed:

$$\sum_{i}^{n} \sum_{j \neq i}^{n} \left[I\left(E_{\alpha}, T_{\alpha i}\right) \beta_j \right] / \left[I\left(E_{\alpha}, T_{\alpha j}\right) \beta_i \right] = min \qquad \textbf{2-9}$$

The subscript α denotes the property value at a given conversion. Note that Vyazovkin (1997) also proposes a similar expression for non-constant heating rates.

Now Starink (2003) claims that errors introduced by approximating the temperature integral are small when the “correct” approximation is chosen, and often are smaller than those introduced by these complex methods, which would imply that there is no further benefit to be gained from the use of these complex methods in activation energy analysis. While this analysis may possibly be true for the methods shown above, there is one major shortfall of all these methods: all methods result in a range in the value of the kinetic parameters, rather than discreet values. As mentioned, the DAEM-based seems to address both concerns: it is both less complex and offers discreet values of the activation energies occurring in a particular system.

2.4. DAEM Based Method for Kinetics Determination

The algorithm presented in Scott et al. (2006) is based on the distributed activation energy model (DAEM). The DAEM as explained in Scott et al. (2006) is presented below. The DAEM was initially developed as means of modelling the pyrolysis of a complex fuel as the first-order decomposition of numerous chemical groups, each characterised by their own activation energy for decomposition. A continuous distribution of activation energies is proposed for complex fuels such as coal where the mass of volatile material with activation energies between E and $E+dE$ at a given time *t* is *m(E,t)dE*, then the total mass $M_v(t)$ is given by equation 2-10 overleaf.

$$M_v(t) = \int_0^{\infty} m(E,t)dE \qquad \textbf{2-10}$$

Then, if it is assumed that the material in the interval E to $E+dE$ decomposes via a first-order reaction, with pre-exponential factor $A(E)$, then

$$\frac{dm(E,t)}{dt} = -A(E)\,exp\left(\frac{-E}{RT}\right)m(E,t) \qquad \textbf{2-11}$$

So $$m(E,t) = m_0(E)\exp\left[-A(E)\int_0^t \exp\left(-\frac{E}{RT}\right)dt\right. \qquad \textbf{2-12}$$

Where $m_0(E)$ is the initial mass of volatile material decomposing in the interval E to $E+dE$. It is noted that $m(E,t)$ cannot be measured in practice, only total amounts, i.e. $M_v(t)$. Therefore, by integrating over all energies equation 4-14 is derived:

$$\frac{M_v(t)}{M_{v0}} = \frac{\mathrm{M_{v0}} - \mathrm{V(t)}}{\mathrm{M_{v0}}} = \int_0^{\infty} g(E) \times \exp\left[-A(E)\int_0^t \exp\left(\frac{-E}{RT}\right)dt\right]dE \qquad \textbf{2-13}$$

Where $g(E)$,the initial distribution of activation energies is given by equation 2-14:

$$g(E) = \frac{m_0(E)}{\int_0^{\infty} m_0(E)dE} \qquad \textbf{2-14}$$

Note too that the double exponential term is referred to as $\Psi(E,t)$, i.e.:

$$\Psi(E,t) = \exp\left[-A(E)\int_0^t \exp\left(\frac{-E}{RT}\right)dt\right] \qquad \textbf{2-15}$$

Such that equation 2-13 can be rewritten as:

$$\frac{M_v(t)}{M_{v0}} = \int_0^{\infty} g(E) \times \Psi(E,t)dE \qquad \textbf{2-16}$$

This approach was initially developed and calculated using isothermal experimentation to reduce the complexity of the integration (Pitt., 1962). The development in that research

noted that although the reactions of the various materials in a complex fuel are likely to be occurring in parallel in reality, they were assumed to be occurring in series, and that the reactions did not overlap each other significantly. This implies that at each fractional conversion, one reaction is dominating (Scott et al., 2006). Another key focus area in the development of this model was the evaluation of the double integral term seen in equation 2-13. Comprehensive research has been done to determine the value of the double integral, for various activation energy distributions(Please et al., 2003). Please et. al. (2003) showed that their correction factor improved the accuracy of the double integral and was also applicable to other activation energy distributions (other than Gaussian distributions as used in the original derivation).

Scott et al. (2006) then noted two other developments based on the DAEM. The first is a method in which various constant heating rate experiments are conducted, and a value of *Ψ(E)* assumed (found by minimising the errors in the pre-exponential factor value *A*) in order to determine the kinetics without assuming values for functions *g(E)* and *A(E)*(Miura and Maki, 1998). The second is a method in which the activation energy values are discretised and the *E* values fixed (Braun and Burnham, 1987). The function *g(E)* is then determined by fitting a model to the experimental data; the same is done to determine the pre-exponential factor *A*. Other similar research has been done (Miura, 1995), each with its own benefits and shortcomings. Some of the approaches taken in these studies have been combined and used by Scott et al. (2006) in order to develop a novel algorithm where no assumptions about the functions *g(E)* and *A(E)* must be made *a priori*. Also, the algorithm is developed to process multiple reactions, using only two heating rates (where most other methods require a minimum of 3 constant heating rate experiments). The full derivation of the algorithm follows below.

Scott et al. (2006) present the algorithm that was developed. The algorithm determines the kinetics from a pair of thermo-gravimetric experiments conducted at different constant heating rates. The algorithm is as given in equation 2-17:

$$\frac{M(t)}{M_0} = w + \sum_{All\ reactions,i} f_{i,0} \exp\left[-A_i \int_0^t \exp\left(\frac{-E_i}{RT}\right) dt\right] \qquad \textbf{2-17}$$

Where $M(t)$ is the mass of the sample at time t, M_0 is the initial mass of the fuel, w is the fraction of inert material and $f_{i,0}$ is the fraction of M_0 which decomposes with activation energy E_i and pre-exponential factor A_i. The double-exponential term can be expressed as Ψ_i. Note that f is the discrete analogue of the continuous fractional density function $g(E)$.

Equation 2-17 can then be written as a matrix equation where, for any set of times t_0, t_1, t_2.. t_f , the mass of fuel remaining, $M(t)$, is given by:

$$\frac{1}{M_0}\begin{bmatrix} M(t_0) \\ \vdots \\ M(t_{\mathrm{n}}) \end{bmatrix} = \begin{bmatrix} \Psi_1(t_0) & \Psi_2(t_0) \cdots \Psi_n(t_0) & 1 \\ \vdots & \vdots \quad \cdots \Psi_n(t_1) & 1 \\ \Psi_1(t_{\mathrm{n}}) & \Psi_2(t_{\mathrm{n}}) \cdots \Psi_n(t_{\mathrm{n}}) & 1 \end{bmatrix} \times \begin{bmatrix} f_{1,0} \\ \vdots \\ f_{\mathrm{n},0} \end{bmatrix} \qquad \textbf{2-18}$$

i.e. $\underline{M} = \underline{\Psi}.\underline{f}$ where the underbars indicate matrix variables.

For experiments with constant heating rate, i.e. $dT/dt = B$.

$$\Psi_i(t) = \Psi_i(T) = \exp\left[-\frac{A_i}{B}\int_{T_0}^{T} \exp\left(\frac{-E_i}{RT}\right) dT\right] \qquad \textbf{2-19}$$

Solving equation 2-18 results in the determination of the initial mass fractions, which is possible since there are usually more experimental points than reactions. It is also possible to solve this equation using linear least squares. Scott et al. (2006) uses the *lsqnonneg* algorithm in Matlab (Matlab R14, The Mathworks Inc.) to do this.

Scott et al. (2006) stated that in order to use equation 2-18, a set of reactions with *E* and *A* values must be proposed, and Ψ calculated. It is first assumed that there will be a single reaction dominating which is first-order, and that for the i^{th} component, the fraction of initial mass remaining is given by equation 2-20 for a constant rate of heating:

$$f_i(T) = f_{i,0}\Psi_{\mathrm{i}}(T) \qquad \textbf{2-20}$$

Now, if the conversion at 2 different heating rates, say B_1 and B_2, is considered and the i^{th} reaction is the only reaction taking place at this conversion, then $f_i(B_1,T_1)=fi(B_2,T_2)$. It then follows, since Ψ is also a function of heating rate, that:

$$\Psi_i(B_1, T_1) = \Psi_i(B_2, T_2) \qquad \textbf{2-21}$$

Then, substituting the heating rate and taking natural logarithms on both sides results yields:

$$\begin{aligned} \frac{1}{B_1}\left[T_0 \exp\left(\frac{-E_i}{RT_0}\right) - \frac{-E_i}{R}\int_{E/RT_0}^{\infty} \frac{\exp(-u)}{u} du - T_1 \exp\left(\frac{-E_i}{RT_1}\right) + \frac{E_i}{R}\int_{E/RT_1}^{\infty} \frac{\exp(-u)}{u} du\right] \\ = \frac{1}{B_2}\left[T_0 \exp\left(\frac{-E_i}{RT_0}\right) - \frac{-E_i}{R}\int_{E/RT_0}^{\infty} \frac{\exp(-u)}{u} du - T_1 \exp\left(\frac{-E_i}{RT_1}\right) + \frac{E_i}{R}\int_{E/RT_1}^{\infty} \frac{\exp(-u)}{u} du\right] \end{aligned} \qquad \textbf{2-22}$$

Equation 2-22 is a non-linear equation that can be solved for the unknown E_i. This method will accurately determine the activation energies of reactions occurring in a material with several components, provided there is only one reaction dominating at a given conversion. Errors are only introduced when several reactions are occurring simultaneously at a given conversion.

Once the activation energy for component *i* has been found using equation 2-22, A_i can be found (Scott et al., 2006). This is done by assuming that the dominating reaction is at some conversion. It is assumed that the reaction of component *i* (not the overall reaction) is at its maximum rate of decomposition. This assumption follows from how the approach is posed, i.e. that the reactions occur in series and that at each fractional conversion, only one reaction is dominating. For one reaction to be dominating, it is safe to assume that its reaction rate is at or near its maximum value. Based on this assumption, the value of conversion *x* that results in this maximum decomposition rate is used in calculation, i.e. where:

$$\frac{d^2 f_i}{dt^2} = 0 \qquad \textbf{2-23}$$

For a first order reaction, a value of $x=1-e^{-1}$ ratifies equation 2-23. Then, if equation 2-20 is written in terms of *x* based on the identity of f_i:

$$\Psi_{\mathrm{i}}(T) = 1 - x \qquad \textbf{2-24}$$

Hence

$$\ln(\Psi_{\mathrm{i}}(T)) = -1 \qquad \textbf{2-25}$$

Then, using this value and the known value of E_i, A_i can be found by solving equation 2-26:

$$\ln(\Psi_{\mathrm{i}}(T)) = \frac{A_i}{B_1}\left[T_0 \exp\left(\frac{-E_i}{RT_0}\right) - \frac{E_i}{R}\int_{E/RT_0}^{\infty} \frac{\exp(-u)}{u}du - T_1 \exp\left(\frac{-E_i}{RT_1}\right) + \frac{E_i}{R}\int_{E/RT_1}^{\infty} \frac{\exp(-u)}{u}du\right] \qquad \textbf{2-26}$$

Where *u* is a dummy variable used in integration.

While this assumption of the value of conversion can be a source of error in determining the pre-exponential factor, it has been found to yield accurate results (Scott et al., 2006; Navarro et al., 2008); thus validating the assumption. This approach can in principle be extended to other reaction models which better describe other reactions such as combustion or the Boudouard reaction. This implies that, since the determination of activation energy is model-free (Saloojee, 2011), all kinetics for any reaction model can be found by simply determining the activation energy and then finding the value of conversion that satisfies equation 2-23 to determine an accurate value of the pre-exponential factor. The mass fraction values are then found using these accurately determined parameters.

The final step (the determination of the initial mass fraction(s)) involves the matrix inversion. This was achieved using Matlab pre-programmed least squares regression (but could be done using any other least squares non-negative regression algorithm). The inversion effectively calculates the area under the conversion-differential versus temperature (*dx/dT – T*) curve, which represents the fractional mass assigned to a reaction at a particular conversion. For multiple (or compounded, indistinguishable) peaks, the sum of the total area under the curve must always equal unity, which is representative of the total fractional mass of the material in the system. The inversion calculates the area under each peak and relates it to a corresponding set of kinetic parameters at a particular conversion. Where the curve lies on the horizontal axis, representing no mass reacting at a specific conversion, the kinetics found at that conversion are deemed spurious. A schematic diagram of the algorithm is provided in Chapter 4.

2.5. Reaction Mechanism

There are various reaction mechanisms proposed to describe various chemical reactions. Common examples include a simple first order (on which the DAEM is based), as well as the shrinking core model, grain model, random pore model, etc (Bhatia and Perlmutter, 1980). A collection of some of these models is given below in Table 2.1 and is based on the following derivation (Joseph, 2000). The fundamental basis is the assumption that reaction rate is dependent on two separate functions: one function of temperature, and one function of conversion. This is presented in equation 2-27.

$$\frac{dx}{dT} = \frac{k(T)}{\beta} f(x) \qquad \textbf{2-27}$$

Then, taking the integral,

$$g(x) \equiv \int_0^x \frac{dx}{f(x)} = \frac{A}{\beta} \int_{T_0}^{T_f} e^{-E/RT} dT \,^{1} \qquad \textbf{2-28}$$

The function *g(x)* therefore gives the integral of positive inverse of the explicit reaction model. This form is the form most commonly used during calculation of kinetic parameters and is indeed the form required for use with the modified DAEM algorithm.

Table 2.1: Reaction Mechanism Expressions (Joseph, 2000)

Reaction Mechanism	g(x)
Power law	$x^{1/n}$
Exponential law	$\ln x$
Avrami Erofe'ev 1	$[-\ln(1-x)]^{1/2}$
Contracting Volume (a.k.a "Shrinking Core Model")	$1-(1-x)^{1/3}$
2 Dimensional Diffusion	$(1-x).\ln(1-x)+x$
First order	$-\ln(1-x)$

[1] Note that the right hand side of equation 2-28 is positive. Since k(T) usually represents the rate of reaction of the gaseous component, this term is expressed as a negative in other instances.

After the discussion in the previous section, it may seem unnecessary to discuss reaction mechanisms if the DAEM-based algorithm is to be used. While the algorithm is model-independent when determining the activation energy, it is not able to determine the pre-exponential factor without an appropriate reaction model.

2.5.1. The Random Pore Model (RPM)

Irfan et. al. (2011) documents the work of many researchers who have used various reaction models, or structural models to determine coal/char-CO_2 gasification kinetics. It is noted that while many researchers use the shrinking core model, and variations thereof, it has been used with little success for the Boudouard reaction. It is however noted that use of the random pore model (RPM) has been used and was found to determine accurate kinetics. The expression for the RPM is presented in equation 2-29 (Gupta and Bhatia, 2000):

$$\frac{dx}{dt} \propto (1-x)\sqrt{1-\varphi \ln(1-x)} \qquad \textbf{2-29}$$

Where φ is a structural parameter, and x is the fractional conversion.

The structural parameter is calculated from a number of equivalent equations, each made up of a collection of physical structural parameters of the sample particle. Examples of these include initial surface area, voidage, etc. Thorough use of the factor and its calculation by way of determining the particles' various physical dimensions is showcased in the work of Perlmutter and colleagues (Su and Perlmutter, 1985). The structural parameter can however also be used as a characterisation parameter whereby the model is fitted to experimental data via regression analysis. It has however been found that for non-uniform pore-size distributions, the approximations made to account for non-uniformity and to improve accuracy in the micro-pore range still result in structural parameter values that may not be accurate, or not representative of the whole sample when using imaging techniques (such as BET analyses) (Everson et al., 2008). Although some research reports differences in the value when calculated directly and when used as a characterisation parameter of between 30-40% (Bhatia and Vartak, 1996), it is still deemed a valid and relevant means of applying the model to experimentally derived data. Other research (Su and Perlmutter, 1985) reports good agreement between the calculated values and the regression-derived values of the parameter. These findings both validate the use of the random pore model when studying the reactivity of coal and coal chars and also supports the use of φ as a characterisation parameter when applying the model to experimental data.

The random pore model expression can written explicitly as in equation 2-30 (Irfan et al., 2011).

$$\frac{dx}{dt} = \frac{r_s S_0 (1-x)\sqrt{1-\varphi \ln(1-x)}}{(1-\varepsilon_0)} \qquad \textbf{2-30}$$

Where S_0, ε_0 and φ are structural parameters (which can be measured experimentally using various imaging techniques, discussed in Chapter 5) and r_s is reaction rate expressed as an Arrhenius type rate equation, i.e. $r_s = -Ae^{-E/RT}.{P_{CO_2}}^n$. The constant terms, (including the concentration term) can be grouped into the pre-exponential factor. The time differential can also be replaced with a temperature differential by means of multiplying by a constant

heating rate. If these two steps are taken, the same approach as taken for entries in Table 2.1 can be applied here. The resulting expression for the function *g(x)* is then given as equation 2-31, where limits are taken between *0* and *x*.

$$g(x) = \frac{2}{\varphi}\left(\sqrt{1 - \varphi \ln(1-x)} - 1\right) \qquad \textbf{2-31}$$

2.5.2. Modified Random Pore Models

The random pore model has also been developed and adapted to account for certain mechanisms not acknowledged entirely in its initial development. Two such adaptations are of primary concern.

The first is an adaptation which adds an additional structural parameter, θ, to the equation. This parameter accounts for the finiteness of the size of the solid reacting particles; here, the rate dependence on conversion is unchanged compared to the original RPM but the form of pore surface area variation is modified (Bhatia and Vartak, 1996). The modified expression is presented below:

$$\frac{dx}{dt} = \frac{r_s S_0 (1-x)(1+\theta)\sqrt{1 - \varphi_E \ln(1-x)}}{(1-\varepsilon_0)} \qquad \textbf{2-32}$$

Where

$$\varphi_E = \frac{\varphi}{(1+\theta)^2} \qquad \textbf{2-33}$$

And θ is a structural term similar to φ but is dependent on the non-overlapping physical measurements of the reacting particle, as well as the radial inter-layer spacing of the atoms of the solid particle. This model showed clear changes in the value of the original structural parameter as well as better agreement with experimental data.

This adaptation with two structural parameters is then developed further to account for the effects of surface chemistry of the particle on the overall reaction rate i.e. to account for when surface complexation and inhibitory functional groups (as well as hydrogen) are present on the initial char surface result in slower initial reactivity (Gupta and Bhatia, 2000). This adaptation adds another factor, which is the ratio of the reactivity of the first layer of the particle to the reactivity of the second and subsequent reaction layers. It was shown that this model was able to successfully predict the anticipated slower initial reactivity of the char oxidation. The addition of factors must however be done with caution since the appeal of the RPM is that is often able to represent the reaction behaviour of porous solids without the use of many arbitrary additional parameters (Bhatia and Vartak, 1996). From this observation, it can be said the original model in its most basic form should be applied initially, and only be disregarded in favour of one of its adaptations if the structural parameters found are not within reason or when the model is simply unable to accurately fit the experimental data.

2.6. Biomass

As noted in Chapter 1 the incorporation of biomass into conventional coal/char gasification has proven beneficial in a number of investigations. Numerous authors have already researched this practice and found favourable results. Vamvuka et. al. (2011) studied the gasification of 3 different biomasses, i.e. Municipal solid waste, untreated sewage sludge, as well as waste paper. It was found that all of these had high ash and volatile content, with calorific values comparable to low-rank coals. The ash was also found to be high in Ca and Si compounds. The alkaline and alkaline earth metals incorporated in the carbonate and sulphate compounds which are inherent in the biomass proved to be catalytic. These compounds increase the reactivity of the samples which results in the biomass degradation starting at lower temperatures. Other research, involving the combined pyrolysis and gasification is presented in Zhu et. al. (2008). This research used Shangwan coal, a Chinese bituminous coal, and wheat straw. Some of the wheat straw was acid-washed to remove alkaline materials, and some straw was used untreated. The coal and straw were pyrolysed and gasified at various rates, in various blend ratios. The ratios included blends of between 20% and 50% biomass, as well as a test of each pure specimen. It was found that gasification reactivity increased with an increasing straw-coal ratio. It was also found that the reactivity of the acid-washed straw and coal blend was comparable to that of unblended coal, indicating that mineral presence is key to increasing reactivity.

The use of biomass, especially for use during CO_2 gasification of coal chars has been widely regarded as a laboratory-scale indication of reactivity and other factors. The information obtained from CO_2 reactivity studies is then used as a reference when studying more conventional feedstock and reducing agent combinations (e.g. steam-coal gasification). While the process of CO_2 gasification and catalysis by addition of biomass is not without its challenges, research has shown its commercial viability (Song et al., 2011). This research notes that the Boudouard reaction is endothermic, requiring energy input, and that CO_2 is not intrinsically reactive, requiring high temperatures and low pressures to react with carbon. It is also noted the reaction can and must be catalysed. This work suggests however that conventional catalyst recovery rates are low and that low-cost abundant carbon-based reducing agents (biomass) show high reactivity with CO_2. It is then noted that highly reactive biomass can be blended with fossil-fuel feedstocks such as coal to increase their reactivity, and shows that this is viable commercially.

What is not taken into account is the negative effect of reacting biomass in this manner. Studies on the slagging caused by the combustion of several biomass species was studied since slagging can result in diminished heat transfer capacity, equipment damage, etc (Miles et al., 1993). It was shown that fast growing plants have higher alkali content and were therefore more prone to slagging. This result is problematic in that the alkali content is what is sought after when co-feeding biomass in the gasification process because it is the alkali material that catalyses the reaction. The research of Miles et al. (1993) notes that some biomass species which have slower growth rates, such as pinewood, cause minimal slagging (as opposed to fast-growing species such as switchgrass or bamboo); Song et al. (2011) reports pinewood char reactivity to be higher than that of coal char and hence possibly catalytic. These findings suggest that if pinewood waste is available, it would make a desirable feedstock for the co-gasification of coal.

Research assessing the effects of coal/biomass-derived syngas on Fischer-Tropsch and water-gas-shift catalysts (Farmer et al., 2011) was also conducted, since coal gasification to produce syngas is used principally in this process. Several catalysts species were operated with multiple contaminant mixtures, containing alkali vapours as well as other vapours such as H_2S. The water-gas-shift catalysts were hardly or not impacted at all by the presence of these contaminant species. The Fischer-Tropsch catalysts were exposed to individual and multiple contaminant mixtures, with varying results. The single contaminant species had no impact on both the iron- and cobalt-based catalysts while declines in CO were registered for multiple contaminant mixtures of alkali vapours and other contaminants such as H_2S and ammonia. This research indicates that while the use of biomass would require some care and control, the implementation would be viable and beneficial.

Blend fraction and particular combinations of different coals and biomass species are also important focus areas which have been studied (Bockelie et al., 2011; Means, 2011). These studies showed that lab-scale blends of equal parts switchgrass or sorghum and coal exhibited reactivity up to six times greater than the plain coal tests (Bockelie et al., 2011). However, a feasibility study found that on a commercial scale, blend percentages above 20% are infeasible, due to transport cost, material characteristics, etc. Bockelie et. al. (2011) showed that a particular biomass had a significant effect on the reactivity of one coal as opposed to the other. This shows that blends must be tested for efficacy and that findings on the effects of addition of a particular biomass on a particular coal's reactivity may not be extrapolated to other coals.

While this approach to improving coal gasification reactivity has some challenges, it is indeed beneficial and commercially viable. The schematic given in Figure 2.1 outlines the overall approach that can be taken commercially to use industrially produced CO_2 rich flue gas as well as abundant, low-cost carbon sources to sustainably improve coal char gasification, by modifying (not replacing) existing infrastructure to become viable CO_2 utilisation processes.

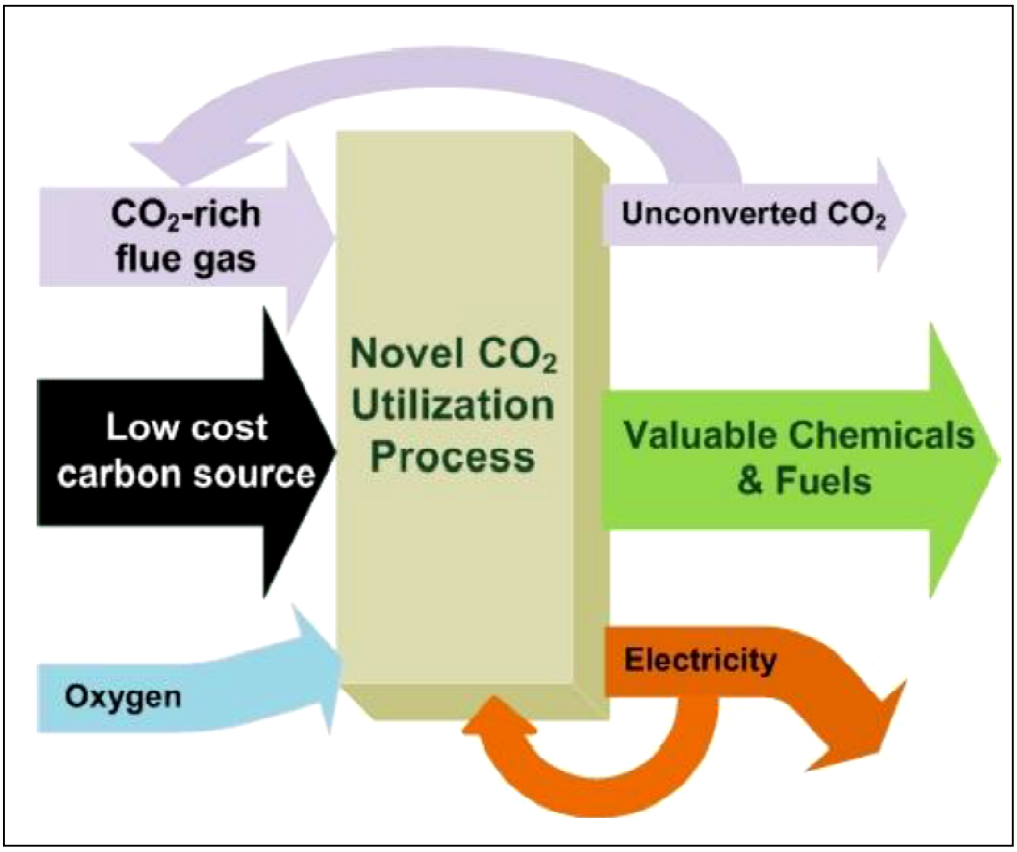

Figure 2.1: Schematic of approach to commercially including biomass to improve coal gasification operation (Song et al., 2011)

These findings suggest that local municipal waste, and other biomass waste, which would otherwise be incinerated or dumped, could be used productively in the coal gasification industry, and indeed prove beneficial. Some research on biomass use for fuel production in a South African context has been conducted where microalgae, (currently available in abundance at the Hartebeespoort Dam due to hypertrophication of the river system), has been used to produce biodiesel (Brink et al., 2011). Australian research has also been conducted on the use of algae to catalyse coal gasification (Kirtania, 2011). Increased reactivity was noted with increased biomass blend percentages, which presents the potential opportunity to utilise the harmful algae occurring in the Hartebeespoort dam for coal gasification, as well as biodiesel production.

2.7. Conclusion

A review of the literature has indicated two distinct opportunities for further investigation. The first is to develop the relatively simple DAEM-based algorithm to process multiple reaction kinetics for systems other than pyrolysis using different structural models such as the RPM. The opportunity exists since isoconversion methods and other algorithmic methods are either not specified to determine multiple reaction kinetics, or are simply too calculation-intensive. Also, extensive research on the effects of using other, more conventional biomass sources for the purpose of co-gasification with South African coals has not been presented. There is hence motivation to investigate the effects of blending South African biomass species with South African coals.

Chapter 3: Research Methodology

3.1. Introduction and Scope

This chapter outlines the scope of this research. The hypotheses posed and the specified objectives which will be achieved are presented. These are then followed by the research methodology. The methodology is two-fold, in that the algorithm will first be modified and developed, using only simulated data. The second tier of the methodology involves testing the modified algorithm on experimental data, as well as using the kinetics data produced by the algorithm to assess the effects of co-reacting biomass and coal in CO_2.

The scope of this research includes the development of a DAEM-based algorithm (based on the original DAEM-based algorithm in Scott et al. (2006)) to accurately process reaction data for processes other than pyrolysis and determine reaction kinetics. The algorithm is modified to process RPM simulated data, for both non-isothermal and isothermal data. The algorithm will then also be applied to non-isothermal reaction data of plain coal and coal-biomass blended chars reacted in CO_2 to determine the effects, if any, of adding biomass to a coal feed during CO_2 reaction. This investigation is limited to a single biomass-coal blend, and a single plain coal. The physical reactivity data is obtained from isothermal as well as non-isothermal experimentation for coal; no isothermal experimentation was conducted for coal-biomass blends.

3.2. Hypotheses and Research Objectives

3.2.1. Hypotheses

- A DAEM-based algorithm can be further developed and modified to accurately determine the entire kinetic triplet for reactions that adhere to models other than the first order model

- The DAEM-based algorithm, modified to incorporate the random pore model (RPM) is capable of processing CO_2 reactivity data and accurately determining the entire kinetic triplet and structural parameter for char-CO_2 reactions, by means of a multiple reaction approach, for isothermal and non-isothermal reaction data.

- The combination of suitable biomass species with coal will improve overall CO_2 reactivity.

3.2.2. Research Objectives

- To assess and confirm the model-independence of the DAEM-based algorithm (Scott et al., 2006) in determining activation energy.

- To develop a method to adapt the algorithm so that other reaction sub-models may be used in determining other parameters of the kinetic triplet.

- To adapt the DAEM-based algorithm to char-CO_2 reactivity (isothermal and non-isothermal) by means of incorporating the RPM. A means of calculating the RPM's structural parameter must also be incorporated

- To investigate the effects of blending a suitable biomass species and a South African coal during CO_2 reactivity on the overall reactivity, by means of assessing the kinetics determined by the algorithm.

3.3. Research Method 1: Data Simulation and Algorithm Development

The first step in the research process is for the original DAEM-based algorithm (Scott et al., 2006) to be coded into Matlab. This coding was tested using the same tests used in Scott et al., (2006) to determine whether the coded algorithm works as shown in the paper presented. Then, the algorithm was adapted to be used in CO_2-char reactivity scenarios by means of incorporating structural reaction models other than the first-order model used originally (The RPM was chosen for this adaptation). The algorithm was also modified to process isothermal CO_2-char reactivity scenarios; this adaptation goes beyond the original algorithm which was developed specifically for non-isothermal data.

Before experimental work is conducted, the chosen reaction model (RPM) will be used to simulate mass-loss with respect to time/temperature data. This data was processed by the modified algorithm to assess the adapted algorithm's efficacy in determining the desired kinetics. As has been done in previous studies (Scott et al., 2006), data was simulated with specified parameters at a pair of heating rates and fed to the algorithm. Then, the values of the algorithm-determined kinetics were compared to the specified values using a relative error analysis.

Since the initial kinetics are not known in physical experimental situations, visual and statistical assessments of quality of fit were used to determine the accuracy of values determined by the algorithm.

The software package, Universal Analysis®, which is used in conjunction with the TA Instruments TGA records the mass loss vs. time/temperature data and can also generate the derivative of this data. These were required for use of the algorithm to determine the desired kinetic parameters. Matlab® (Matlab R14, The Mathworks Inc.) will be used to code and run calculations of the algorithm. All coding is provided, with explanations in Appendix B.

3.4. Research Method 2: Physical Experimentation

3.4.1. Sample Material

Coal

The coal used in these experiments was sourced from a Witbank coal field in Mpumalanga, South Africa. The sample supplied was dried and pulverized by previous students at the University and was made ready for use in the TGA. The coal was pulverized in a centrifugal mill, with the product consisting of particles with a nominal diameter up to 150 microns. The

gases used for the proximate analysis were ultra high purity N_2 and ultra high purity dry bottled air. A proximate analysis of the coal is provided in Chapter 5.

Biomass

The biomass material used in these experiments was pinewood produced in the furniture making industry. It is readily available and is produced in large quantity. The wood was obtained as large blocks. To reduce the particle size of the biomass to that suitable for mixing with the coal sample, an attempt was made to mill the blocks in a centrifugal mill. Because the wood is not has brittle as coal, it did not break as desired and could therefore not be milled. Instead, the wood was abraded with an electric sander. The sawdust produced (approximately 10g) was collected.

To ensure accurate blends (50% coal to 50% wood by mass), the two materials were not mixed in bulk. Rather, each sample to be loaded into the TGA was mixed individually, (using a scale to determine the mass of each material) and mixed in the TGA crucible. The sample was then reacted in the TGA. A proximate analysis of the 50:50 coal-biomass blend is provided in Chapter 5.

The combinations of coal and biomass will be specified by weight fraction of each. Biomass mass fractions to be used will be 0%, and 50%.

3.4.2. Thermo-gravimetric Analysis (TGA)

Once the algorithm is successfully adapted to process RPM data, it was used to determine the kinetics of char-CO_2 reactions. The algorithm requires a minimum of 2 heating rates per sample to be able to determine the kinetics. In this study, 3 heating rates for each sample were used to enable the use of different heating rate combinations, which will serve as an additional tool for assessing the efficacy of the modified algorithm.

Since this research focuses on char reactivity, all samples were charred before being reacted in CO_2. Note that all runs mentioned thus far are under non-isothermal conditions. The algorithm was also used to process isothermal CO_2-char reactivity experimental data following its adaptation to handle simulated isothermal random pore model reactions.

Table 3.1 overleaf provides a summary of the experimental runs that will be done and reported.

Table 3.1: Matrix of planned experimental data to be produced and collected

	Non-Isothermal			Isothermal		
plain coal	20K/min charring in N_2 12K/min reactivity in CO_2	20K/min charring in N_2 15K/min reactivity in CO_2	20K/min charring in N_2 20K/min reactivity in CO_2	20K/min charring in N_2 1050°C reactivity in CO_2	20K/min charring in N_2 1080°C reactivity in CO_2	20K/min charring in N_2 1100°C reactivity in CO_2
50:50 blend	20K/min charring in N_2 12K/min reactivity in CO_2	20K/min charring in N_2 15K/min reactivity in CO_2	20K/min charring in N_2 20K/min reactivity in CO_2			
Plain Biomass	20K/min charring in N_2 12K/min reactivity in CO_2	20K/min charring in N_2 15K/min reactivity in CO_2	20K/min charring in N_2 20K/min reactivity in CO_2			

Two main TGA sequences were developed; an isothermal and a non-isothermal sequence. Both sequences however included identical char preparation steps. The char was prepared by treating the fresh material (pulverized coal, plain pinewood sawdust, or coal-pinewood blend) in pure N_2 and heating from ambient temperature to 1250°C at a rate of 20°C/min. The furnace was allowed to cool, and held at 700°C for 15 minutes to ensure that any residual volatile matter was removed from the sample before the CO_2 reactivity commenced.

After this standardised char-preparation sequence, the non-isothermal CO_2 reactivity treatment commenced. The gas was switched to CO_2 and the temperature was increased from 700°C up to temperatures between1250°C and 1350°C depending on whether the observed reaction reached completion.

For the isothermal experimentation, after the char was prepared in the manner described above, the gas feed was switched to CO_2. The temperature was then set to jump to the required temperature (between 1050°C and 1100°C). The hold time was specified depending on the observed completion of the reaction, approximately 70 minutes.

See Appendix A for further details of the experimental sequences.

3.4.3. Equipment

Standard Equipment

A key consideration in this experimental portion of the research is the equipment being used. The School of Chemical and Metallurgical Engineering at the University of the Witwatersrand acquired a TA instruments SDT-Q600 high-temperature TGA for use in this research. Along with fellow students, the unit was commissioned and calibrated. The DTG and DSC calibrations were conducted and also form part of the experimental work done in this research. The unit is able to operate up to 1500°C. Figure 3.1 and Figure 3.2 are images of the unit and its balance and furnace mechanism respectively.

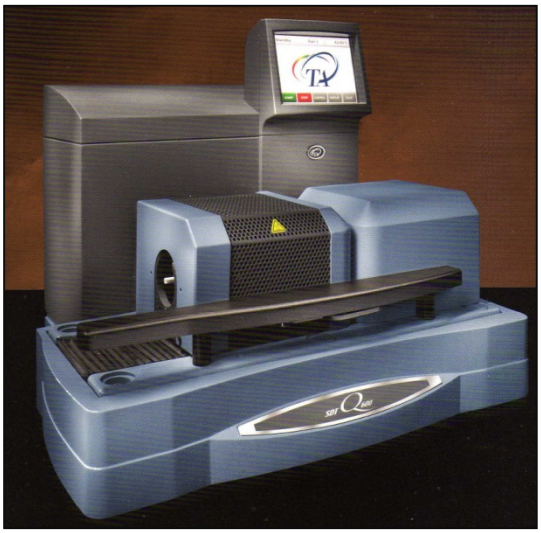

Figure 3.1: TA Instruments SDT-Q600 (TA Instruments, 2010)

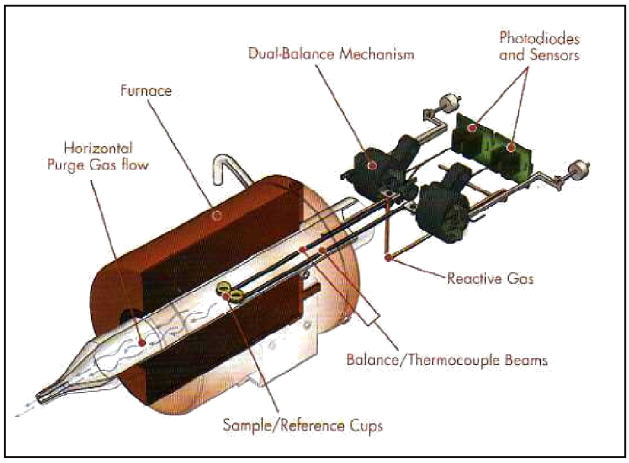

Figure 3.2: SDT-Q600 Furnace and Balance Mechanism (TA Instruments, 2010)

Note that the balance arms have in-built thermocouples since the unit is also able to conduct differential scanning calorimetry measurements. The two balance beams can be used to run simultaneous experiments in order to compare runs and ensure that data is consistent and accurate. When only one balance beam is used, the other holds an empty crucible, which the instrument uses as a reference sample, to account for buoyancy effects within the furnace environment. This functionality ensures that data produced using this instrument is accurate and reliable.

Equipment Modification

According to a TA instruments technician however, the unit cannot process CO_2 through its own in-built mass-flow controllers. The reason stated was that CO_2 can form acidic compounds, which would damage the delicate internal valves, fittings and balances. It was therefore required to design and build an add-on flow controller that could be used through the unit's reactive gas port in order to bypass the unit's balance mechanism. Figure 3.3 is a schematic diagram of the Gas Switching Accessory (GSA) unit and the mass flow controller configuration that was designed and incorporated into the standard TGA configuration to enable safe and prolonged use of CO_2 (as well as pure O_2).

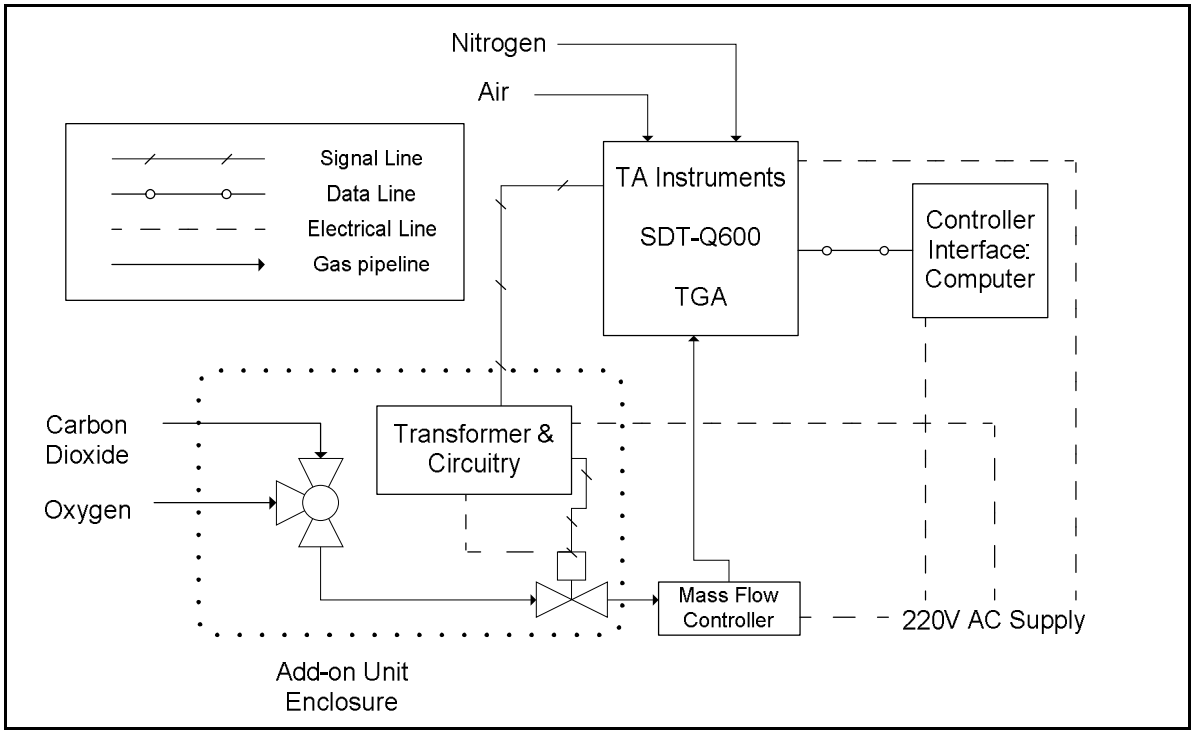

Figure 3.3: Schematic Diagram of the Modified TGA Configuration

The reactive gasses (ultra high purity CO_2 and O_2) are passed through a manual 3-way valve (only one of these gases can be used per run sequence). The desired gas is selected, and the MFC switch is set to the corresponding reactive gas. The signal from the TGA is passed through the GSA's circuitry to operate a solenoid valve that opens and closes when the TGA's "external event" signal is set to on or off within the pre-programmed run sequence. The gas is fed to the calibrated MFC that modulated the gas supply to the TGA. The steady reactive gas supply is then fed through the TGA's reactive gas port which bypasses the delicate balance mechanism and is fed directly into the furnace environment, where it reacts with the loaded sample.

This presents a novel and cost-effective way of adapting relatively affordable equipment to be able to operate under conditions that would otherwise only be possible with far more costly equipment. The alternative, according to the unit's supplier, would be to purchase a unit four times the price of the current one, which was not feasible.

3.5. Conclusion

This chapter has outlined a number of key aspects of how this research was carried out and what was intended to be found. The research objectives and hypothesis were defined, along with the scope of the research. A description of the materials, equipment, and research methods used has also been provided. The research approach has now been structured, and the beginning of the investigation follows in Chapter 4.

Chapter 4: Algorithm Development

4.1. Introduction

Many adaptations of the original Distributed Activated Energy Model (DAEM) method for determining reaction kinetics have been attempted and implemented, as illustrated in the literature review. This chapter details the steps taken to modify the DAEM-based algorithm developed in Scott et al. (2006) to be used for kinetics determination of thermo-chemical coal/char reactions in other reactive atmospheres, where the reactions adhere to reaction models other than the first-order model. This is done so as to extend the application of this algorithm to systems other than pyrolysis. Firstly, the algorithm, as presented in Scott et al. (2006) was coded into Matlab® (Matlab, The Mathworks Inc). Other researchers' work on modification of the algorithm is then presented, followed by a detailed presentation of the adaption conducted in this research. A series of steps were taken in this study to develop the algorithm to determine the kinetics of char-CO_2 reaction, which according to literature, follows the random pore model (RPM) (Irfan et al. 2011). The method will also be generalised so that the algorithm can be adapted to other general reaction models. This study then shows that the algorithm can be further modified to analyse isothermal reactions, also using any reaction model, which is a novelty since other DAEM adaptations have only been used for non-isothermal conditions. (Note that all Matlab® coding written to complete the simulations and calculations discussed and presented in this chapter are presented in Appendix C)

4.2. Original First Order Algorithm

4.2.1. Algorithm Steps and Approach

Without presenting the same detailed explanation of the original algorithm given in the literature review, this section serves to highlight the most important steps and equations used in the algorithm, which also later become the main focus points for its modification to other situations. A reproduction of the algorithm schematic presented in Scott et al. (2006) is provided in Figure 4.1 below:

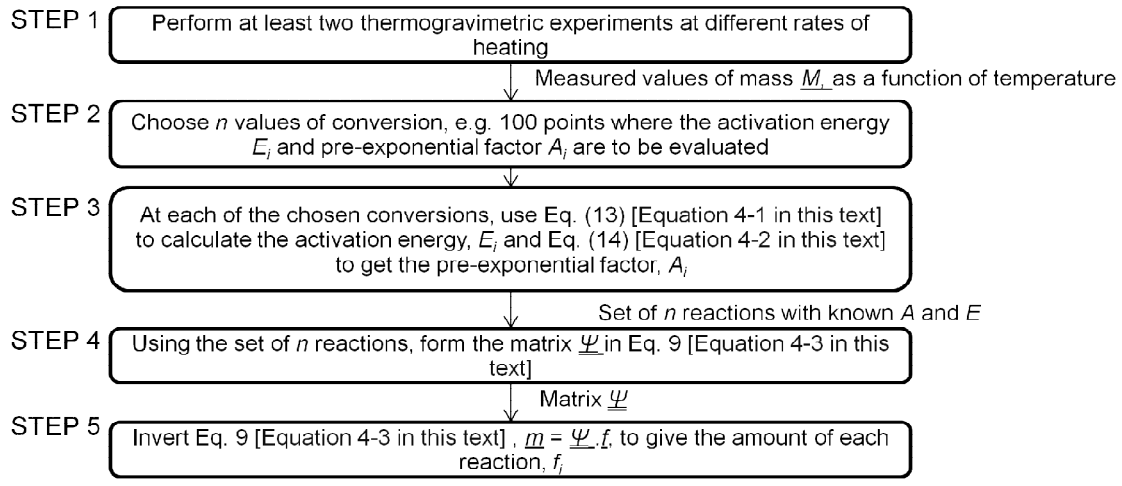

Figure 4.1: Schematic of Algorithm (Scott et al. 2006)

The three main equations referred to in the schematic are given below. The first is the equation which equates the two Ψ expressions which are at different temperatures and heating rates, but at the same fractional conversion. This equation is used to calculate the activation energy, *E*, and is referred to in Scott et al. (2006) as "Eq. 13", and is given in this text as equation 4-1:

$$\Psi_i(B_1,T_1) = \Psi_i(B_2,T_2)$$
$$or\ substituting$$
$$\frac{1}{B_1}\left[T_0\exp\left(\frac{-E_i}{RT_0}\right)-\frac{-E_i}{R}\int_{E/RT_0}^{\infty}\frac{\exp(-u)}{u}du - T_1\exp\left(\frac{-E_i}{RT_1}\right)+\frac{E_i}{R}\int_{E/RT_1}^{\infty}\frac{\exp(-u)}{u}du\right] \quad \textbf{4-1}$$
$$= \frac{1}{B_2}\left[T_0\exp\left(\frac{-E_i}{RT_0}\right)-\frac{-E_i}{R}\int_{E/RT_0}^{\infty}\frac{\exp(-u)}{u}du - T_1\exp\left(\frac{-E_i}{RT_1}\right)+\frac{E_i}{R}\int_{E/RT_1}^{\infty}\frac{\exp(-u)}{u}du\right]$$

The second principle equation in the algorithm is the expression which uses the activation energy that has been found, as well as a known value of ln(Ψ) to find the pre-exponential factor, *A*. This equation is given in Scott et al (2006) as "Eq. 14" and is given in this text as equation 4-2:

$$\ln(\Psi_i(T)) = \frac{A_i}{B_1}\left[T_0\exp\left(\frac{-E_i}{RT_0}\right)-\frac{E_i}{R}\int_{E/RT_0}^{\infty}\frac{\exp(-u)}{u}du - T_1\exp\left(\frac{-E_i}{RT_1}\right)+\frac{E_i}{R}\int_{E/RT_1}^{\infty}\frac{\exp(-u)}{u}du\right] = -1 \quad \textbf{4-2}$$

This step is particularly important since this is the first step in which a reaction model is involved in the determination of the kinetic parameters. While finding the activation energy only involves the numerical integration of the temperature integral, the determination of the pre-exponential factor needs a known value of the natural logarithm of Ψ_i, (i.e. $ln(\Psi_i)$). This value can be determined, according to Scott et. al. (2006) by assuming that the dominating reaction is at some conversion. It is assumed that each candidate reaction (i.e. the reaction of the i^{th} component dominating at each overall fractional conversion) is reacting such that decomposition rate is a maximum. Mathematically, one must find the value of f_i, or conversion *x,* such that $\frac{d}{dT}\left(\frac{dx}{dT}\right) = 0$, and the corresponding value of ln(Ψ_i) to substitute into equation 4-2. (Note that time and temperature differentials are interchangeable as long as heating rates are constant.) As is stated in Scott et. al. (2006), this assumption increases the possibility of erroneous results since the actual value of Ψ could be anything between zero and unity. This approach is then defended since the matrix inversion which is the next pivotal step in the algorithm always negates spurious results by allocating 0% of the reactive mass to those particular kinetics. Scott et. al. (2006) also notes that when several reactions are occurring (as is the case in real thermo-chemical treatment of complex fuels), for a reaction to be dominating, its reaction rate must be high, thus, it is likely that the rate of reaction of the i^{th} component is at a maximum, and therefore that the actual value of Ψ is close to the calculated value.

Equation 4-3 is used in the matrix inversion step which uses the Ψ-matrix and the mass loss data to calculate the initial mass fractions of each reaction. The non-zero mass fractions correspond to the actual reactions that occurred, thereby negating the spurious reaction kinetics found since these correspond with 0% of the reactive mass. It is given as "Eq. 9" in the original text.

$$\underline{M} = \underline{\Psi}.\underline{f} \quad \textbf{4-3}$$

A key aspect of the algorithm is calculating the correct mass fractions. If this is not done accurately, even though the correct activation energy and pre-exponential factor are found in one of the candidate reactions generated by the algorithm, one would not know which of them are correct. Scott et al. (2006) again uses a model dependent approach to find this value; this approach must be borne in mind when adapting the algorithm to other situations.

Before the algorithm is adapted, the original algorithm will be tested. The following section, section 4.2.2, presents the simulations and kinetics determination of first order reactions, as was done in Scott et al. (2006).

4.2.2. Validation of the Algorithm

In Scott et al. (2006), thermo-gravimetric experiments were simulated using specified kinetic parameters and specified reaction kinetics (i.e. a specific reaction model was used – in this case, the first-order reaction model.). The simulated data is then fed to the algorithm, where the algorithm should ideally find the same kinetic parameters specified during simulation. The results in this section will be assessed by analysis of relative error between the specified kinetics, and those found by the algorithm. A visual comparison of the plots generated from the specified and algorithm-determined kinetics is also given.

Test 1: Simulation of a Single First-Order Reaction

The first test illustrates the most basic functionality of the original algorithm. For this test, a single first order reaction was simulated. The activation energy E=200kJ/mol and grouped pre-exponential factor A=1E+15sec^{-1} correspond to a total mass fraction of 1. The simulation is presented in Figure 4.2. Note that no ash content has been simulated in this instance.

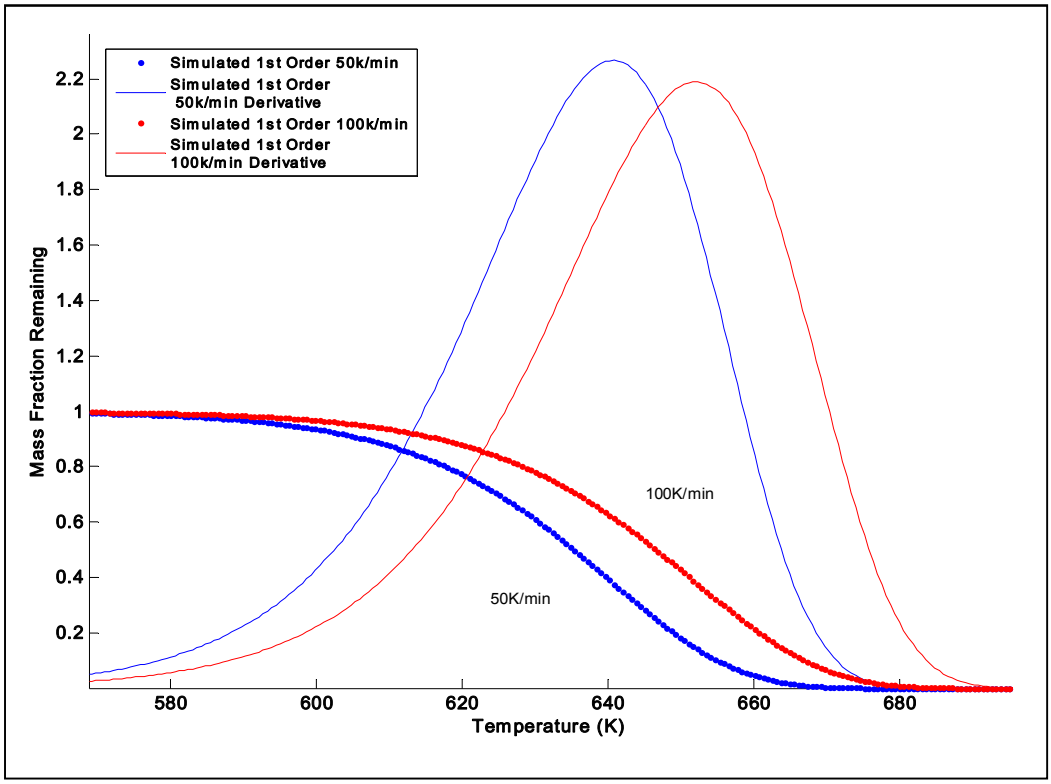

Figure 4.2: Simulated Single First Order Reaction at Different Heating Rates

This data is then fed to the algorithm, which follows the steps outlined in Figure 4.1. The algorithm then generates the kinetic data results presented in Figure 4.3.

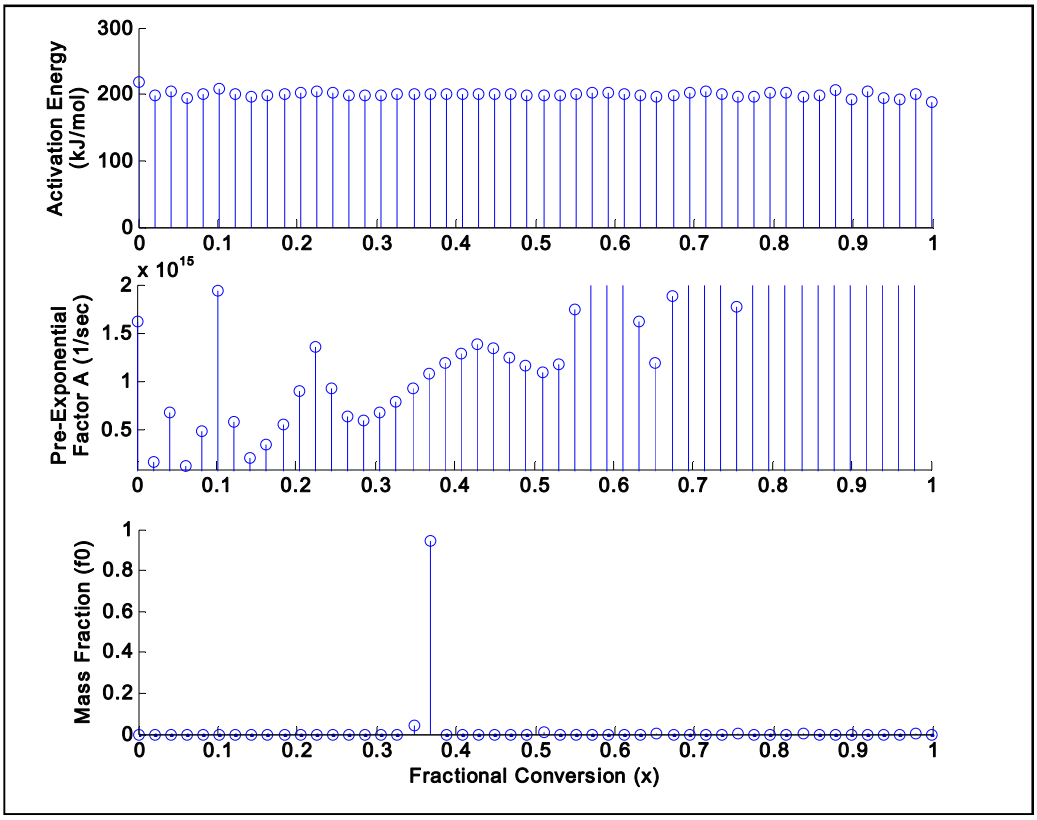

Figure 4.3: Stem Plots of Algorithm Derived Activation Energy and Initial Mass Fraction

From Figure 4.3, it can be seen that the algorithm has evaluated the activation energy, pre-exponential factor, and initial mass fraction at each of the 50 candidate reactions across the entire range of conversion. While *E* and *A* values have been found for each reaction, the algorithm has only allocated mass to 1 set of parameters, those being the kinetics around the conversion of x≈0.368. This is value of conversion used in Scott et al. (2006) in equation 4-2. It can also be noted that due to the numeric nature of the algorithm, the results tend to be straddled across 2 adjacent reactions; such is the case observed in Figure 4.3 where the two nodes straddling this value of conversion are both allocated mass. These results can be taken to represent a single reaction, especially since the parameter values are so close. A weighted average (based on mass fraction) of the parameters *E* and *A* is therefore calculated and presented in Table 4.1.

Table 4.1: Error Analysis for Simulated Single First Order Kinetics Determination

	Activation Energy *E* (kJ/mol)	**Pre-Exponential Factor *A* (sec^{-1})**	**Initial Mass Fraction *f0***
Specified Value	200	1E+15	1
Algorithm Derived Value	199.93	9.992E+14	0.9998
Relative Error (%)	<1%	<1%	<1%

Table 4.1 shows the high accuracy with which the algorithm was able to determine the kinetics. This indicates that the original algorithm has been successfully reproduced, and that the algorithm itself is reliable when determining single first order reaction kinetics.

The algorithm-derived kinetics are then used to generate new simulated data, which is plotted over the original data. This serves to illustrate the quality of the kinetics found. As can be seen in Figure 4.4, the algorithm kinetics produced a plot that correlates strongly with the original simulations. This is expected since the value of the parameters found correlate well with the parameters specified. This form of analysis is more useful when comparing simulated data produced after finding the kinetics to the experimental data. The comparison indicates the quality of choice of model.

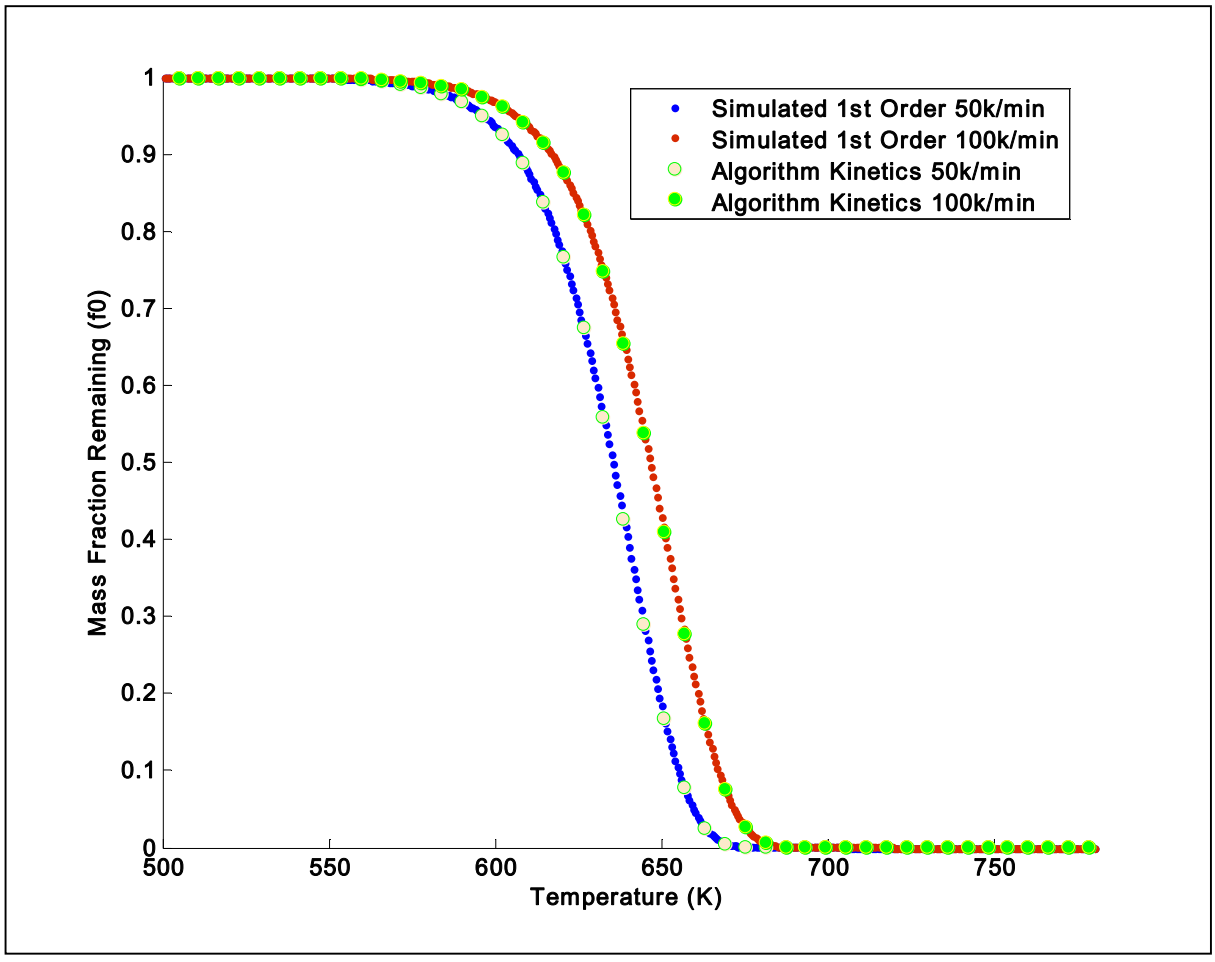

Figure 4.4: Algorithm kinetics simulation plotted over original single first order simulation

Test 2: Simulation of Seven First-Order Reactions

As was done in the original presentation of the algorithm (Scott et. al. 2006), the next test is to simulate several reactions to determine whether the algorithm can determine the kinetics of multiple reactions occurring during one thermal decomposition of a complex fuel. Unlike the original test by Scott et al. (2006), this test will be applied to the simulation of several reactions with the presence of ash, whereas ash was not initially included in simulation. The multiple reaction simulation is presented in Figure 4.5 overleaf.

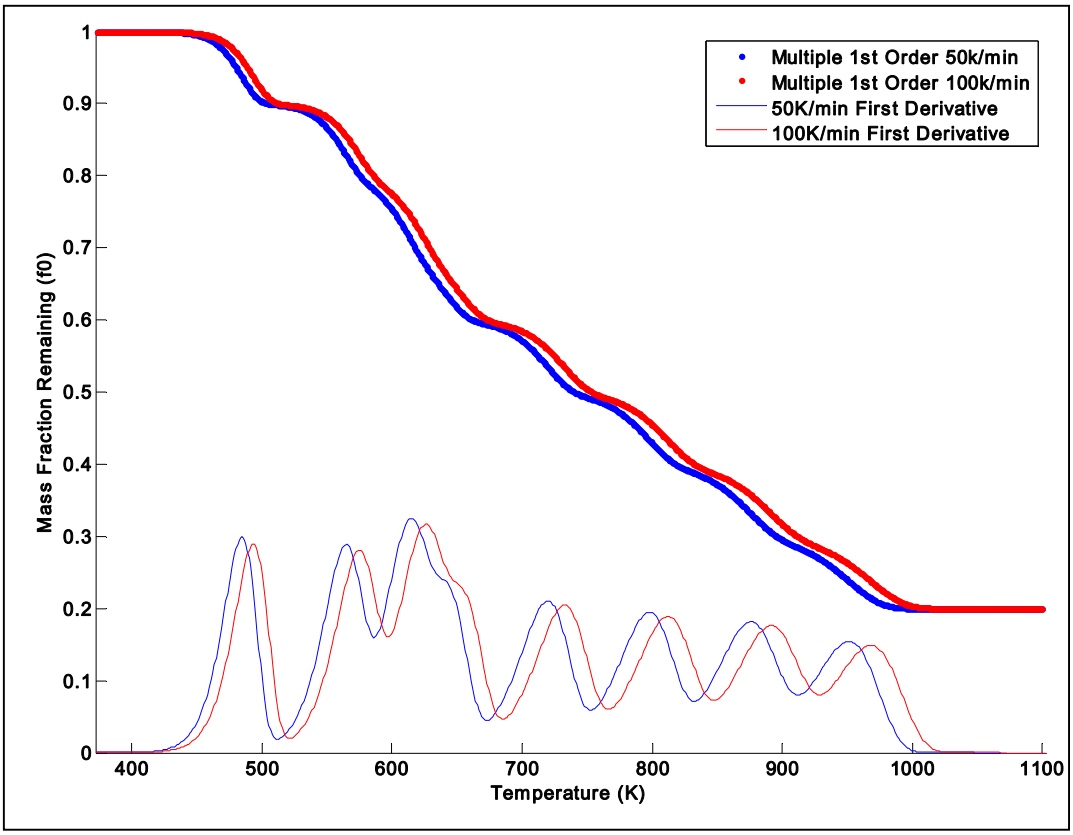

Figure 4.5: Simulated Multiple First-Order reaction with Ash Content

The data presented in Figure 4.5 represents multiple first order reaction occurring with the presence of inert ash content, as would be observed from experimental TGA data. The figure also includes the first derivative data. Each peak or inflection point represents a distinct reaction. It is evident that the beginning and end of each reaction cannot be identified precisely, especially for the second, third and fourth reaction. A numeric method is required to determine the area under each individual reaction peak. This simulated data is then fed to the algorithm which calculates the activation energy *E*, Pre-exponential Factor *A*, and lastly, initial mass fraction related to each *E-A* pair which is represented by the area under each individual reaction peak in the derivative data. These results are provided as follows in Figure 4.6 overleaf.

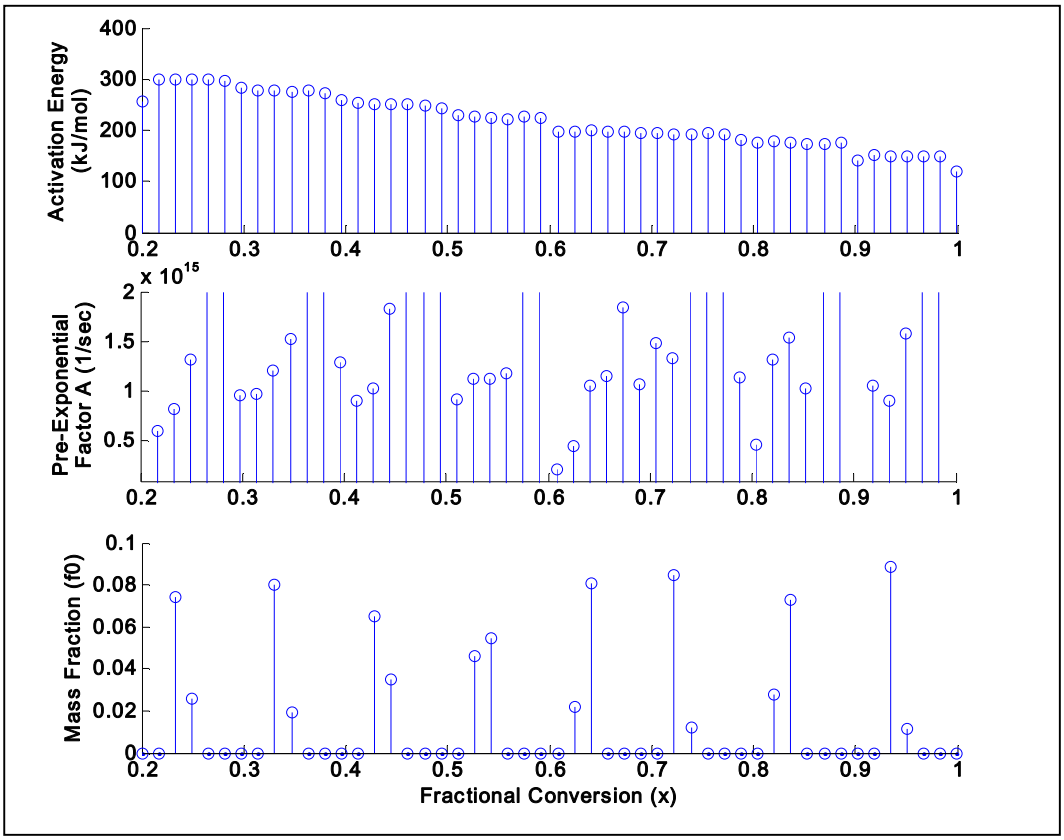

Figure 4.6: Kinetic Parameters of Simulated Multiple First Order Reactions Determined by the Algorithm

Again, the algorithm determines an activation energy and pre-exponential factor for each of the fifty specified candidate reactions. The spurious values are identified by means of correlation of the *E-A* set to the initial mass fractions (*f0*) of 0% as determined by the matrix inversion. Those initial mass fractions which are non-zero indicate which kinetics to regard as non-spurious. Note that 8 reactions were specified, each allocated an initial mass of *f0=0.1*. The remaining 20% of the mass is then regarded as inert ash. The activation energy values were chosen between 150kJ/mol and 300kJ/mol. Note too that two values have been specified with marginal difference in value, i.e. 190kJ/mol and 200kJ/mol are both specified. This has been done to determine whether the algorithm is able to identify independent reactions even if their kinetics are very similar. The values of the specified and algorithm-determined kinetics are given as follows in Table 4.2:

Table 4.2: Error Analysis if Algorithm Derived Multiple First Order Reaction Kinetics

Algorithm-Determined f0 (summed)	Specified f0	Relative Error (%)
0.1001	0.1	0.13%
0.1005	0.1	0.52%
0.0974	0.1	2.61%
0.1018	0.1	1.85%
0.1003	0.1	0.32%
0.1002	0.1	0.16%
0.0994	0.1	0.59%
0.1003	0.1	0.32%

Table 4.2 Continued: Analysis if Algorithm Derived Multiple First Order Reaction Kinetics

Algorithm-Determined E (kJ/mol) (summed)	Specified E (kJ/mol)	Relative Error (%)
150.29	150	0.19%
176.55	175	0.88%
192.29	190	1.21%
200.21	200	0.11%
225.97	225	0.43%
251.29	250	0.52%
276.59	275	0.58%
299.61	300	0.13%
Algorithm-Determined A (1/sec) (summed)	**Specified A(1/sec)**	**Relative Error (%)**
1.09E+15	1E+15	8.96%
1.40E+15	1E+15	40.49%
1.62E+15	1E+15	61.86%
1.08E+15	1E+15	8.04%
1.20E+15	1E+15	20.46%
1.24E+15	1E+15	23.77%
1.28E+15	1E+15	27.74%
9.93E+14	1E+15	0.66%

Table 4.2 shows that the algorithm was able to identify 8 distinct reactions, even with two of the activation energies being specified close together. As in the previous example, the values produced by the algorithm straddle 2 consecutive candidate reactions. What has been done in this case is to sum the adjacent mass fractions, and calculate a weighted average of the activation energy and pre-exponential factor values. It can be seen the errors in the activation energy *E* and initial mass fraction *f0* are desirably low, all within the order of ±3%. The errors in the pre-exponential factor values are admittedly high, but a graphic analysis of the quality of fit using the algorithm-derived kinetics can also indicate whether or not the kinetics found are reliable. These error ranges correlate with those found in the original demonstration of the algorithm's use (Scott et al., 2006). The graphical analysis is presented in Figure 4.7.

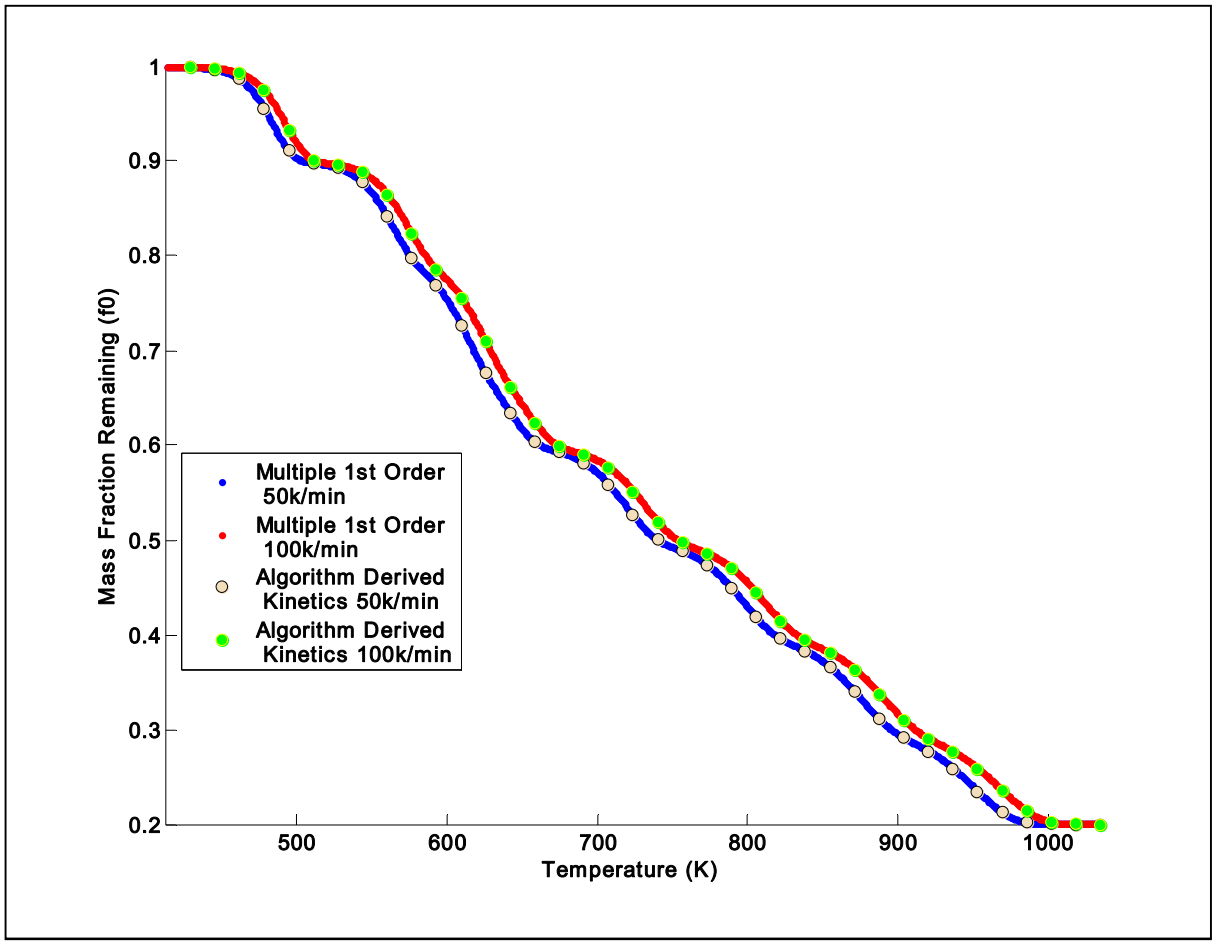

Figure 4.7: Overlay Plot of the Multiple First Order Reaction Simulation Using Algorithm-Derived Kinetics

Despite the pre-exponential factor error margin, Figure 4.7 illustrates a very accurate fit when comparing the data generated by using the algorithm-derived kinetics to the original simulation. This observation has been observed and studied to assess whether an inter-dependence exists between the kinetic parameters (Koga, 1994). Koga (1994) suggests that there exists some compensation effect where *E* and *A* values may vary but still represent the equivalent reaction behaviour.

4.3. Other Uses and Developments of the First Order Algorithm

Having showcased the original algorithm and its ability to process simulated first order data, this section highlights other developments based on the original algorithm.

4.3.1. Application of the Algorithm to Simulated Char Combustion

Saloojee (2011) applied the unmodified algorithm to simulated char combustion, which follows the shrinking core model (Sadhukhan et al., 2010). Unlike the original algorithm, reaction simulations were conducted primarily with the use of ODE solvers, whereas the original algorithm simulations were conducted using a semi-analytical approach. A novelty of the research in Saloojee (2011) is that the DAEM-based algorithm developed in Scott et al. (2006), developed solely for first-order reactions, is able to determine the activation energy of any thermo-chemical decomposition, regardless of model. Since this finding relates

directly to the current research, the full derivation, as given in Saloojee (2011) is given below.

The DAEM-Based Algorithm's Model-Free Determination of Activation Energy

Firstly, a generic reaction model is proposed for a component *i* of a complex fuel, such as coal:

$$\frac{df_i}{dt} = -A^* \exp\left(\frac{E_i}{RT}\right) g(f_i) \qquad \textbf{4-4}$$

Where the pre-exponential factor A^* is a grouped factor which may include a reactive gas partial pressure term, as well as initial fuel particle structural parameters; and $g(f_i)$ represents a generic function (reaction model) describing the behavior of component *i*.

Then, equation 4-4 is separated according to its variables, and both sides of the equation are integrated. The time differential is converted to a temperature differential by means of multiplication of a constant heating rate, *B* (Scott et al., 2006) resulting in equation 4-5 below:

$$\int_{f_{i,0}}^{f_i} \frac{df_i}{dg(f_i)} = -\frac{A}{B}\int_{T_0}^{T} \exp\left(\frac{-E_i}{RT}\right) dT \qquad \textbf{4-5}$$

Where T_0 and $f_{i,0}$ are the initial temperature and initial mass fraction of component *i* respectively. The integral form of the left hand side is written as $G(f_i)$ and right hand side can be written as $ln(\Psi_i)$, where Ψ is a function of temperature, *T* and heating rate, *B*. Then if the right hand side is integrated between the specified limits, and the identity of the right hand side is used, equation 4-5 can be written as:

$$G(f_i) - G\left(f_{i,0}\right) = ln(\Psi(B,T)) \qquad \textbf{4-6}$$

At a given conversion, the mass fraction, f_i is equal for two different heating rates at different temperatures, such that $ln(\Psi(B_1,T_1)) = ln(\Psi(B_2,T_2))$(Scott et al., 2006). Since the value of f_i is equal for both sets of temperature, the left hand side of equation 4-6 falls away; hence determination of activation energy *E* using the DAEM based algorithm (Scott et al., 2006) is a "model-free" method (Saloojee, 2011).

Determination of Shrinking Core Model Activation Energy

Here, reactions adhering to the shrinking core model (SCM) are considered. The Shrinking Core Model (Everson, Neomagus, Kasaini, et al., 2006) is given as equation 4-7:

$$\frac{dx}{dt} = r\frac{S_0(1-x)^{2/3}}{(1-\varepsilon_0)} \qquad \textbf{4-7}$$

Where *x* is fractional conversion, *t* is time, S_0 *and* ε_0, are initial particle structural parameters and *r* is the reaction rate, defined as $r = -Ae^{-E/RT}.{P_{O_2}}^n$.

Equation 4-7 can be re-written in terms of temperature instead of time by multiplying through by a constant rate of heating. This has been done since non-isothermal reactions are being studied. Unlike the original algorithm, reaction simulations were conducted primarily with the

use of ODE solvers to solve equation 4-7 whereas the original algorithm simulations were conducted using a semi-analytical approach (The use of these methods is explained in the following section, 4.3.2). The activation energy was specified as *E=200kJ/mol*; the pre-exponential factor was specified as $A=1E+15sec^{-1}$, and the mass fraction of material reaction with these kinetics was specified as $f_0=1$. The simulation for heating rates of 50K/min and 100K/min are presented in Figure 4.8.

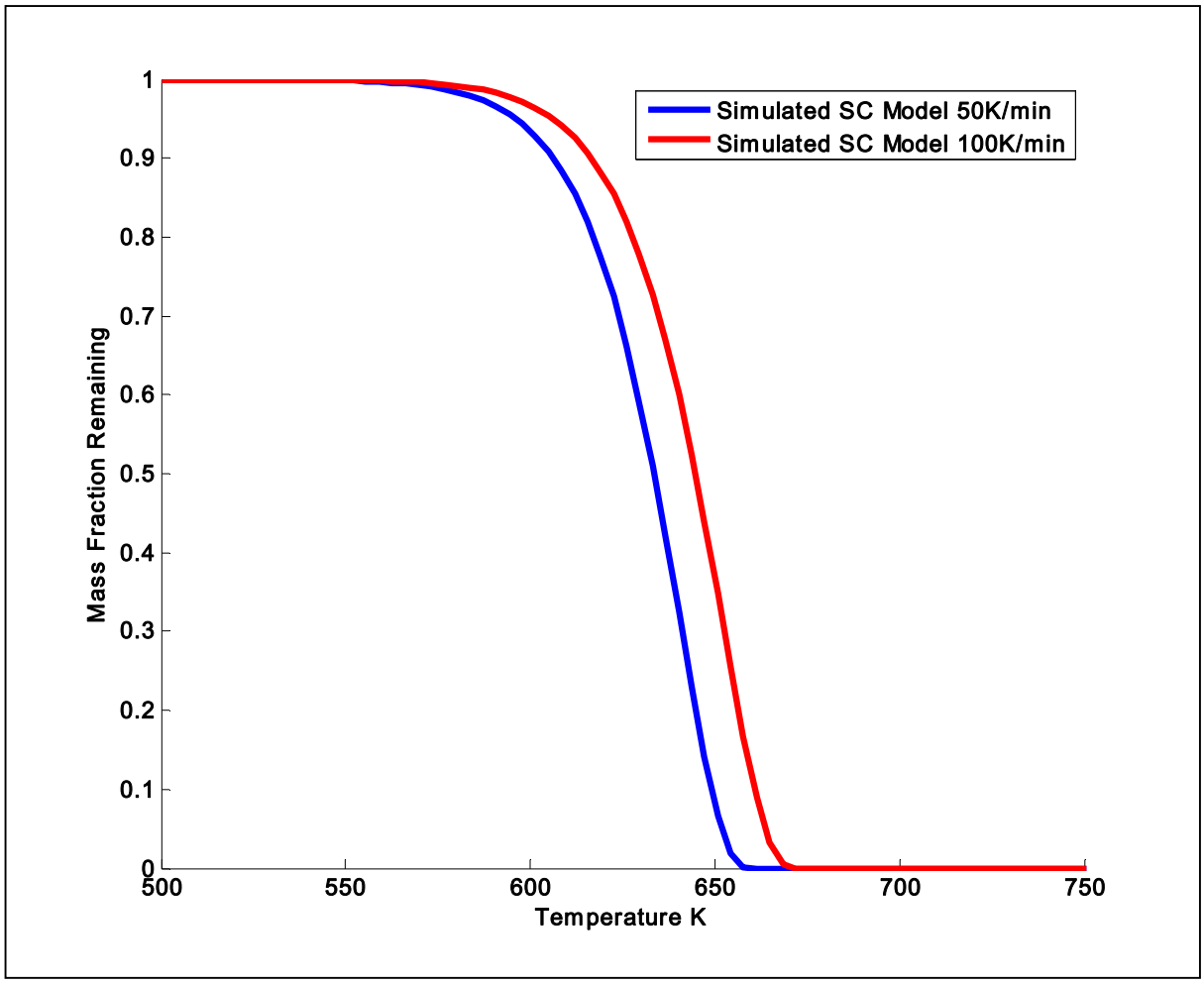

Figure 4.8: Simulated Single Shrinking Core (SC) Model Reaction at Different Heating Rates

As was done before, the algorithm then uses the simulated data to determine the kinetic triplet. Note that no alterations to the original algorithm were made when attempting to determine these shrinking core model kinetics. The algorithm was again set to calculate 50 candidate reactions across the range of conversion. The results obtained from the algorithm are presented in Figure 4.9 overleaf.

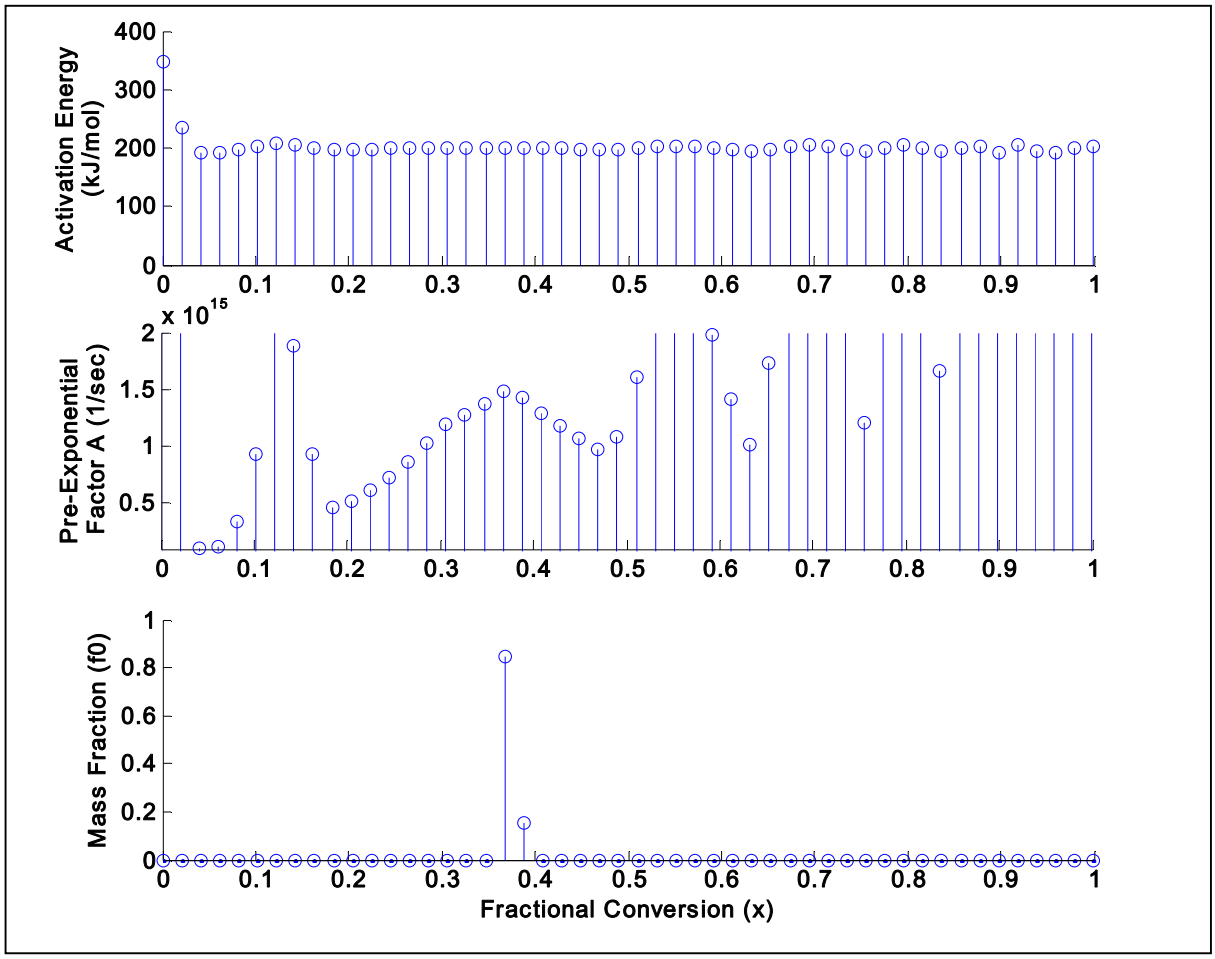

Figure 4.9: Kinetics Results for Simulated Single Shrinking Core Model Reaction

The results again straddle the point at which $x \approx 0.368$, i.e. the conversion at which a first-order reaction is at its maximum rate of decomposition, and that which is specified in equation 4-2. From Figure 4.9, it can be see that while the entire range of activation energy values found is very close the specified value, the values of the pre-exponential factor values vary greatly. It can also be seen that the value of the pre-exponential factor indicated to be non-spurious by the non-zero value of f_0, is far greater than the value specified.

Table 4.3: Error Analysis for Simulated Single Shrinking Core Reaction Kinetics

	Activation Energy *E* (kJ/mol)	**Pre-Exponential Factor *A* (sec^{-1})**	**Initial Mass Fraction f_0**
Specified Value	200	$1*10^{15}$	1
Algorithm Derived Value	201.42	1.47E+15	1.0017
Relative Error (%)	<1%	47%	<1%

Table 4.3 indicates that the mass fraction and activation energy have still been found with great accuracy, despite the use of the supposed first-order model on shrinking core model data. The value of the pre-exponential factor however has a great margin of error. This

shows that the original model can be used to determine the activation energy, but cannot be used for determining the pre-exponential factor. The kinetics found by the algorithm were used to simulate SCM reactions at the same heating rates to compare against the original simulations. This comparison is presented in Figure 4.10.

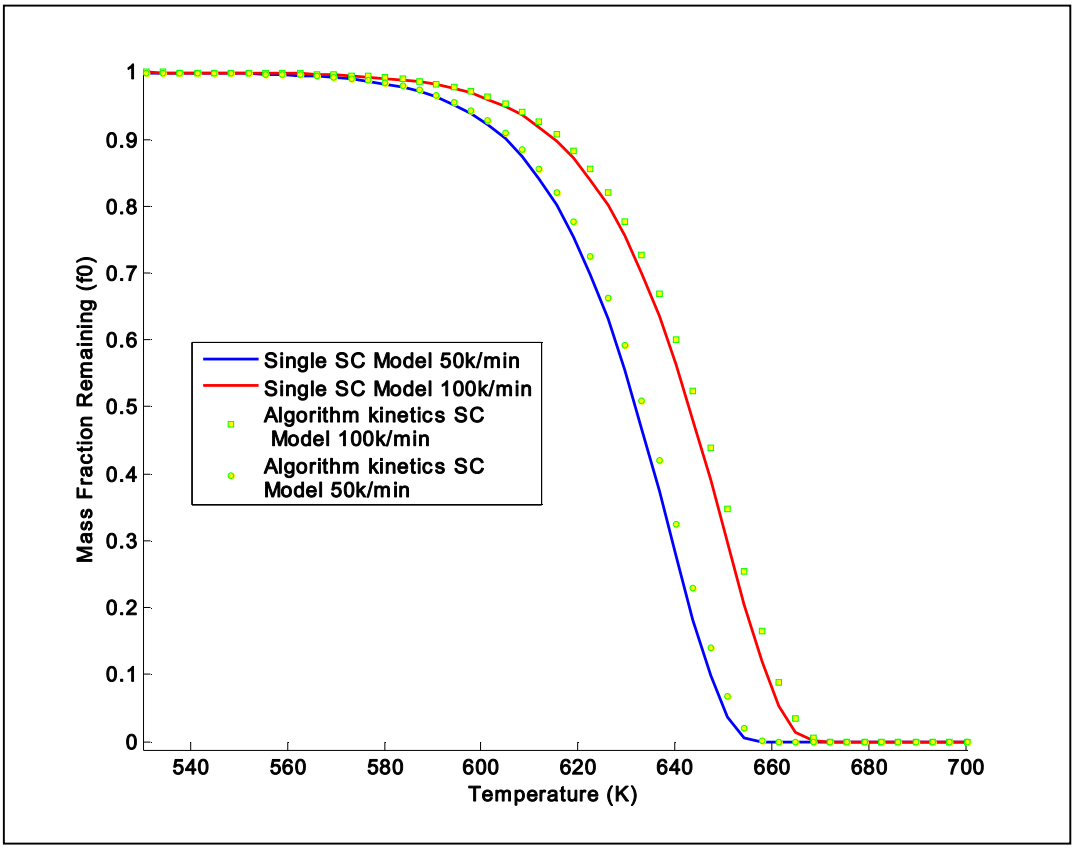

Figure 4.10: Comparison of First-order-Algorithm kinetics simulation and originally specified kinetics simulation of a single SCM Reaction

Plotting the curves under the same conditions and using the algorithm derived kinetics, it can be seen in Figure 4.10 that the incorrect value of the pre-exponential factor A^* results in consistently over-predicted values of the mass fraction remaining. The value of the activation energy can however be used in order to find the pre-exponential factor.

Determination of the Pre-exponential Factor A

Saloojee (2011) details a method in which the reaction model is used directly, along with the activation energy *E* found from the use of the algorithm and the known values specified when simulating the data and determining *E*. Equation 4-7 is used, with the Arrhenius form of the rate expression substituted, and grouped pre-exponential factor. The resulting expression is given in equation 4-8:

$$\int_0^x \frac{dx}{(1-x)^{2/3}} = -\frac{A}{B}\int_{T_0}^{T} \exp\left(\frac{-E}{RT}\right) dT \qquad \textbf{4-8}$$

The limits of integration are of principle importance when using this method. Saloojee (2011) notes that the limits of integration with respect to conversion *x* lie between the initial conversion, which is zero, and the value of *x* at which the reaction undergoes a maximum

rate of decomposition, i.e. $x \approx 1-e^{-1} \approx 0.632$ (Scott et al., 2006) and the temperature limits are between the initial temperature, usually 298K and the temperature corresponding to the non-zero mass fraction, f_0. Saloojee (2011) reports errors of less than 2% using this method, which is a significant improvement over the original algorithm's accuracy when processing shrinking core model data. It must however be noted that the conversion value used is still related to first-order. A more robust approach when using this method would be to find the conversion resulting in a maximum rate of decomposition for the particular reaction model being used.

4.3.2. Comparison of Simulation Methods: ODE Solvers vs. Semi-Analytical Method

Ordinary Differential Equation (ODE) Solvers

When using an ODE solver, very little mathematical manipulation of the reaction model is required. A major consideration in this approach however is how to select the most appropriate solver to use. Since different solvers utilise different mathematical algorithms each suited to certain situations, one must investigate which solver is best suited to a given reaction model. This dispels the notion that using an ODE solver is an easier, less "labour-intensive" means of simulating data. The penalty for bypassing this suitability analysis is that the accuracy of the simulated data will not be as high if the wrong solver is chosen. Figure 4.11 shows a comparison of the results of two arbitrarily chosen ODE solvers. Figure 4.11 depicts the simulated mass loss curves and their derivatives of a 50K/min regime produced using each ODE solver. Table 4.4 shows the results obtained using the first-order algorithm.

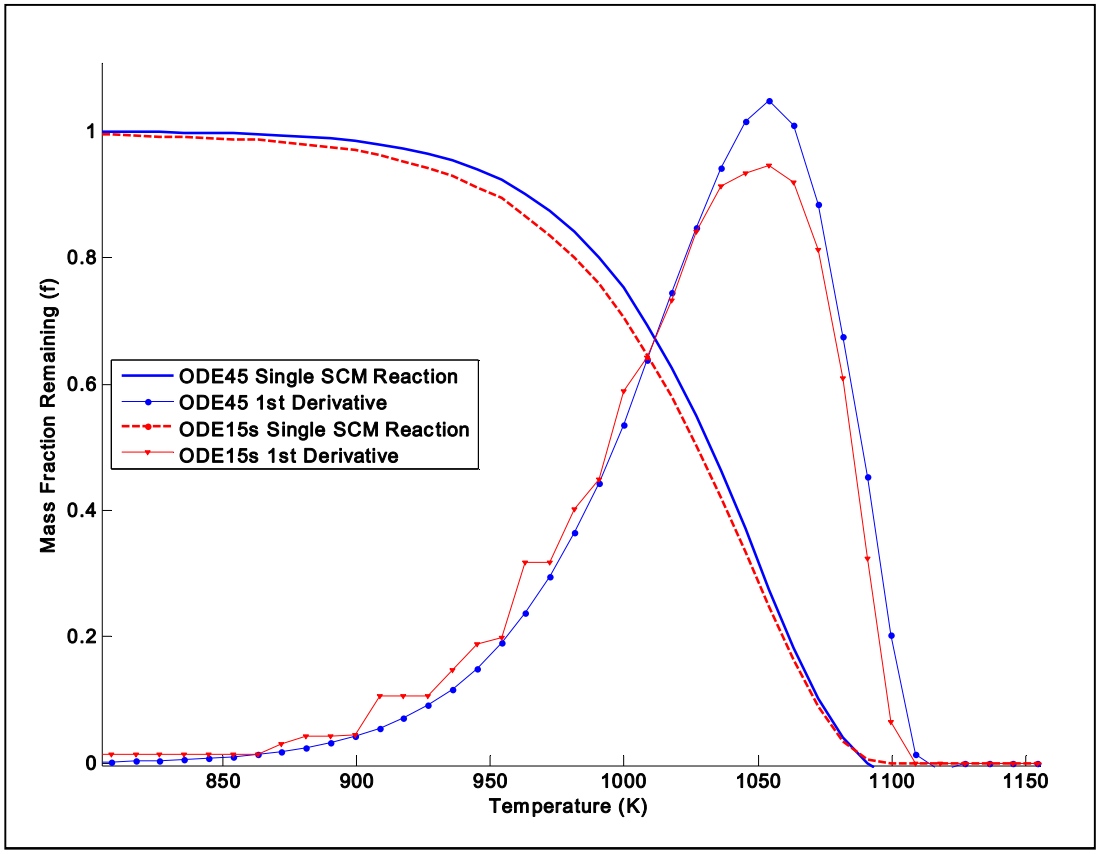

Figure 4.11: Comparison of Data Produced Using Different ODE Solvers

Table 4.4: Kinetics Results Obtained From Data Produced Using Different ODE solvers

	Activation Energy	Mass Fraction
Specified Value	200kJ/mol	1
ODE45 ***(%error)***	200.41kJ/mol *(0.20%)*	1.0034 *(0.34%)*
ODE15s ***(%error)***	203.61kJ/mol *(1.81%)* 142.82kJ/mol *(spurious reaction)*	0.9886 *(1.14%)* 0.0109*(spurious)*

As can be seen, the results differ appreciably. It must also be noted that the second solver, ODE15s inaccurately simulates two separate reactions, even though just one activation energy value is specified. The jagged curve of the derivative of the ODE15s simulation results in the algorithm identifying multiple reactions; also mass loss seems to occur at lower temperatures and at a slower rate using the ODE15s solver. These results show that while some ODE solvers can be used to generate accurate simulations which in turn result in an accurate determination of the kinetics, use of others can lead to significantly inaccurate results. As a result of this, ODE solvers should be carefully chosen, or a more certain method of data simulation should be used entirely.

Semi-Analytical Methods

The successful use of the semi-analytical method has already been demonstrated when using the original algorithm. The semi-analytical method is used by separating variables, integrating and generating an explicit expression of mass fraction remaining (or conversion) in relation to an explicit temperature function. The temperature interval is pre-defined and divided into a set number of intervals, corresponding to the number of conversion points at which the integral will be evaluated.

The reason this method is referred to as semi-analytical and not completely analytical is because no analytical solution for the temperature integral exists, and must hence be solved numerically. This is done using *quad,* an in-built numerical integration function in Matlab®, which applies adaptive Gaussian quadrature. It evaluates the temperature integral at each candidate reaction, represented by each specified fractional conversion and corresponding temperature. The method also uses the activation energy and pre-exponential factor values specified.

The resulting matrix generated from this numerical integration, (with rows representing each complete reaction represented by each specified *E-A* pair) is multiplied by the specified mass fraction vector. This multiplication normalises each reaction to its specified initial mass, so that the sum of total fractional mass loss across all reactions (as well the addition of ash, if specified) sums to unity. This enables one to simulate multiple reactions and/or ash content in the same way that one would simulate a single ashless reaction; no modifications to the mathematical approach are required. This is a key benefit as compared to the ODE solver method, which would require the solver to be applied to each *E-A* pair in order to simulate multiple reactions and/or ash content. Since ODE solvers require one to specify initial and/or final conditions, it would be possible (but cumbersome) to simulate multiple reactions. This limitation would then exclude the use of ODE solvers for multiple reaction kinetics determination for experimental data, because the initial and final conditions of each reaction occurring would not be known.

While an integrated expression is not needed in the ODE solver method, it is also less versatile. The ODE solver method can be used for simulating rudimentary situations but must be used with care, especially when choosing the solver. Hence, the simulations in the sections that follow all use the semi-analytical method.

4.4. Application of the Algorithm to Gasification Reactions using the RPM

An approach similar to that of Saloojee (2011) was taken in this study, to adapt the algorithm to the RPM, which describes the reaction of char with CO_2 (Irfan et al., 2011). The unchanged algorithm is initially used to determine whether the correct activation energy can be found for RPM simulations. Then, instead of using the activation energy to calculate the pre-exponential factor outside of the algorithm, the algorithm is essentially re-written to include the RPM where model-dependent steps are used. The benefit of this is that RPM data can be processed without user input or interference, as was achieved in the original algorithm presented by Scott et al. (2006).

4.4.1. Method of Simulation of RPM Non-Isothermal Reactions

This section will illustrate the steps used in working with the model to produce simulated RPM data. The *g(x)* expression for the RPM, equation 2-31, is used and equated to the temperature integral term, as shown in equation 4-9:

$$g(x) = \frac{2}{\varphi}\left(\sqrt{1-\varphi\ln(1-x)}-1\right) = \frac{A^*}{\beta}\int_{T_0}^{T}\exp\left(\frac{-E}{RT}\right)dT \qquad \textbf{4-9}$$

Where A^* is a grouped pre-exponential factor, including the partial pressure term ($P_{CO_2}{}^n$) assumed constant, as well as other initial particle structural parameters, such that the units of A^* are $s^{-1}.m^{-1}$. The structural term φ is calculated for all simulations using values applicable to common porous solids (Bhatia and Perlmutter, 1980). The values provided result in a structural parameter value of ***φ=0.88***. This is the structural parameter value used for all simulated RPM data that follows.

The aim is to make the fraction of initial sample mass remaining, *f*, the subject of the formula, which is achieved by making the *(1-x)* term in equation 4-9 the subject, since *f=1-x* when the initial mass fraction, $f_0=1$. Hence, the following expression is obtained by manipulating equation 4-9:

$$f_i = 1 - x_i = exp\left(\frac{1}{\varphi}\left(1-\left(\frac{\varphi}{2}\left(\ln\Psi_{\mathrm{i}}+\frac{2}{\varphi}\right)\right)^2\right)\right) \qquad \textbf{4-10}$$

Where

$$\Psi_{\mathrm{i}} = \exp\left(\frac{A_i^*}{\beta}\int_{T_0}^{T_f} e^{-E_i/RT}\,dT\right) \qquad \textbf{4-11}$$

Note the subscript *i*, indicates the property relating to the i^{th} component, reacting during each candidate reaction.

Since equation 4-10 is explicit function of temperature, it can be used to simulate a reaction over a specified range of temperature, by specifying the kinetic parameters and heating rate.

The derivative of the curve can be calculated numerically by determining the change in mass fraction between simulated points and the corresponding change in temperature. The derivative is important since, mathematically, the area under the derivative curve is equal to the fraction of mass reacted, and the peak(s) of the first derivative indicate the number of reactions occurring. This information is less important for simulated data since the mass fractions and number of reactions are specified, but is useful for experimental data as the calculated values could be compared to the experimentally determined values. The second derivative is also significant, but will be discussed in section 0.

4.4.2. Determination of Activation Energy, *E*

The unchanged DAEM-based algorithm (which incorporates the first-order reaction model) was used to determine the activation energy of a single simulated RPM reaction. The kinetics were specified as *E=200kJ/mol* and $A^{*}=10E+10s^{-1}.m^{-1}$. Heating rates are now specified lower, at 5k/min and 10K/min, which is more in line with the experimental rates that will be used in the following chapter. The structural parameter used, as mentioned is previously is *φ=0.88.* The plot of the simulated data and the derivative indicating a single reaction occurring is given below in Figure 4.12.

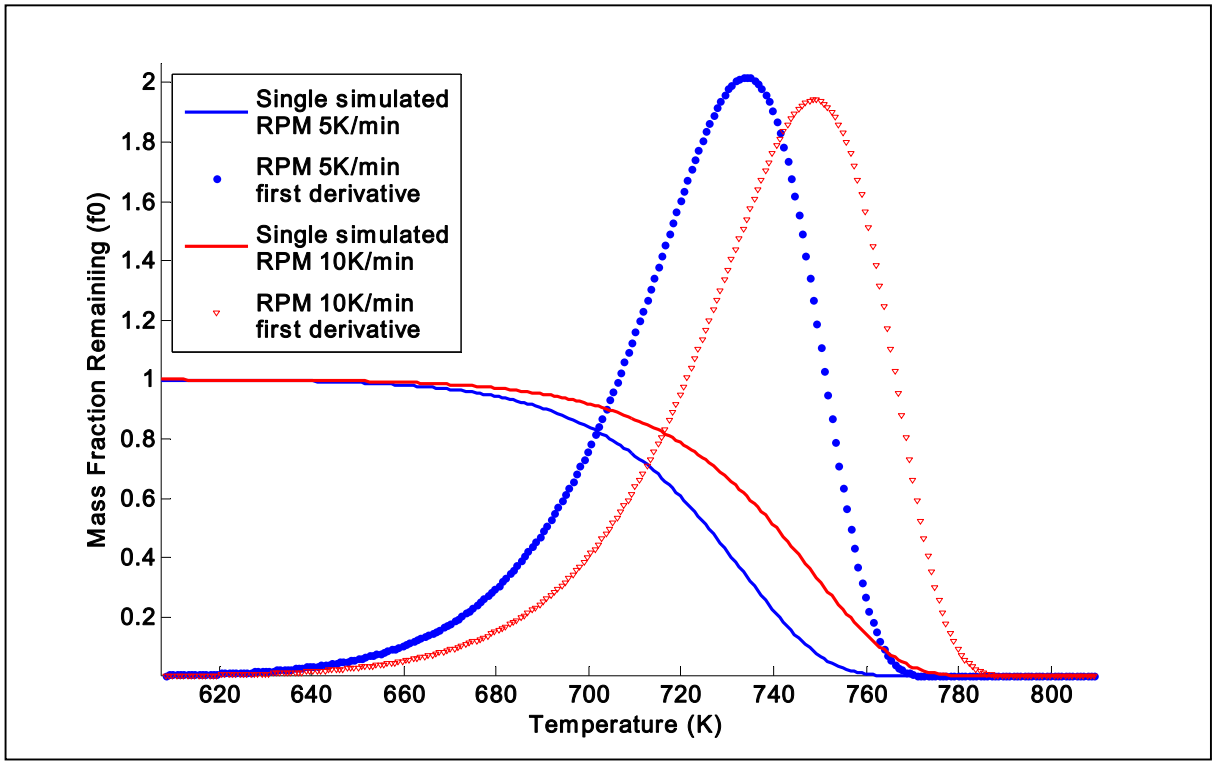

Figure 4.12: Single Simulated Random Pore Model Reaction at 5k/min and 10k/min

This data is again fed to the first-order algorithm which produced the following results, as given in Figure 4.13.

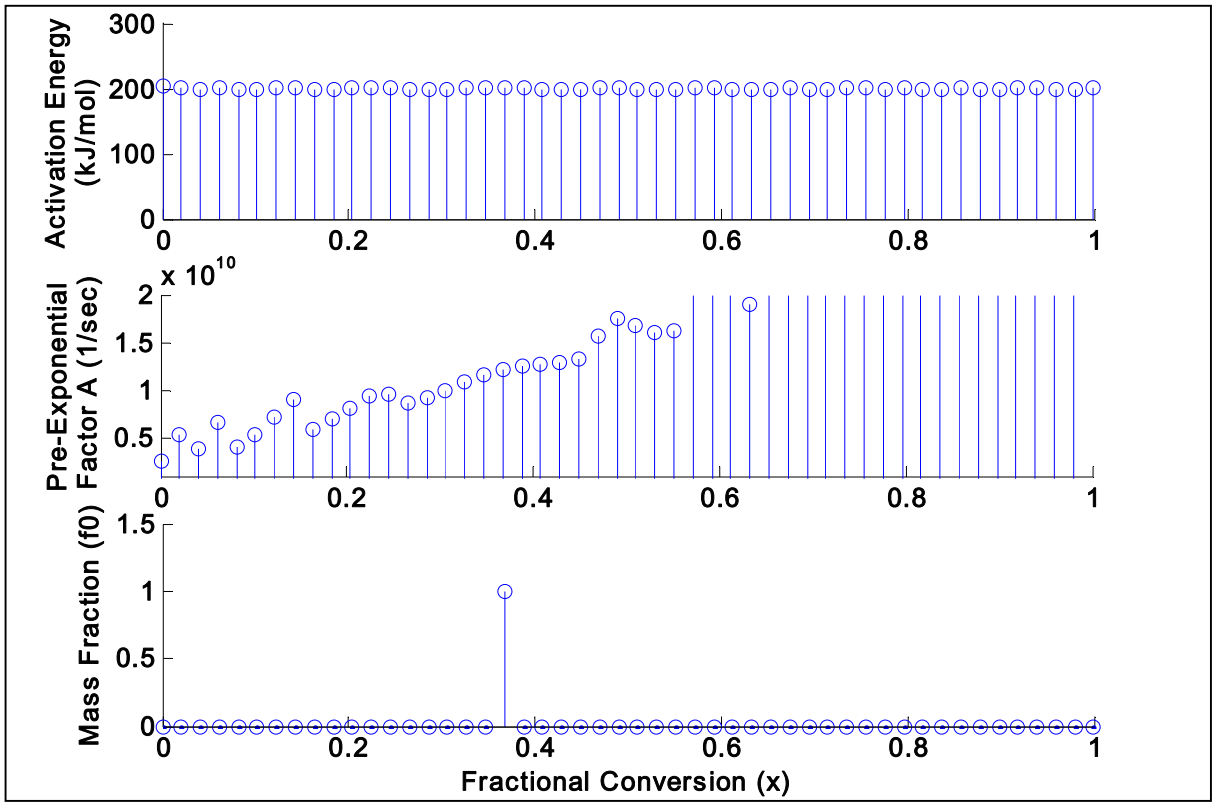

Figure 4.13: Simulated Single RPM Reaction Kinetics Determined using the 1st-order Algorithm

From Figure 4.13, it can be clearly seen that the value of the pre-exponential factor has been over-predicted, while the values of the activation energy and mass fraction found seem to correspond to the values specified during simulation. The values plotted in Figure 4.13 are tabulated and compared to the original specified values in Table 4.5 below.

Table 4.5: Analysis for Simulated Single RPM Reaction Kinetics Determined using the 1st-order Algorithm

	Activation Energy *E* (kJ/mol)	**Pre-Exponential Factor *A* (sec^{-1})**	**Initial Mass Fraction *f0***
Specified Value	200	1E+10	1
Algorithm Derived Value	200.19	1.22E+10	1.0018
Relative Error (%)	<1%	22%	<1%

As observed when processing the shrinking core kinetics, the original first-order algorithm is unable to accurately determine the value of the pre-exponential factor. As a result of this, other methods must be explored to determine the pre-exponential factor accurately.

4.4.3. Determination of the Pre-exponential Factor *A*

Using the Integral Method

The "integral method" is the method where the algorithm-determined pre-exponential factor is neglected, but the other kinetic parameters found are substituted in to the integrated form of the reaction model to calculate the pre-exponential factor directly (Saloojee, 2011). For the RPM, the equation to solve is given as:

$$\int_{x_0}^{x_f} \frac{dx}{(1-x)\sqrt{1-\varphi \ln(1-x)}} = \frac{A^*}{\beta} \int_{T_0}^{T_f} \exp\left(\frac{-E}{RT}\right) dT \qquad \textbf{4-12}$$

Where A^* is again a grouped pre-exponential factor, and the limits of integration go from the initial conversion, $x=0$ to $x_f \approx 1-e^{-1} \approx 0.632$ (Scott et al., 2006). The temperature limits go from the initial temperature, usually 298K, to the temperature T_f corresponding to the specified conversion, at the specified heating rate.

As before the activation energy specified as 200kJ/mol, the specified pre-exponential factor value was $10^{10} s^{-1}.m^{-1}$ and heating rates of 5K/min and 10K/min were specified. The algorithm again found $E=200.19 kJ/mol$. This value was found at the specified first-order conversion of $x \approx 0.632$ and the temperature at this conversion for the 5K/min simulation was $T_f=603.39K$.

All of these values are then substituted into equation 4-14 and A^* is made the subject. The resulting value is $A^*=5.1636 \times 10^9$. This translates to a 48.36% relative error.

This margin of error is far greater than that found when using this approach with the shrinking core model. This result indicates that using the conversion value at maximum decomposition of a first-order reaction is not viable when determining RPM kinetics. The appropriate value for the model being used must be found in order to determine reaction kinetics accurately.

Using the Maximum Rate of Decomposition Assumption

As has been explained, the value of the pre-exponential factor, A^* is calculated using the activation energy found during the first model-free step as well as some assumed value of conversion. For 1st order the assumed value is $x \approx 0{,}368$. This assumed conversion value is also used for multiple reactions. For multiple reactions, this value is adjusted over the specific range of mass fraction represented by each reaction. For example, consider a multiple reaction scenario occurring where each reaction is represented by half the total material mass, such that $f_{0,1}=0.5$, and $f_{0,2}=0.5$. For 1st-order if the first reaction spans the overall x-region of 0 - 0.5, then correct value of A^* will be found at the x which results in a maximum rate of decomposition in that range, which is approximately $x \approx 0{,}368*0.5 \approx 0.184$. The A^* for the second reaction, occurring over the x-region of 0.5 - 1 will be indentified at $x \approx 0.5+(1-0.5)*0.368 \approx 0.684$. Given the effective use of this approach in the previous section, the value of conversion at the maximum rate of decomposition (x_{max}) for a random pore model reaction must be determined, i.e. the value of x that satisfies the following equation, equation 4-14 must be found.

$$\frac{d}{dT}\left[\frac{A^*}{\beta}\exp\left(\frac{-E}{RT}\right)(1-x)\sqrt{1-\varphi\ln(1-x)}\right]=0 \qquad \textbf{4-13}$$

Finding the Maximum Decomposition Rate Conversion Graphically

To avoid the need to find the complex expression for the analytical derivative of the reaction model, or if the analytical derivative cannot be found, the conversion value at the maximum decomposition rate can be determined graphically. The reaction model can be manipulated and used to simulate a reaction and produce reaction data. The numerical derivative of the reaction data can then be used to determine the conversion value at maximum decomposition. Also, finding the *x*-value of the reaction data that corresponds to the maximum conversion value of the first derivative is analogous to finding that which corresponds to the zero-value of the 2nd derivative. This was done graphically. Since these calculations are done using a number of numerical approximations (e.g. numerical integration when simulating the reaction), a sensitivity analysis was conducted to assess how changes in the specified kinetic parameters affect this maximum decomposition conversion value. The graphical approach used is plotted in Figure 4.14 and Figure 4.15 below. The sensitivity analysis results are presented in Table 4.6.

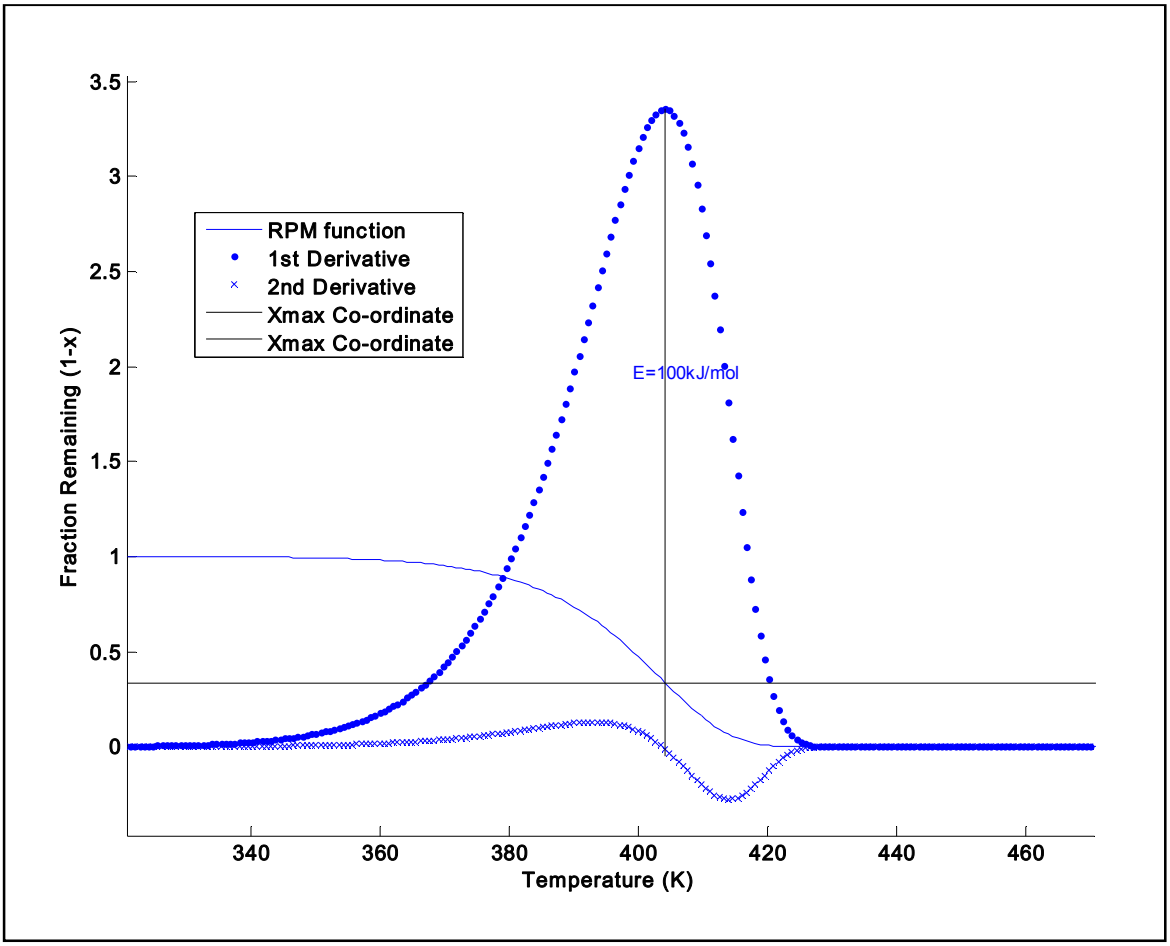

Figure 4.14: Example of Plots used to find x_{max}

Figure 4.14 is an example of the plots used to find x_{max}. The same plot is repeated in Figure 4.15 overleaf for varying activation energy values.

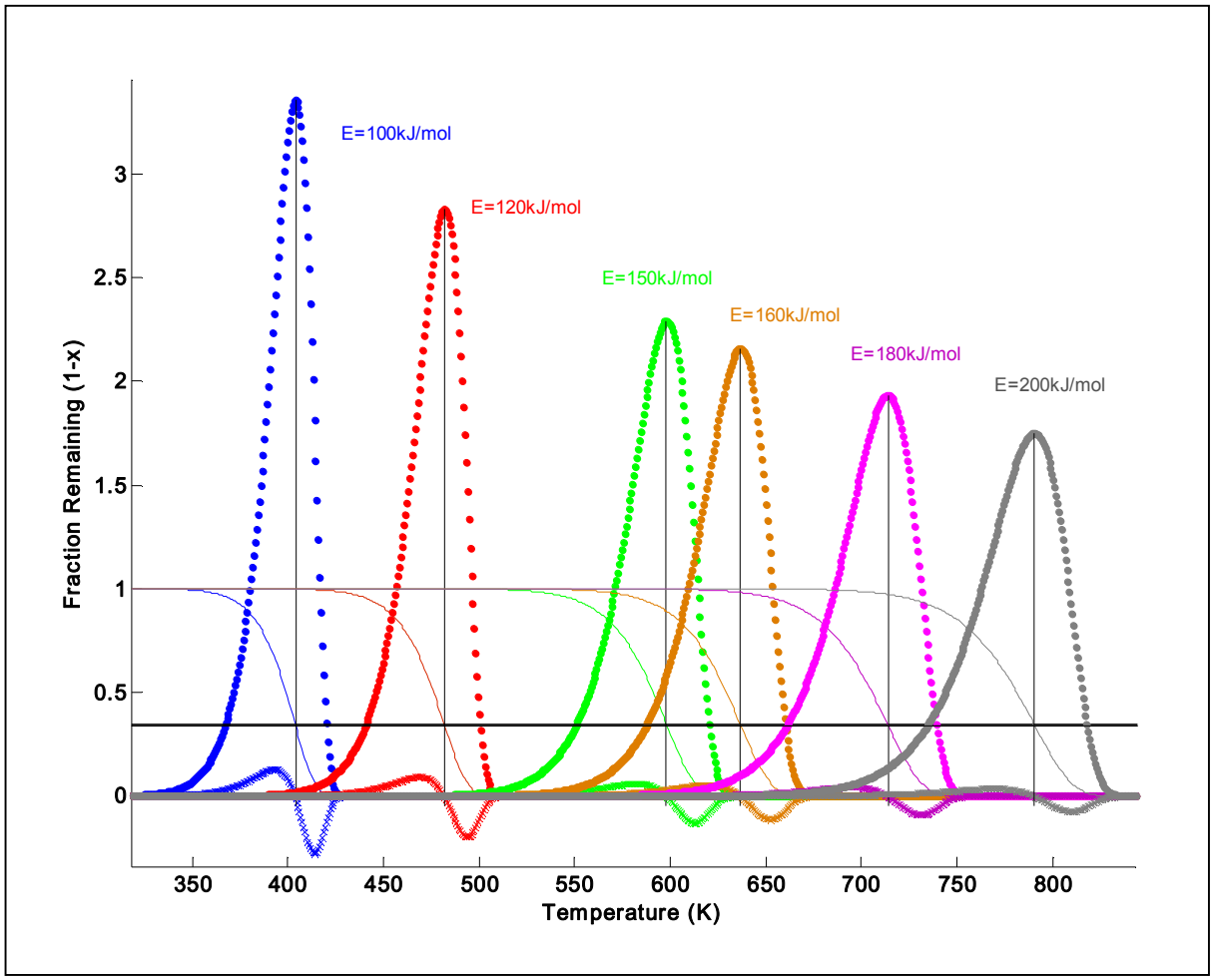

Figure 4.15: Determination of Conversion at Maximum Decomposition for Varying Kinetic Parameters

In Figure 4.15, the solid coloured lines represent the function (integrated RPM) values; the round markers represent the first derivative and the cross markers represent the second derivative for each simulation using a specific activation energy. Each activation energy dataset is plotted in its own colour. The black lines indicate how the value of conversion is found i.e. the function value of *x* corresponding to the maximum point of the first derivative.

The graphical analysis conducted in Figure 4.15 was also done for varying pre-exponential factors and heating rates. From Figure 4.15 it can be seen that the value of *x* found is fairly constant regardless of the change in activation energy. A full sensitivity analysis of all the varying parameters and resultant *x*-values is given in Table 4.6 overleaf.

Table 4.6: Sensitivity Analysis of Graph-Derived x_{max} values

Activation Energy E (kJ/mol)	Pre-exponential Factor A	Heating Rate B (K/min)	Graph-Derived Values		
			X_{max}	T_{max} (K)	
100	1x10^12	100	0.6651	404.2	**Variance**
120	1x10^12	100	0.6555	481.9	1.37E-05
150	1x10^12	100	0.6556	598.2	**Mean**
160	1x10^12	100	0.6548	636.7	0.6556
180	1x10^12	100	0.6579	713.8	**Average**
200	1x10^12	100	0.6544	790.4	*0.6572*
150	**1x10^8**	100	0.6497	834.9	
150	**1x10^10**	100	0.6515	697.6	**Variance**
150	**1x10^11**	100	0.6491	644.0	1.04E-04
150	**1x10^12**	100	0.6556	598.2	**Mean**
150	**1x10^13**	100	0.6646	558.4	0.6601
150	**1x10^15**	100	0.6682	492.1	**Average**
150	**1x10^16**	100	0.6689	464.4	*0.6608*
150	**1x10^18**	100	0.6788	417.4	
150	1x10^12	**1**	0.6553	522.9	**Variance**
150	1x10^12	**10**	0.6646	558.4	2.22E-05
150	1x10^12	**50**	0.6555	585.5	**Mean**
150	1x10^12	**100**	0.6556	598.2	0.6555
150	1x10^12	**150**	0.6596	606.0	**Average**
150	1x10^12	**500**	0.6515	629.5	0.6559
150	1x10^12	**1000**	0.6491	644.0	

It is evident that the average x_{max} value of each range of the parameters is similar, but varies over a greater range than is desirable. The reason for this is that this method finds the maximum value of the derivative from the given data, and not necessarily the true mathematical maximum. The numerical solution to the temperature integral will also result in the x_{max} value varying slightly; an (unattainable) analytical solution to the indeterminate integral would give precise results. The number of simulation points and the temperature range specified during simulation can both affect whether the true maximum derivative value has actually been calculated or whether a point close to the true maximum has been calculated/identified. The average value found overall in the graphical method is x_{max}=*0.6580*. An even more accurate value for x_{max} can however be determined by using the analytical derivative of the reaction model to ensure confidence in the kinetic parameter results determined by the modified algorithm.

Finding the Maximum Decomposition Rate Conversion Analytically

The alternative is to determine the 2nd derivative analytically. The complexity of this approach is encountered when applying the chain rule to the reaction model, since the dx/dT term generated must be represented in the solution by the model expression itself. This results in what can become quite a complex expression, or one that cannot be separated in terms of variables explicitly. Equation 4-14 is the analytical solution to equation 4-13:

$$\frac{\varphi A^{*2}\exp\left(\frac{-2E}{RT}\right)(1-x)}{2\beta^2}-\frac{A^{*2}\exp\left(\frac{-2E}{RT}\right)(1-x)(1-\varphi\ln(1-x))}{\beta^2}$$
$$-\frac{A^{*}E\exp\left(\frac{-E}{RT}\right)(x-1)\sqrt{1-\varphi\ln(1-x)}}{\beta RT^2}=0 \qquad \text{4-14}$$

Equation 4-14 cannot be written explicitly in terms of *x*. The value of x_{max} must therefore be found using an error minimization calculation. The *fzero* function in Matlab® was used to find the zero value of the above expression for the same range of parameters as used in the graphical method. The sensitivity analysis results follow in Table 4.7.

Table 4.7: Sensitivity Analysis of Equation-Derived x_{max} values

Activation Energy E (kJ/mol)	Pre-exponential Factor A	Heating Rate B (K/min)	Equation-Derived Values		
			Xmax	Tmax (K)	
100	1x10^12	100	0.6493	403.7	**Variance**
120	1x10^12	100	0.6496	481.7	2.45E-07
150	1x10^12	100	0.6499	597.9	**Mean**
160	1x10^12	100	0.6501	636.5	0.6500
180	1x10^12	100	0.6504	713.5	**Average**
200	1x10^12	100	0.6508	790.1	0.6500
150	**1x10^8**	100	0.6431	834.4	
150	**1x10^10**	100	0.6497	697.3	**Variance**
150	**1x10^11**	100	0.6486	643.9	1.23E-05
150	**1x10^12**	100	0.6499	597.9	**Mean**
150	**1x10^13**	100	0.6511	557.9	0.6505
150	**1x10^15**	100	0.653	491.7	**Average**
150	**1x10^16**	100	0.6538	464.0	0.6505
150	**1x10^18**	100	0.6551	416.9	
150	**1x10^12**	**1**	0.6521	522.8	**Variance**
150	1x10^12	**10**	0.6511	557.9	1.24E-06
150	1x10^12	**50**	0.6503	585.3	**Mean**
150	1x10^12	**100**	0.6499	597.9	0.6499
150	1x10^12	**150**	0.6497	605.6	**Average**
150	1x10^12	**500**	0.649	629.4	0.6501
150	1x10^12	**1000**	0.6486	643.9	

It can be seen in Table 4.7 that the equation derived values have much smaller variances compared to the results in Table 4.6, and the difference in average x_{max} values between the parameter ranges are also significantly smaller. (Variation in the result is unavoidable since numerical integration is still used to calculate the temperature integral.) The average value found overall is $x_{max}=0.6502$. Given the evident precision of this method compared to the graphical method, this method's value will be used. The graphical method is still useful however if the 2nd derivative of a function cannot be determined.

Unlike in the original algorithm (Scott et al., 2006), the *Ψ-x* relation for the RPM is not *ln(Ψ)=1-x*. This relationship is first-order specific. The value of *ln(Ψ)* must therefore be calculating using equation 4-12, where the right hand side is equivalent to *ln(Ψ)*, and the limits of integration of the left hand side go from *x=0* to $x=x_{max}=0.6502$. This results in *ln(Ψ)=-0.8801.* As opposed to the original first-order value of *ln(Ψ)=-1*. (refer to section 4.4.4 for further explanation of the *Ψ-x* relationship)

To demonstrate the difference between these $ln(\Psi_i)$ values for various models, integrated forms of the reaction model expressions (*g(x)* functions), as well as the determined values of the x_{max} and the corresponding $ln(\Psi_i)$ values are presented below in Table 4.8.

Table 4.8: Comparison of $ln(\Psi_i)$ values for various reaction models using x_{max}

Reaction Model	$\int_{x_0\approx 0}^{x} \frac{dx}{f(x)} = g(x)$	x_{max}	$g(x_{max}) = \ln(\Psi_i)$ For Equation 4-2
First-Order	$\ln(1-x)$	[2] $x_{max} = 1 - e^{-1} \approx 0.6321$	$\ln(\Psi_i) = -1$
Shrinking Core Model (SCM)	$3\left[\sqrt[3]{1-x} - 1\right]$	[3] $x_{max} = 0.6921$	$\ln(\Psi_i) = -2.6921$
Random Pore Model (RPM)	$\frac{2}{\varphi}\left(\sqrt[2]{1-\varphi\ln(1-x)} - 1\right)$	$x_{max} = 0.6502$	$\ln(\Psi_i) = -0.8801$

Pre-exponential Factor Results Using New x_{max}

The pre-exponential factor calculated at every candidate reaction (for the i^{th} component) will now be a RPM-derived value. All that is left for the algorithm to do is to identify the non-spurious result by accurately calculating the initial mass fraction f_0, which corresponds to the correct conversion, temperature, pre-exponential factor and activation energy.

The single RPM reaction simulated previously is again fed to the algorithm to assess whether changing the value of *ln(Ψ)* to a RPM-specific value has enabled the algorithm to accurately determine the kinetic triplet specified in the simulation. The kinetics determined by the modified algorithm are presented in Table 4.9.

Table 4.9: Extract of Algorithm results for all candidate reactions of a single simulated RPM reaction

Initial Fraction f0	Activation Energy E (kJ/mol)	Grouped Pre-exponential factor A ($s^{-1}.m^{-1}$)	Temp at β_1 (K)	Conversion x
1.001862	200.0	1.1813E+10	830.3	0.3673
0	199.9	1.1221E+10	831.6	0.3469
0	199.9	1.0562E+10	832.8	0.3265
0	200.0	1.0228E+10	834.2	0.3061
0	200.1	9.9087E+09	835.5	0.2857

[2] Value obtained from Scott et al. (2006)
[3] Value Determined by finding the maximum decomposition rate conversion graphically

From Table 4.9 it is evident that the algorithm now generates a different set of values for the pre-exponential factor A^* compared to results from the original algorithm, since the values are now model specific. It fails however to identify the correct E-A^* pair by finding the corresponding non-zero mass fraction at the corresponding conversion.

The values of A^* are all closer to the specified value since the value of $ln(\Psi)$ has been amended. However, the algorithm has allocated mass to a candidate reaction with a pre-exponential factor of 1.1813E+10, and not the specified 1E+10. This translates to an 18% relative error. It can be seen however that the following candidate reactions all have results that would be within an acceptable margin of error (±5%). This indicates that the correct kinetics are being calculated, they need only to be correctly identified by the correct f_0 correlating to the "correct" temperature and conversion.

The next and final step in adapting the algorithm to handle RPM reactions is to reassess the way the initial mass fraction, f_0, is determined.

4.4.4. Determination of Mass Fraction Remaining, f_0

The f_0 values for each component i, are calculated using linear least squares. Equation 4-3 is used by specifying an E and A^* value and generating the candidate reactions to populate the matrix $\underline{\Psi}$. This is done with the assumption that at a particular conversion, one reaction will be dominating (Scott et al., 2006). The $\underline{M}$ vector from equation 4-3 is the predetermined mass loss profile of the simulated or experimental reaction. Note that resulting matrix $\underline{\Psi}$ is not a square matrix. Therefore when the $\underline{f}$ vector is calculated using matrix inversion such that $\underline{M}.\ \underline{\Psi}^{-1}=\underline{f}$, there is no exact solution. The least squares (non-negative constraint) function in Matlab (*lsqnonneg*) is therefore used to numerically determine the f_0 elements in the $\underline{f}$ vector that satisfy $\underline{M}.\ \underline{\Psi}^{-1}=\underline{f}$, the manipulated form of equation 4-3.

The modification of the original algorithm (Scott et al., 2006) is needed in the generation of the $\underline{\Psi}$ matrix. The original algorithm uses the first-order identity of Ψ to generate the matrix and subsequently calculate the f_0 values. This is why the f_0 determined in the previous section still relates to the first-order value of x_{max}. In calculation of the matrix $\underline{\Psi}$, the RPM specific equivalent of the Ψ expression must be used. Equation 4-9 equates $g(x)$ to the temperature integral such that:

$$g(x) = \ln(\Psi) \qquad \textbf{4-15}$$

Therefore,

$$\Psi = e^{g(x)} = \exp\left(\frac{2}{\varphi}\left(\sqrt{1-\varphi\, ln(1-x)}-1\right)\right) \qquad \textbf{4-16}$$

Whereas, for first-order:

$$\Psi = e^{g(x)} = \exp\,(1-x) \qquad \textbf{4-17}$$

Equation 4-16 is used to calculate the matrix $\underline{\Psi}$ which is then used in the *lsqnonneg* algorithm in Matlab® to do the matrix inversion and generate the vector $\underline{f}$.

After this change has been made, the RPM reaction simulation used in previous sections is again fed to the algorithm to assess whether it is able to accurately identify the complete kinetic triplet. The original single RPM reactions simulated at heating rates of 5 and 10 K/min, as well as the simulation using the algorithm derived kinetics is presented in Figure 4.16.

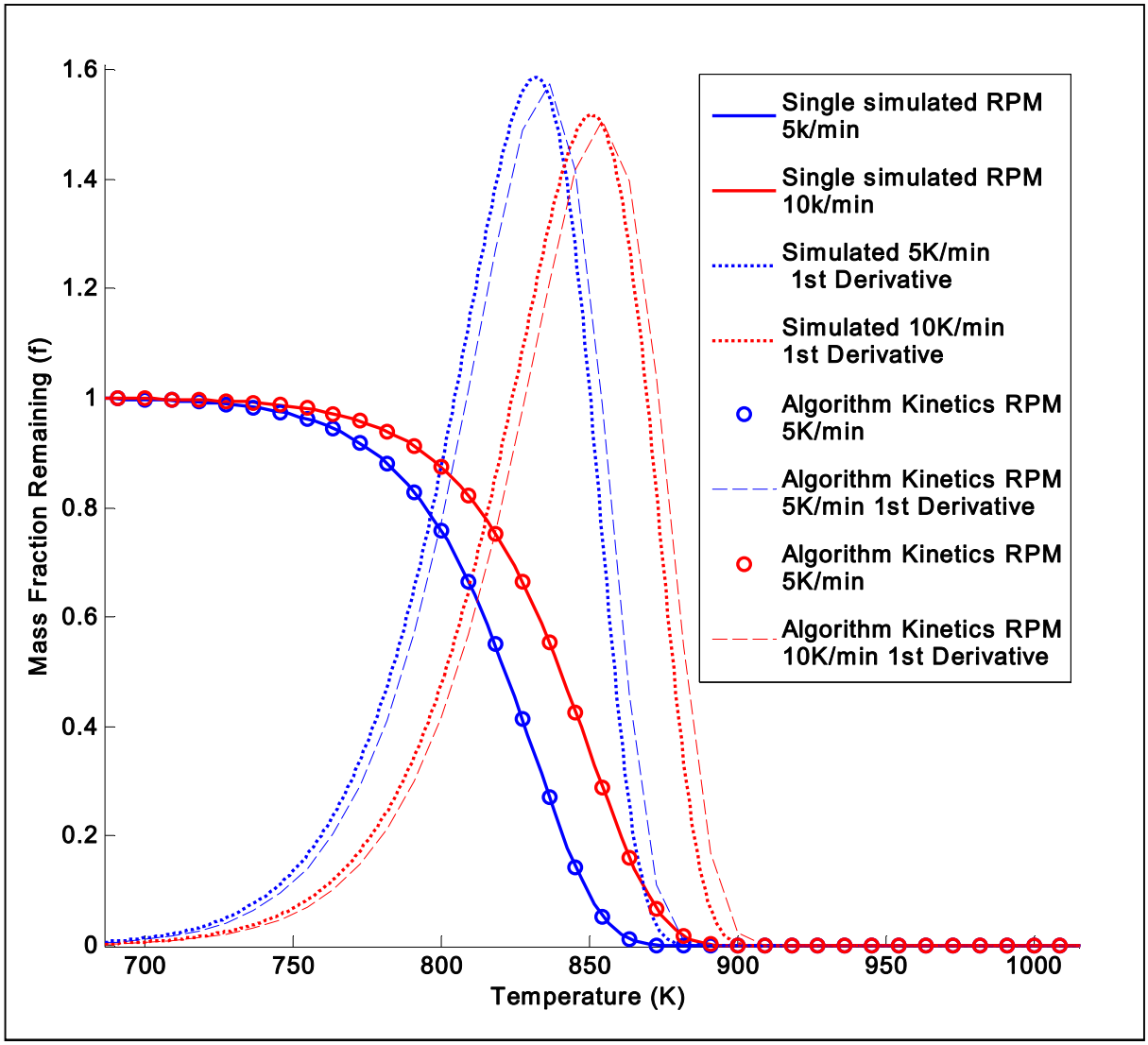

Figure 4.16: Single Simulated RPM reactions and 1st Derivatives at 5K/min and 10K/min With RPM Algorithm-derived Kinetics Simulations Overlaid

As can be seen in Figure 4.16, the reaction behaviour of the original kinetic parameters and that of the algorithm-derived kinetics correlate very closely, throughout the entire range of conversion. The deviations in the derivatives are slight. These are expected since the derivative is very sensitive to the values of the kinetics. The slight deviation indicates that while the kinetic parameter values determined are very close to those originally specified, they have not been determined exactly. The algorithm results for each candidate reaction follow in Figure 4.17. The error analysis of the kinetic parameter values found is presented in Table 4.10.

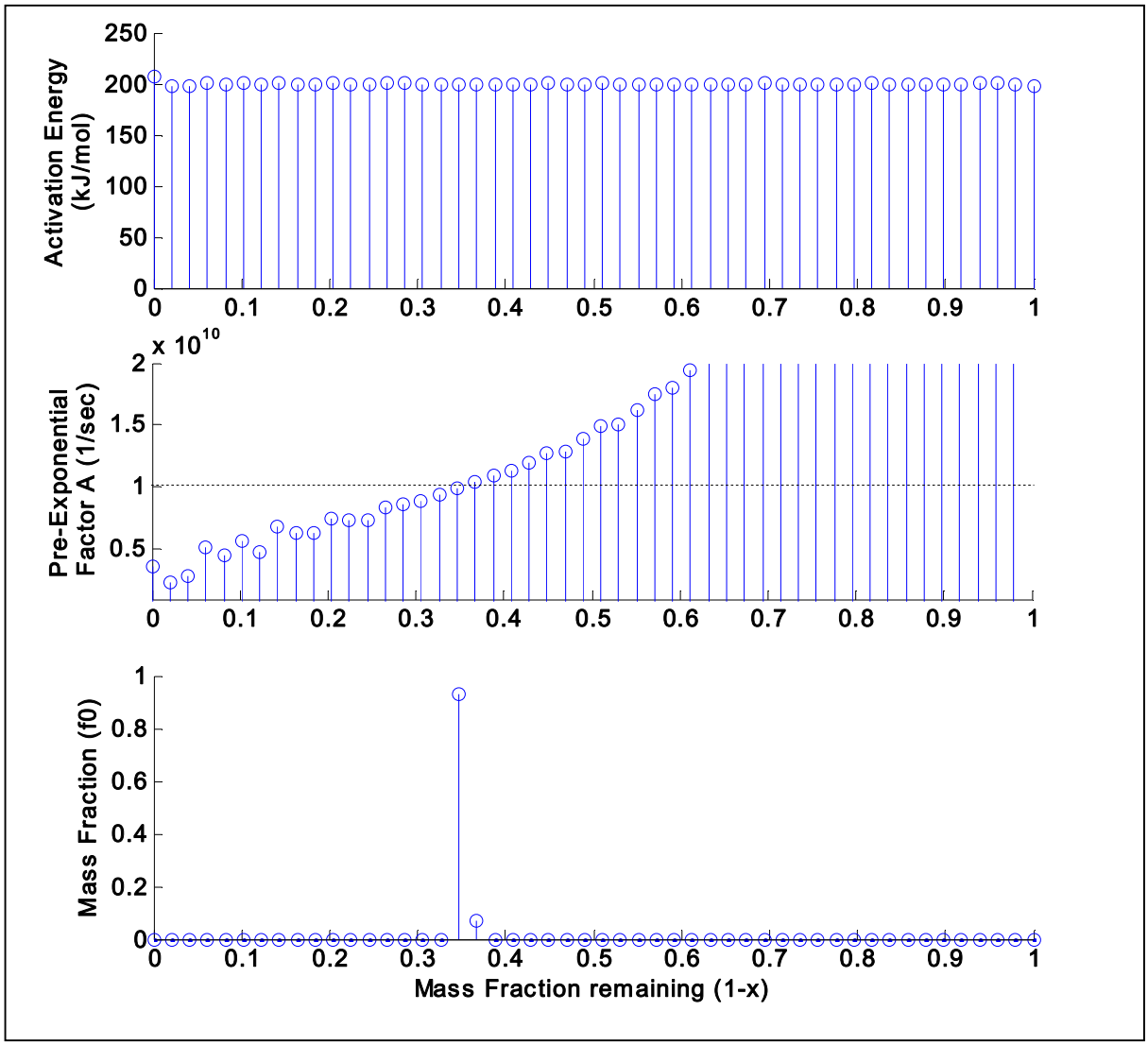

Figure 4.17: Stem Plots of Activation energy, Pre-exponential Factors and initial mass fraction results from the RPM modified Algorithm

Figure 4.17 shows how the algorithm has identified the correct kinetic parameter values by 'assigning' a non-zero mass fraction to it, and negating all others.

Table 4.10: Comparison between Specified and Algorithm Derived Kinetic Parameters for a single simulated RPM reaction

	Activation Energy *E* (kJ/mol)	**Pre-Exponential Factor A^* (sec^{-1})**	**Initial Mass Fraction *f0***
Specified Value	200	1E+10	1
Algorithm Derived Value	200.05	1. 02E+10	0.9995
Relative Error (%)	<1%	2%	<1%

Activation energy and mass fraction values found are almost exact while the pre-exponential factor is found with a desirably low error of only 2%. The results in Table 4.10 show that the algorithm is now capable of accurately determining the kinetics of a simulated RPM reaction.

4.4.5. Application of the Successfully Modified Algorithm

Having shown the capability of the modified algorithm to determine the kinetics of a single RPM reaction, other scenarios must also be simulated and analysed.

Multiple RPM Reactions

The following simulation will include multiple RPM. Reactions with close activation energy values will be chosen to determine whether the algorithm is able to identify each individual reaction. E_1, E_2, and E_3 were specified as 120kJ/mol, 135kJ/mol and 200kJ/mol respectively. A^*_1, A^*_2, A^*_3 were specified as 1E+10, 1E+9, and 1E+9, respectively. The mass fractions f_1, f_2, f_3 were specified respectively as 0.3, 0.5 and 0.2. The structural parameter value used is φ=0.88. Figure 4.18 is a plot of the simulation.

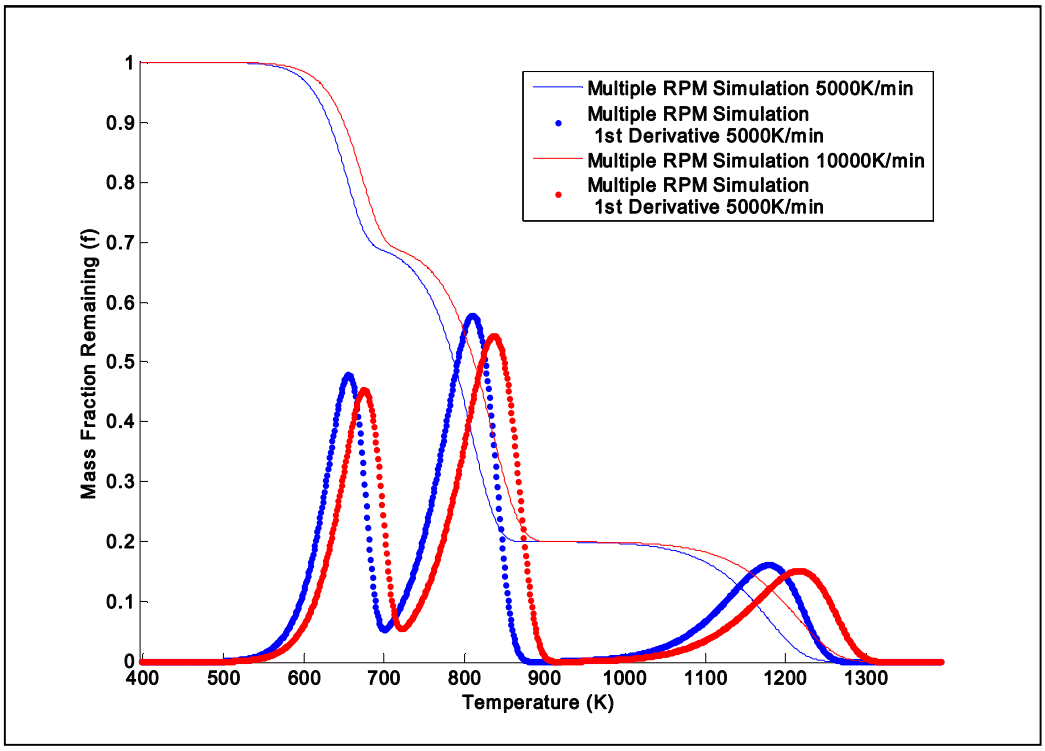

Figure 4.18: Multiple RPM Reaction Simulation At high Heating Rates

The reactions were simulated at very high heating rates to indicate that the algorithm is able to process high heating rates which are not uncommon in practice. It can be seen that the first two reactions are close together and seem to shoulder each other, but the derivatives have also been included to clearly identify each distinct reaction. Table 4.11, which follows, compares the algorithm-derived and specified kinetic values. Table 4.11 indicates that the modified algorithm is able to identify and accurately predict the kinetics of multiple reactions. All relative error is within an acceptable and desired margin of error of 5% between the specified and determined kinetics. Beyond this limit, deviations between the plots of the algorithm based data and original data become too apparent. It must be noted that the algorithm manages to accurately determine the kinetics not only at low heating rates, usually related to lab-scale experimentation, but also at high heating rates, akin to large scale reactions.

Table 4.11: Kinetics Data Analysis for Multiple Simulated RPM Reactions

Algorithm-Determined *f0*	Algorithm-Determined *f0 (summed)*	Specified *f0*	Relative Error (%)
0.0954	0.3000	0.3	**0.01%**
0.2046			
0.1832	0.5000	0.5	**0.01%**
0.3168			
0.0849	0.2001	0.2	**0.03%**
0.1152			
Algorithm-Determined *E (kJ/mol)*	**Algorithm-Determined *E (kJ/mol) (summed)***	**Specified *E (kJ/mol)***	**Relative Error (%)**
120.31	120.28	120	**0.24%**
120.27			
135.02	134.99	135	**0.01%**
134.98			
199.99	200.00	200	**0.00%**
200.01			
Algorithm-Determined *A(1/sec)*	**Algorithm-Determined *A (1/sec) (summed)***	**Specified *A(1/sec)***	**Relative Error (%)**
1.2E+10	1.06E+10	1E+10	**5.96%**
1.0E+10			
1.1E+09	1.00E+09	1E+09	**0.03%**
9.6E+08			
1.1E+09	1.01E+09	1E+09	**0.75%**
9.0E+08			

4.5. General Adaptation of the Original Algorithm to use Any Structural Model

Following the approach used to adapt the algorithm to process RPM simulations, the algorithm can be modified to almost any known structural reaction model, provided the conversion and temperature variables are separable, and that the inverse of the conversion function can be integrated. It has been demonstrated that for 3 different reaction models, the algorithm was able to accurately predict the activation energy value specified in simulation with high accuracy without the need for any modification to the original algorithm. Then, two fairly simple steps must be applied to convert the rest of the algorithm to accurately determine the remaining two parameters of the desired kinetic triplet. Firstly the x_{max} value for the given model must be found. This should be done analytically, but can also be done graphically if the 2nd derivative of the function cannot be found explicitly or if the x_{max} value cannot be easily determined from the analytical expression. Then, the expression used to calculate the elements of, and populate the matrix $\underline{\Psi}$ must be rewritten to be model specific so that the f_0 will correctly identify the non-spurious reaction parameters among all values found for the candidate reactions.

More specifically, the algorithm uses the model-free temperature integral to find a value of E at each candidate reaction, evenly spaced along the full range of conversion. The algorithm then uses the assumed value of conversion in equation 4-2 to find a value of A^* at each

candidate reaction along the full range of conversion. In the final step (the matrix inversion) f_0 will only be non-zero at the point where x equals that specified in equation 4-2 i.e. where $x=x_{max}$. Hence, for models other than the 1st order model, the model specific value of ln(ψ) must be determined to calculate the correct value of A^*. Furthermore, the expression used to calculate f_0 must also be model specific so that when the parameters, namely E, A^*, x, and T are substituted into it, it corresponds to the values obtained when calculating A^* with the model-specific value of ln(ψ) found using the x_{max} value.

A schematic similar to Figure 4.1 is presented in Figure 4.19 which illustrates the steps needed to adapt the algorithm for use with other structural models.

Step 1
Collect Mass loss vs. Temperature data for at least 2 different constant heating rates (collect via experimentation or simulation)

Step 2
Choose *n* values of conversion. This is the number of equally spaced points over the range at which the activation energy and pre-exponential factor for each component *i* will be evaluated.

Step 3
Propose a reaction model (Or use the reaction model used for the simulation) and find the value of conversion at which the reaction reaches a maximum rate of decomposition. Find the corresponding value for Ψ_i from the model-dependent equivalent of the $\ln(\Psi_i)$ expression

Step 4
Using the expanded form of the equation

$$\Psi_i(B_1, T_1) = \Psi_i(B_2, T_2)$$

Find activation energy values for each component *i*. This is model independent.

Step 5
The value found in step 3 influences the value of the pre-exponential Factor. Using this value, and the known E_i the following can be solve for A_i

$$\ln \Psi_i = \left[T_0 exp\left(\frac{-E_i}{RT_0}\right) - \frac{E_i}{R}\int_{-E_i/RT_0}^{\infty} \frac{\exp(-u)}{u} du - T_1 exp\left(\frac{-E_i}{RT_1}\right) + \frac{E_i}{R}\int_{-E_i/RT_1}^{\infty} \frac{\exp(-u)}{u} du \right]$$

Step 6
Then, using the set of *n* reactions each with its own E and A value, find each reaction's initial mass fraction f_0 using matrix inversion in

$$\underline{M} = \underline{\Psi}.\underline{f}$$

The equation used to find each element of f_0 must be model-dependent. Non-zero mass fractions corresponding to E and A values found for each reaction indicate which values are to be used.

Figure 4.19: Schematic of Generalised Adaptation of Original DAEM-Based Algorithm

4.6. Extension of the Model to Simulate and Analyse Isothermal Data

Following the approach outlined above, the RPM adapted algorithm was further modified to process isothermal data. The equations presented overleaf show the time-based integration and mathematic manipulation of the RPM and of the Ψ identity in order to simulate and determine the kinetics of isothermal RPM reactions.

Firstly, the RPM is rewritten and integrated with respect to time:

$$g(x) = \frac{2}{\varphi}\left(\sqrt{1-\varphi\ln(1-x)}-1\right) = \frac{A^*}{\beta}\int_{t_0}^{t}\exp\left(\frac{-E}{RT}\right)dt = \ln\left(\Psi_t(t)\right) \qquad \textbf{4-18}$$

It can be noted that since the temperature and activation energy are now kept the constant, the right hand side of 4-18 is no longer an indeterminate integral. Then, simplifying as was done in equation 4-10 and making the fraction remaining (*f*) the subject:

$$f = 1 - x = exp\left(\frac{1}{\varphi}\left(1-\left(\frac{\varphi}{2}A^*\exp\left(\frac{-E}{RT}\right)t+1\right)^2\right)\right) \qquad \textbf{4-19}$$

This expression applies for when $t_0=0$, which is often the case when processing isothermal data. If not, the *t* term must be replaced by $(t- t_0)$.

Then, the Ψ_t expression must be re-evaluated in terms of time:

$$\Psi_{t,i} = \exp\left(\frac{A_i^*}{\beta}\int_{t_0}^{t_f} e^{-E_i/RT}\,dt\right) \qquad \textbf{4-20}$$

This expression will be used in the algorithm in the same way that equations 4-1 and 4-2 are used in the original algorithm. As in equation 4-2, the grouped pre-exponential factor, A^* will be determined according to the following expression:

$$A_i^* = \ln\left(\Psi_{t,i}(t)\right) / \exp\left(\frac{-E_i}{RT}\right).t \qquad \textbf{4-21}$$

Where the $\ln(\Psi_i)$ value must be determined from the model-specific equivalent of equation 4-20, which will be a function of *x*.

Figure 4.20 overleaf shows the isothermal simulations of a single RPM reaction at 850K and 900K. The kinetic parameters used were: $E=200kJ/mol$, $A=1E+10s^{-1}.m^{-1}$ and $\varphi\approx0.88$.

It can be seen that the derivative of the curves do not go through a maximum at some point within the range; the only maximum is at $t=0$. This rules out the possibility of finding the value of x_{max} graphically. To overcome this, the algorithm was run, and the *E* and A^* values specified in the simulation were hardcoded so that every candidate reaction was given the precise kinetic values to calculate the initial mass fraction f_0. The value of *x* which corresponded to the non-zero value of f_0 found by the algorithm was then used to determine the value of $ln(\Psi_t)$. This value was then substituted back into the calculation of A^*. The hardcoded parameters were then removed, and the kinetics recalculated to assess the efficacy of the algorithm. This method of determining the x_{max} value in order to find a model-specific $\ln(\Psi_i(t))$ (used to calculate A^*) was repeated for various *E* and A^* values. It was found that a consistent value of $\ln(\Psi_i(t))\approx0.9090$ was calculated regardless of the kinetic parameters specified. (A similar method was applied to finding the $\ln(\Psi_i(t))$ value for the shrinking core model. It was found to be $\ln(\Psi_i(t))=0.2312$, and also produced accurate factor values)

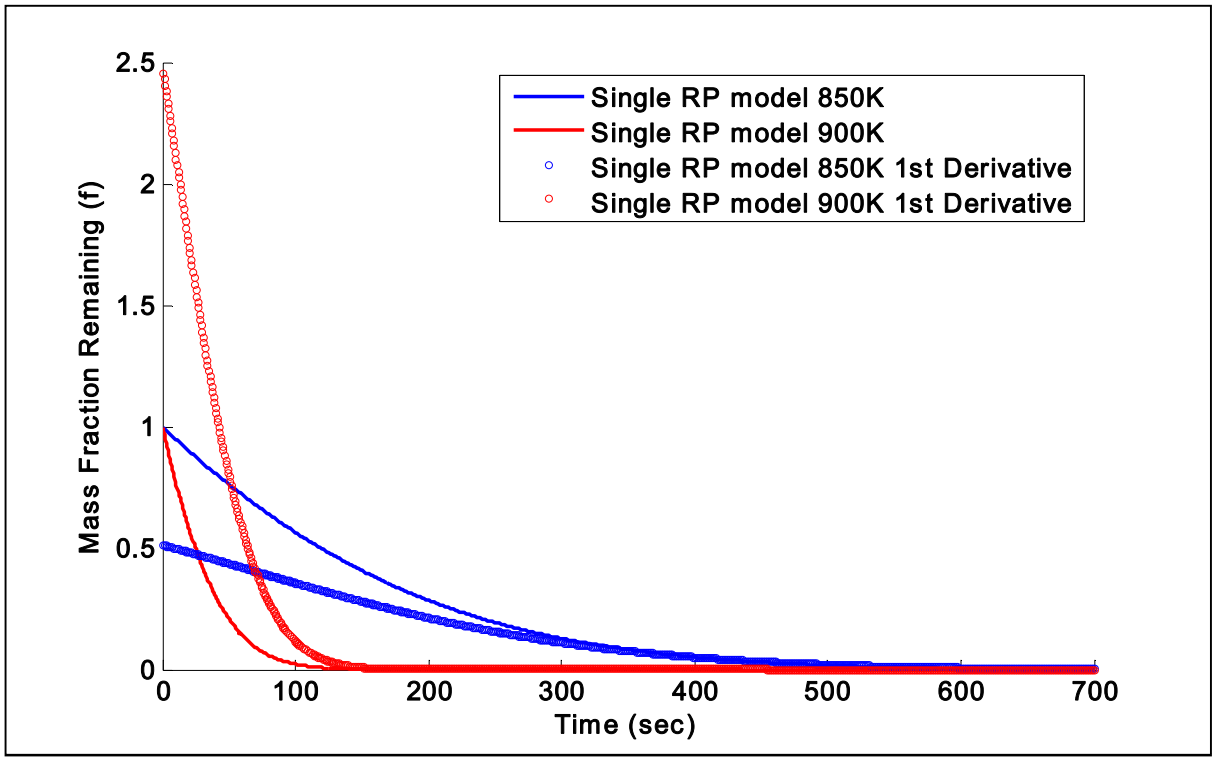

Figure 4.20: Single Simulated Isothermal RPM Reaction at Different Temperatures

Note that the higher temperature simulation reaches completion before the lower temperature, unlike the behaviour observed with non-isothermal reactions. The non-isothermal reactions with higher heating rates tend to reach completion at higher temperatures than lower heating rate reactions. The specified kinetic parameters and the kinetics found by the algorithm are presented and compared in Figure 4.21. The complete results of RPM modified isothermal algorithm for all candidate reactions is presented in the stems plots in Table 4.12.

Table 4.12: Error Analysis Of Kinetics Determined for Single Simulated Isothermal RPM Reaction

	Activation Energy *E* (kJ/mol)	**Pre-Exponential Factor A^* (sec^{-1})**	**Initial Mass Fraction f_0**
Specified Value	200	$1*10^{10}$	1
Algorithm Derived Value	199.92	9.857E+9	1.0001
Relative Error (%)	<1%	1.43%	<1%

Table 4.12 shows that the algorithm is still able to determine the desired kinetic parameters with high accuracy. These results also ratify the method used to determine the value of $\ln(\Psi_i(t))$ used to find A^*.

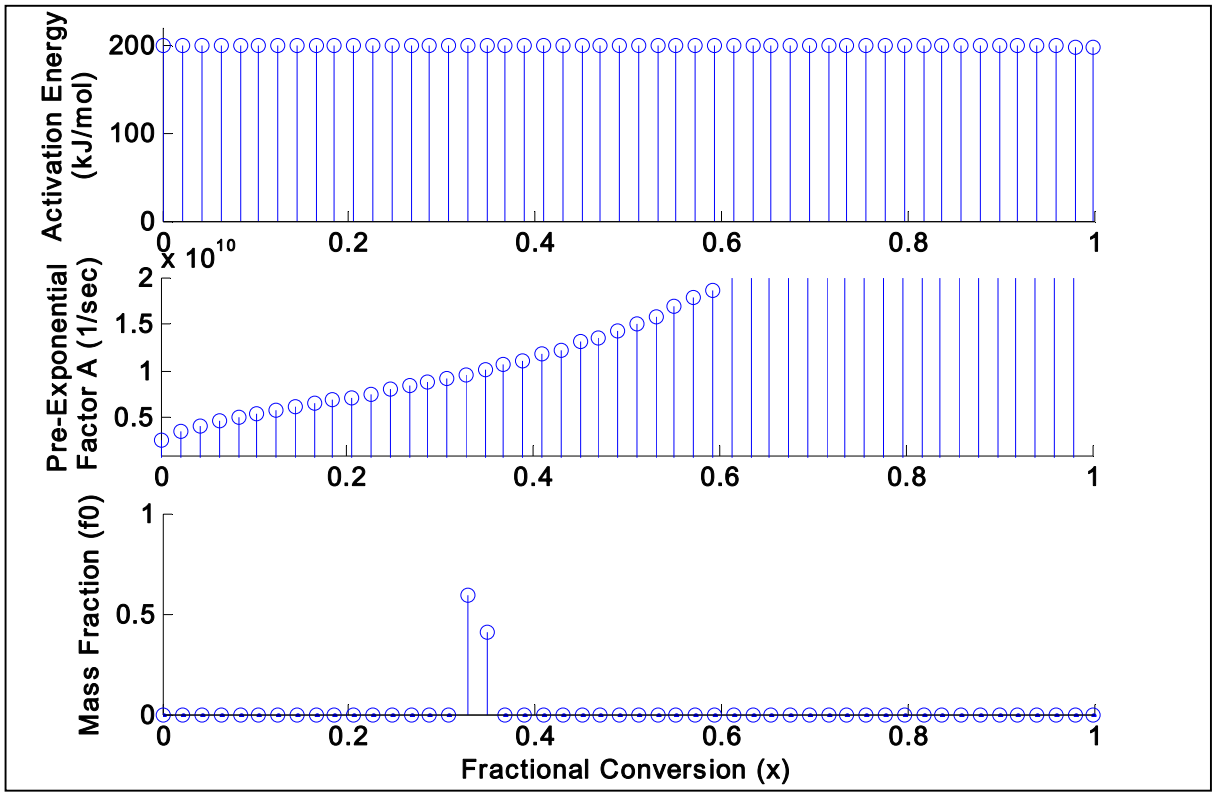

Figure 4.21: Kinetic Parameter Results for an Isothermal RPM Simulation

It can be seen in Figure 4.21 that the activation energy values for all the candidate reactions has again be found with a great degree of precision and accuracy. The algorithm has determined that all the mass is allocated to two adjacent candidate reactions and has identified a pre-exponential factor value close to that specified in simulation.

As an additional assessment of the accuracy of the isothermal algorithm results, a third higher temperature simulation was run. The original kinetics as well as the algorithm-determined kinetics were both used to simulate an RPM reaction at the same temperature (1000K). The datasets are presented in Figure 4.22 overleaf.

The simulated data presented in Figure 4.22 was not used in any way in the determination of the kinetics. As can be seen, the algorithm-determined kinetics simulation correlates very well with the specified kinetics simulation. The derivative data shows a very close correlation as well. This result reaffirms the accuracy with which the algorithm is able to predict reaction kinetics as well as predict the reaction behaviour under different conditions using the kinetics found.

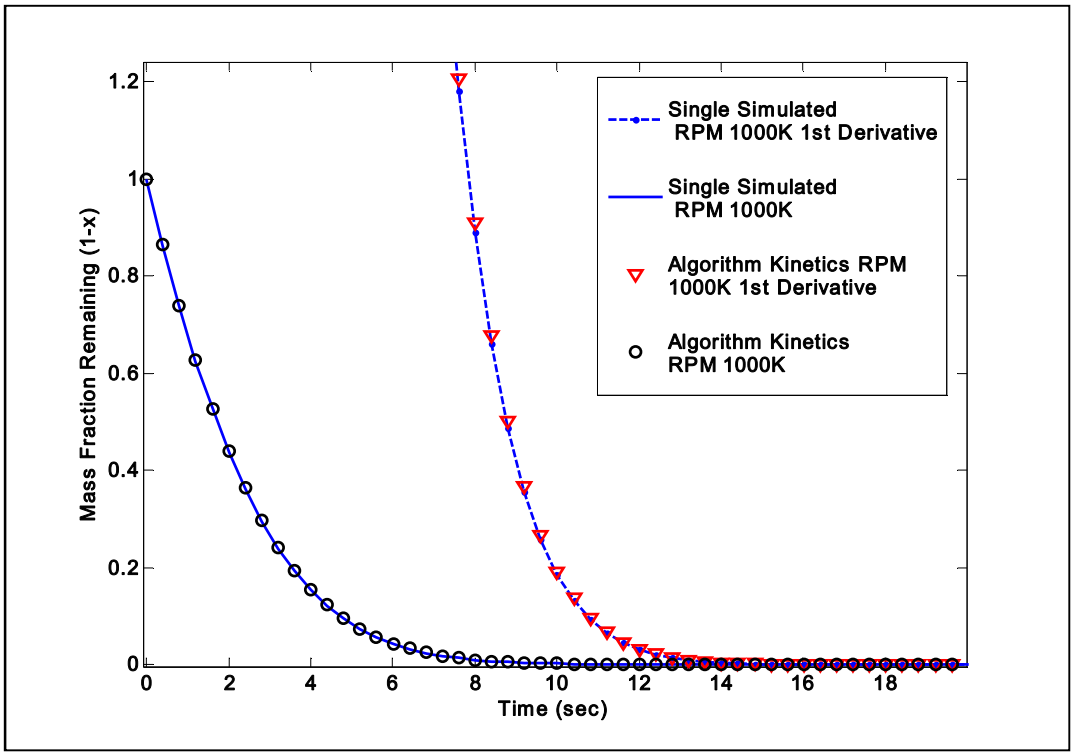

Figure 4.22: Single RPM reaction simulated using specified and algorithm-derived kinetics

4.7. Conclusion

The development in this chapter has shown that the DAEM-Based algorithm (Scott et al., 2006) can be adapted to various other situations. This development has also illustrated a method to adapt the original algorithm to be used in conjunction with almost any known structural model. This can be done by following two relatively uncomplicated steps. The steps required were applied to the shrinking core model and are presented in Table 4.8. This table contains the manipulated x(T) functions required to simulate curves, and for substitution into the parts of the algorithm that are model-dependent. The x_{max} values are also presented, for 1st-order, shrinking core and random pore models. Even once modified, a high level accuracy is achieved when processing simulated data, as was done with the original algorithm.

Another important finding is the ability of this DAEM-based algorithm to process multiple reaction simulations for reaction models other than first order. This is significant since many other well-established kinetics determination methods that use the RPM use a single reaction assumption. Where multiple reactions are occurring, an algorithm capable of processing multiple reactions will prove significantly more accurate than other established methods.

The specific adaptation of the algorithm to incorporate the RPM to process simulated char-CO_2 reactivity has been found to give accurate results for both non-isothermal and isothermal simulations. This result suggests that experimental data will be processed with a good level of accuracy, if the reactions indeed adhere to the RPM. The next assessment of the algorithm is therefore to determine its efficacy when processing experimental data.

Chapter 5: Experimental Results: Char Reactivity

5.1. Introduction

This chapter presents the experimental data produced by means of thermogravimetric analysis as well as data captured from other research. Firstly, the statistical methods used to fit the data and evaluate the quality of fit will be explained. Then, the modified algorithm, shown to be effective in processing simulated CO_2-Char reaction(s) (under both isothermal and non-isothermal conditions) is used on experimental data to determine the reaction kinetics of the materials being studied. Two sets of plain coal data are evaluated: that of Sangtong-Ngam and Narasingha (2008), as well as new reactivity data produced for this study. The new data conducted in this study includes non-isothermal as well as isothermal data. Next, the algorithm is applied to chars from coal-biomass blends, and the kinetics compared to determine whether such blends result in synergistic interactions and improved reactivity of the South African coal and the biomass. (Note that all Matlab® coding written to complete the simulations and calculations discussed and presented in this chapter are presented in Appendix C.)

5.2. Statistical Methods for Fitting Data and Assessing Quality of Fit

When using simulated data, the evaluation of the accuracy of the algorithm was done by comparing the specified kinetic parameters to those produced by the algorithm. This is inherently possible because the kinetics are known during a simulation. However, this is not the case when processing experimental data. In this chapter, a regression analysis will be used to determine the quality of fit of the model to the experimental data.

5.2.1. Correlation Coefficient

The regression tool be used for this analysis is the R^2 statistic, also known as 'the coefficient of multiple determination' or the "correlation coefficient" which measures the proportion of the total variation about the mean value of data (Draper and Smith, 1981). The following equation gives the expression for the R^2 statistic (GraphPad Software Inc, 1999) written in the notation found in Draper & Smith (1981):

$$R^2 = 1 - \frac{\sum(Y_i - \hat{Y}_i)^2}{\sum(Y_i - \bar{Y})^2} \qquad \textbf{5-1}$$

Where $\hat{Y}_i$ is the model-predicted dependent variable value, Y_i is the observed (experimental) dependent variable value and $\bar{Y}$ is the mean of the experimental values.

The value of R^2 is $0<R^2<1$ where $R^2=1$ denotes that there is no error in the fitted data, i.e. the fit is perfect; and $R^2=0$ denoted that the model proposed approximates the experimental data only as well as a straight line through the mean of experimental points. An acceptable value of R^2 is relative to the variance of the data being analysed, and for this application, a

significantly high degree accuracy is desired i.e. the model should estimate most, if not all the observed points accurately; Hence, R^2 values close to unity are regarded as good fits.

The R^2 value will be calculated between the observed values of a third experimental run (not used during the kinetics determination calculations), and the values generated by simulating a reaction at the experimental heating rate (or temperature), using the intrinsic kinetics found by the algorithm.

5.2.2. Calculation of the Structural Parameter *φ*

Another key factor when dealing with the random pore model in particular is the structural parameter, *φ*. While this parameter value is specified during simulation, it must be measured from experimental data, or used as a characterisation parameter to fit the data. The former approach can be achieved by measuring pore structure using mercury porosimetry, pycnometry, and measuring nitrogen and CO_2 adsorption at various temperatures (Su and Perlmutter, 1985). These methods produce all the physical dimensions and measurements required to physically calculate the structural parameter, *φ*. However, the same research reports that there is good agreement in the value of the parameter when calculating it experimentally and where *φ* is found using regression analysis. This study as well as other studies (Bhatia and Vartak, 1996; Everson et al., 2006) suggest that it is best to find the structural parameter via regression analysis to avoid the need for lengthy experimental procedures, as well to ensure improved accuracy and reliability of the kinetics results.

Many effective methods have been proposed to find the structural parameter value numerically. Everson et al. (2008) notes that many researchers estimate the value using the maximum rate of reaction. This approach is heavily dependent on the numerical accuracy in determining the maxima. Everson et al. (2008) goes on to develop an effective means of calculating *φ* using regression analysis on isothermal data, which was found to be effective and accurate. In this research, *φ* will be used as a characterisation parameter but will be calculated primarily using non-isothermal data. A least squares regression method will be used where the parameter is varied until the square root of the mean squared deviation is minimised (Sangtong-Ngam and Narasingha, 2008). This approach is characterised by equation 5-2:

$$\sigma = \sqrt{\frac{err_1^2 + \cdots + err_n^2}{n}} \qquad \textbf{5-2}$$

Where err_1 is the error between the calculated and experimental data at point *1*, and err_n is the error between the calculated and experimental data at point *n*, and *n* is the number of points in the data set. The *fminbnd* algorithm in Matlab (Matlab R14, The Mathworks Inc.) is used to vary the value of *φ* within a predetermined range until *σ* is minimised. The quality of fit is then assessed by evaluation of the R-Squared parameter explained above.

5.3. Thai Lignite Char Oxidation

Sangtong-Ngam and Narasingha (2008) present research using thermogravimetric analysis in which Thai-lignite was charred under various conditions and reacted in oxygen. Although the use of oxygen generally results in combustion, the reactivity is described as gasification in this work and the RPM (rather than a core model) is used to fit the data; the first-order or 'homogenous' model is also used and the fits compared.

Sangtong-Ngam and Narasingha (2008) fitted the char-O_2 reaction data with the RPM, using the structural factor φ as a characterisation parameter for the regression analysis. It was assumed that a single reaction was occurring. The RPM was found to fit the data well, and with much greater accuracy than the homogenous reaction model (Sangtong-Ngam and Narasingha, 2008). In this section, a comparison between the accuracy of fit obtained when assuming a single reaction versus the assumption of multiple reactions is conducted, given the same data and reaction model.

The data presented in this work for Char A was captured graphically in Matlab ® (Matlab R14, The Mathworks Inc.) using the *ginput* command. The data points were interpolated using the *spline* function, which results in a fairly smooth curve, but a fairly 'noisy' derivative. The derivative is still useful however in determining roughly whether one or multiple reactions are occurring, even when the mass-loss curve seems to represent only one reaction. The data is presented below in Figure 5.1.

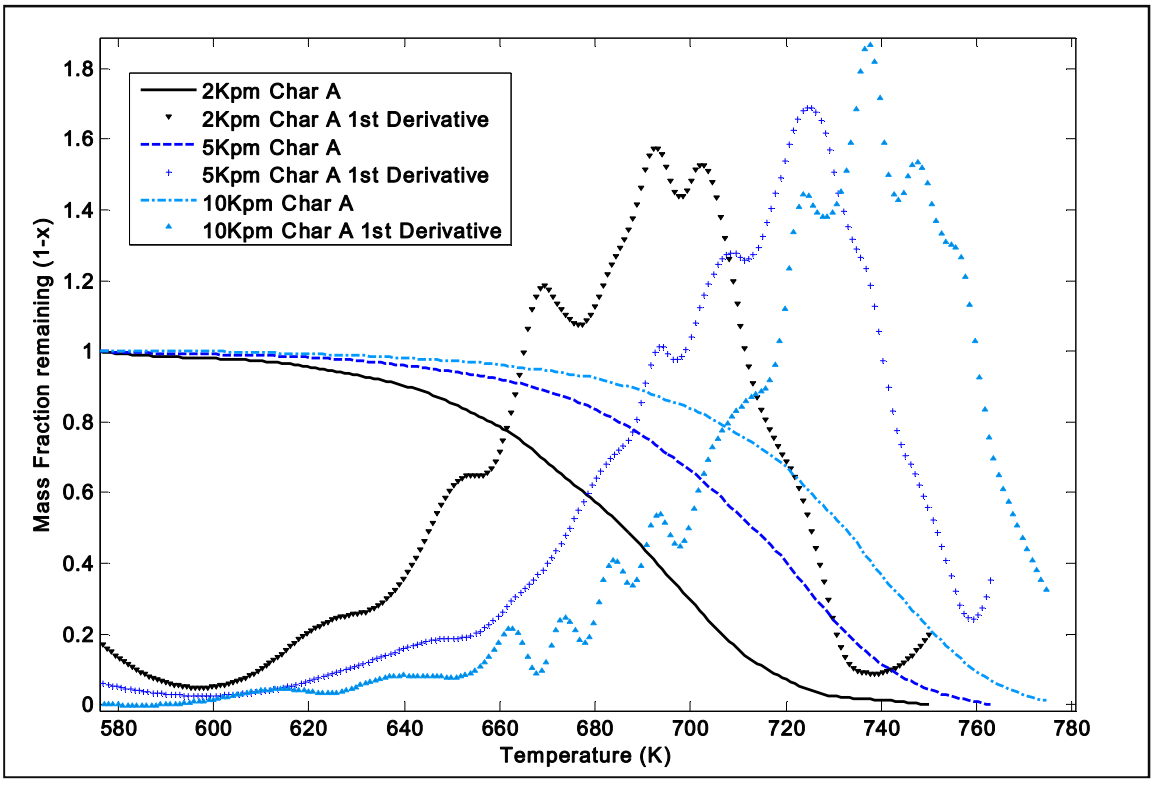

Figure 5.1: Thai-Lignite Char Oxidation at 2Kpm, 5Kpm and 10Kpm (Sangtong-Ngam and Narasingha, 2008)

The original work finds the activation energy (E) by means of an Arrhenius plot and another straight-line fit to find the pre-exponential factor, and then fits the data with the RPM to find φ. For char A, activation energy of 136.5kJ/mol is reported, with a pre-exponential factor of

18.1E+6. The kinetic parameters determined in the study are presented in Table 5.1. While the fits are said to be good, this method is limited to the assumption that only one reaction is occurring. As can be seen in Figure 5.1, the derivatives suggest multiple reactions.

Table 5.1: Char A single reaction kinetics determined by Arrhenius plots (Sangtong-Ngam and Narasingha, 2008)

	Initial Mass Fraction (f_0)	Activation Energy E (kJ/mol)	Pre-exponential Factor A ($s^{-1}.m^{-1}$)	Structural parameter φ
Reaction 1	1	136.5	18.1E+6	0.61

Having presented the results of the single reaction assumption, the multiple reaction assumption is used by applying the RPM-modified DAEM-based algorithm presented in Chapter 4. Unlike the conventional method, only two heating rates are required to determine the kinetic data, leaving the third rate to be used to assess the quality of fit. Since three heating rates are available, three different combinations can be produced. However, since the algorithm only uses the data from one of the two heating rates to calculate the pre-exponential factor values (i.e. only one dataset is used to substitute into equation 4-2 to calculate A^*), six combinations exist. Each of these need not be calculated, but each combination is presented overleaf in Figure 5.2 to assess and compare the accuracy of all the combinations. The kinetic data is presented in Appendix B.

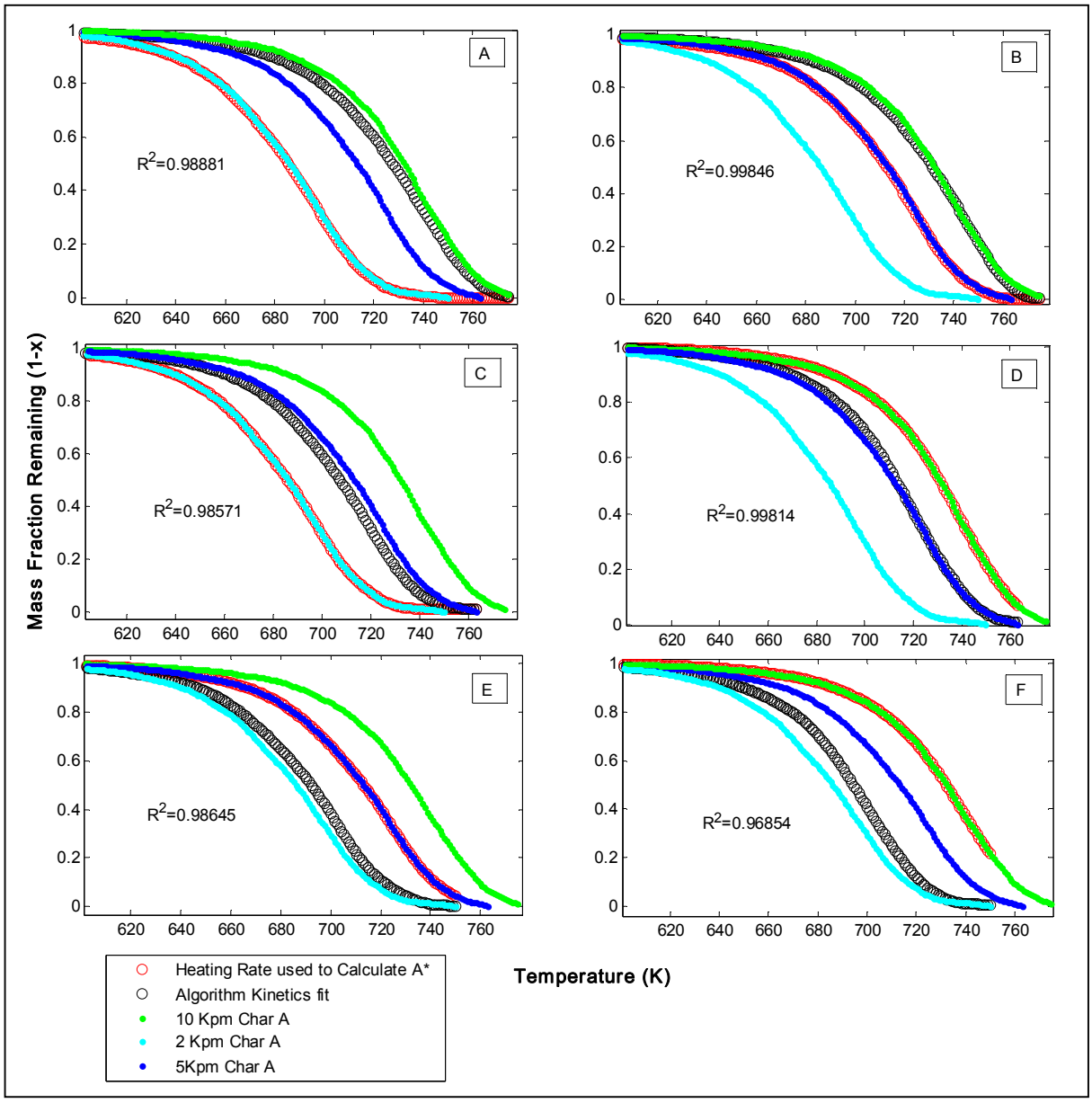

Figure 5.2: All combinations of the 3 available heating rates used to calculate kinetics and predict 3rd independent heating rate

From Figure 5.2 it is evident that most combinations produce a fair quality of fit, but some are better than others. The R-Squared values for each combination range from 0.968 to 0.998. Figure 5.2B presents the best statistical and visual fit, while Figure 5.2F presents the least accurate fit. What can be deduced from the differences in accuracy presented in Figure 5.2 is that it is generally best to use lower heating rate reactions to predict higher heating rate behaviour. This is evident since plots A and B in Figure 5.2 are among the most accurate plots, as opposed to plots E and F which are less accurate. Attempting to predict reaction behaviour within the heating rate range of those used will also result in less accurate fits, since Figure 5.2C provides one of the least accurate fits. Also, in choosing which heating rate to use to calculate the pre-exponential factor, it is best to use the heating rate that is the higher of the two rates, especially if the heating rate being predicted is higher than those being used to calculate the kinetics. Having assessed the differences between the results of the different combinations, a general best-practice as to how to choose the

best combination has been established, and will be tested on other datasets presented later in this chapter.

Given the findings on how best to choose a combination of heating rates, the 2K/min and 5K/min data were used to calculate the kinetics and predict the behaviour at 10K/min. The 5K/min data was used to calculate the A^* for each candidate reaction. Figure 5.3 presents the lower two heating rate dataset plots and the algorithm iteration plots conducted to calculate the structural parameter value.

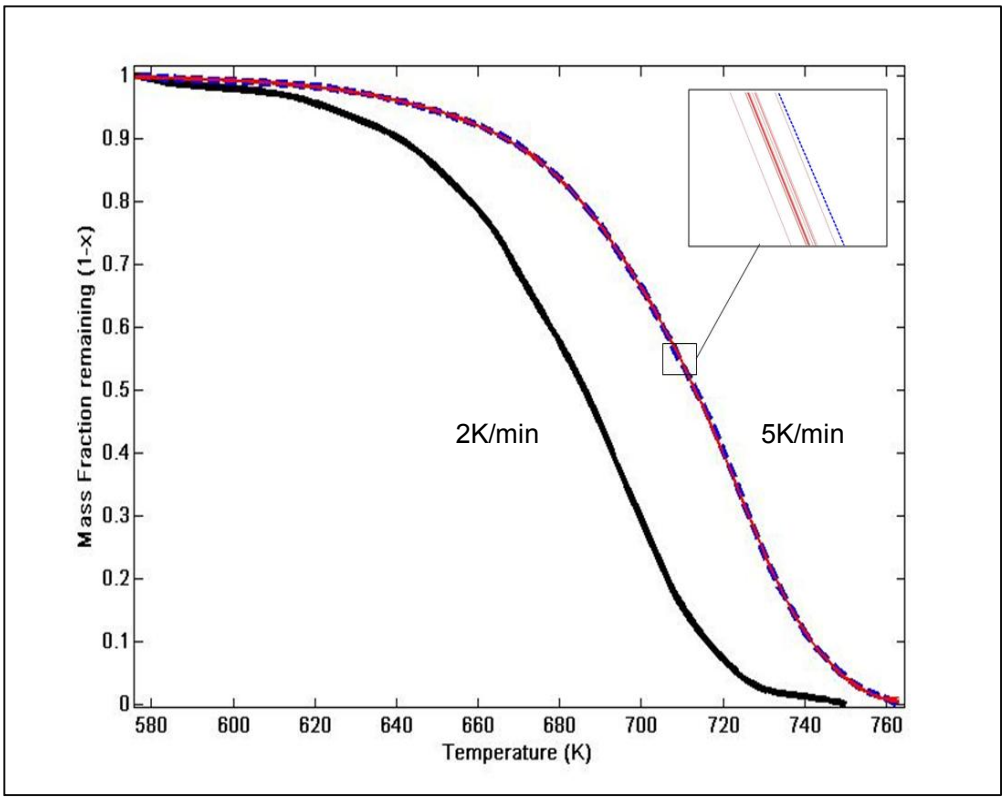

Figure 5.3: Curve Fitting to Find Structural and Kinetic Parameters

Figure 5.3 illustrates the steps taken by the algorithm to find the desired parameters. Here, the black and blue lines represent the 2Kpm and 5Kpm experimental data respectively. Each red line represents an iteration by the algorithm in which a value of φ is proposed and the error between the modelled and experimental points is calculated. The iteration is repeated for different values of φ until this error is minimised (see equation 5-2). Unlike the findings of Sangtong-Ngam and Narasingha (2008), the DAEM-based algorithm finds 3 independent reactions, as given in Table 5.2. In instances where the initial mass fractions straddle a specific conversion point, the kinetics are summed and averaged appropriately, as explained in Chapter 4). The structural parameter found is much higher than that reported, at $\varphi=18.9$. This value is however of the order applicable to the model (Bhatia and Perlmutter, 1980).

Table 5.2: Char A multiple reaction kinetics as determined by the RPM modified DAEM Algorithm

	Initial Mass Fraction (f_0)	Activation Energy E (kJ/mol)	Pre-exponential Factor A ($s^{-1}.m^{-1}$)	Structural parameter φ
Reaction 1	0.21	123.65	3.27E+06	18.9
Reaction 2	0.68	150.41	8.29E+07	
Reaction 3	0.10	310.62	9.32E+18	

The first two reactions correspond with the single reaction's activation energy originally reported and the third has a much higher activation energy and pre-exponential factor. These kinetic parameters are then used to predict the highest heating rate presented, 10K/min.

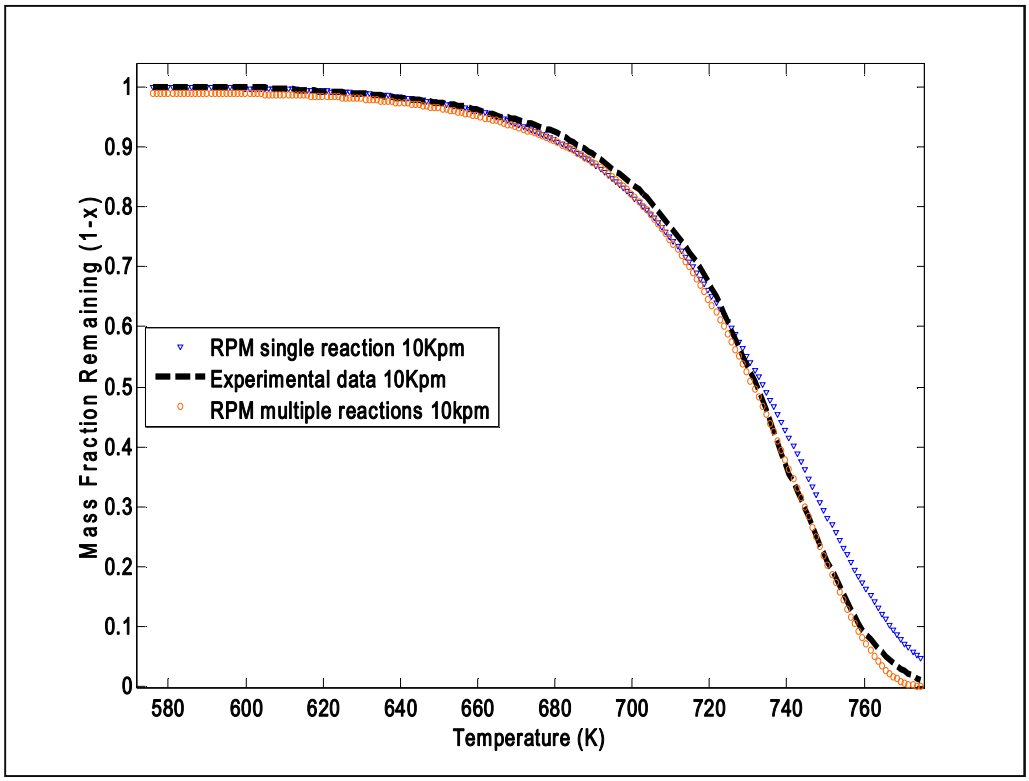

Figure 5.4: RPM Fits for Char A in O_2 at 10Kpm Using Different Kinetics Determination

Figure 5.4 presents the comparison of simulations produced using the two sets of kinetic parameters determined; one set using the Arrhenius plots to find single reaction kinetics, and the other produced using the DAEM-based algorithm to find multiple reaction kinetics. As can be seen, the use of the multiple reaction kinetics results in an accurate prediction of the measured experimental data. Slight deviations can be attributed to heating rate discrepancy as explained in Saloojee (2011). If the simulated curve could be shifted along the x-axis as is observed when adjusting the heating rate, an even closer fit would be achieved. Since the actual measured heating rate is not available in the original work, the programmed rate used by the original researchers is used in simulation. The single reaction simulation fits well until $1-x \approx 0.6$, but then deviates from the experimental data appreciably.

An objective assessment of the quality of fit is given by the R-squared statistic. The R-squared value for the multiple reaction fit of the experimental data is $R^2=0.998$. This high R-squared value is expected since it can be seen in the figure that the multiple reaction simulation fits the data more closely over the entire range of conversion. The R-squared value for the single reaction simulation was found to be $R^2=0.991$. When assessing the R-squared statistic for these fits, it must be borne in mind that the statistic is a comparison between the fit of the curve to the data and the fit of the mean to the data. Both simulated curves make a very good approximation to the experimental data, when compared to the

mean, hence high values of R-squared are always expected. Because of this, slight variations in the value still indicate a significant difference in the quality of fit. In assessing these fits, a difference of 0.007 is regarded significant. The greater value of the R-squared value for the multiple reaction simulation, along with the clear graphical representation shows that the DAEM-based RPM algorithm is an accurate, easy and reliable way to determine the kinetics of RPM reactions, especially in the event of multiple reactions.

What is also of concern in char reactivity simulation is behaviour at high heating rates, observed in drop-tube furnaces as well as in industry in fluidised bed operations. Heating rates of the order of 10^4K/min are not uncommon in these applications. Therefore, Figure 5.5 presents a comparison of the simulations obtained at such a heating rate using both sets of kinetics.

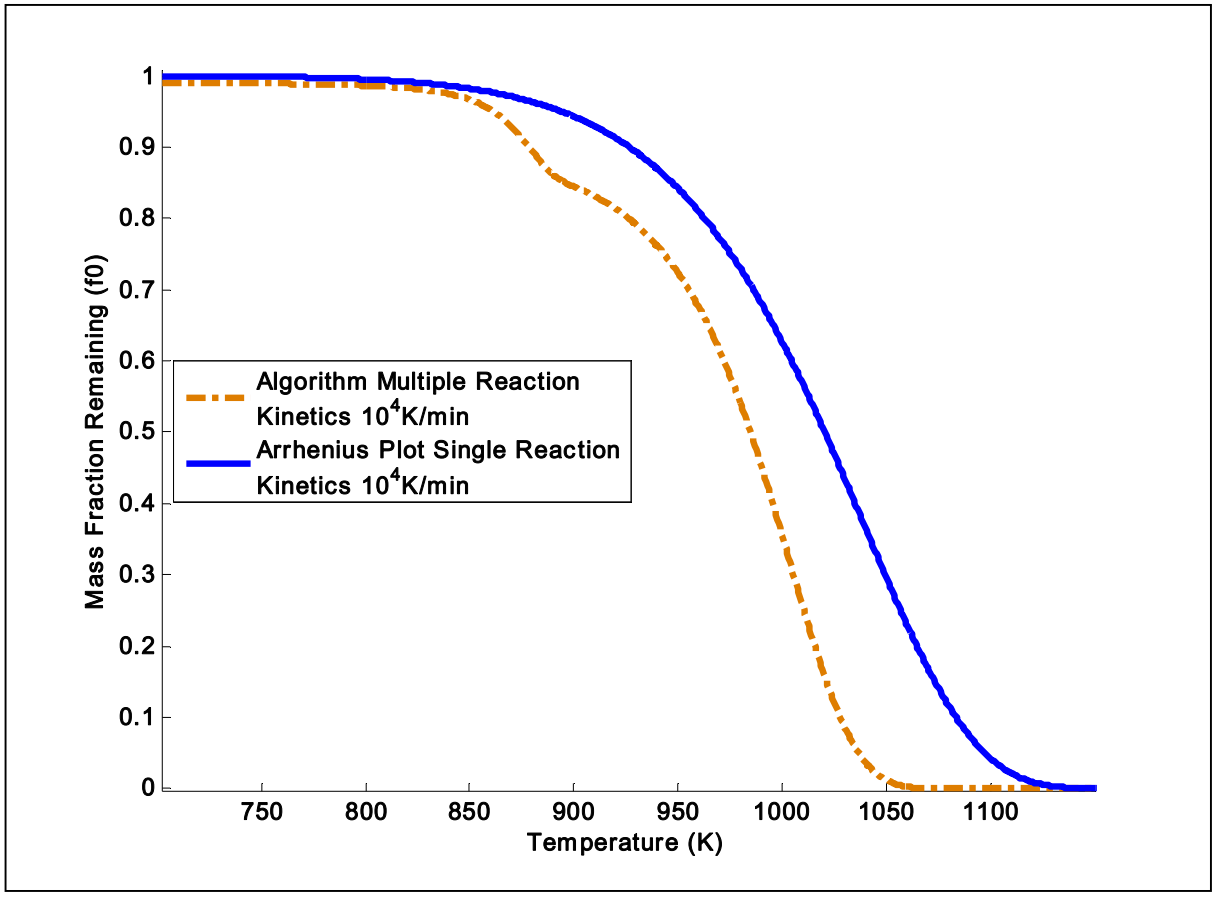

Figure 5.5: Comparison of single reaction and multiple reaction kinetics simulations of a High heating rate (10^4K/min)

It is clear that the simulations at this high heating rate are significantly different. The observation of multiple reactions becomes far more evident at such high heating rates; thus a single reaction approximation may not accurately predict the material behaviour as accurately. One of these curves would presumably predict the actual physical behaviour of the char better than the other, and given these findings it seems prudent to always consider the possibility of the occurrence of multiple reactions. While the developed algorithm is able to identify and process single as well as multiple reaction scenarios, most other methods, especially for RPM applications, can only function on the premise of a single reaction.

5.4. Plain Coal Char Reactivity

After processing the data from other research, raw experimental data produced for this research is assessed. The coal used was sourced from a South African coal field in Witbank. The sample preparation as well as the various experimental procedures used to conduct proximate analyses, non-isothermal and isothermal thermogravimetric analyses are outlined in Chapter 3.

5.4.1. Proximate Analysis

The proximate analysis of the coal is provided in Figure 5.6 and Table 5.3.

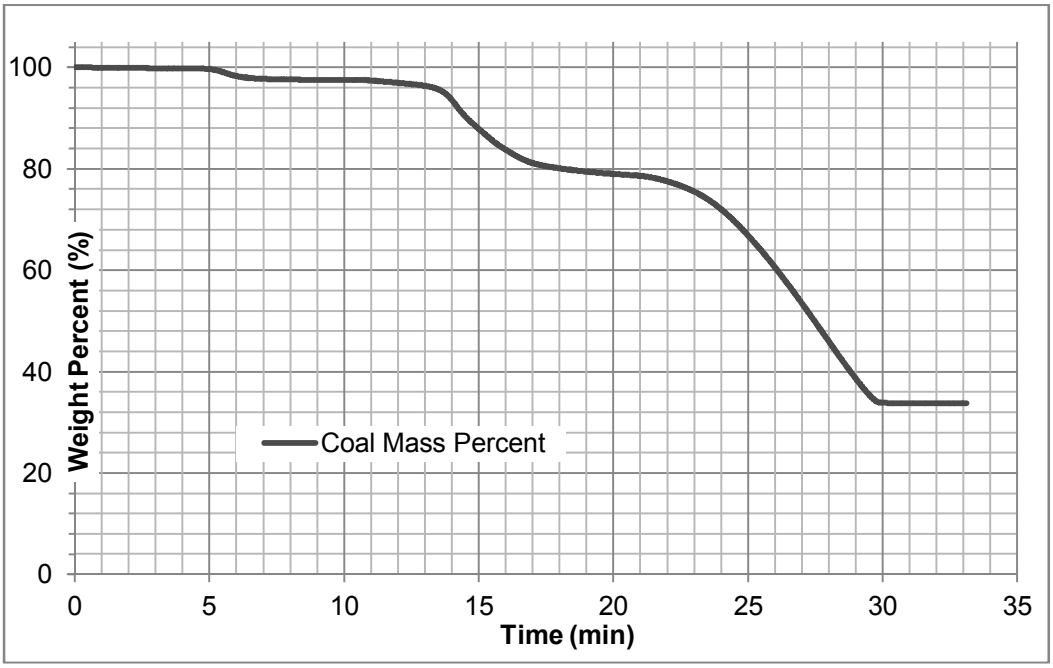

Figure 5.6: Coal Proximate Analysis Data

Table 5.3: Coal Proximate Analysis Results

Component	Weight Percentage
moisture	2.44
Volatile matter	18.93
fixed carbon	44.80
Ash Content	33.83
total	**100**

It is evident that the coal being used has a large ash-fraction and low moisture content.

5.4.2. CO_2 Reactivity

Figure 5.7 overleaf presents reactivity data of the Witbank coal char. The data was produced by reacting the char (produced under the same condition for all three heating rates shown below) in CO_2. Since the raw data produced by the TGA includes the initial charring mass-loss data, the CO_2 reactivity data had to be extracted and normalised. Even though the algorithm is able to process ash data, the ash data is not processed here, because it was noted that precisely equivalent ash percentages were not preserved when normalising each

of the three heating rates. Hence, the data presented below is normalised 'ashless' CO_2-reactivity data of a plain coal char at heating rates of 12K/min, 15K/min and 20K/min.

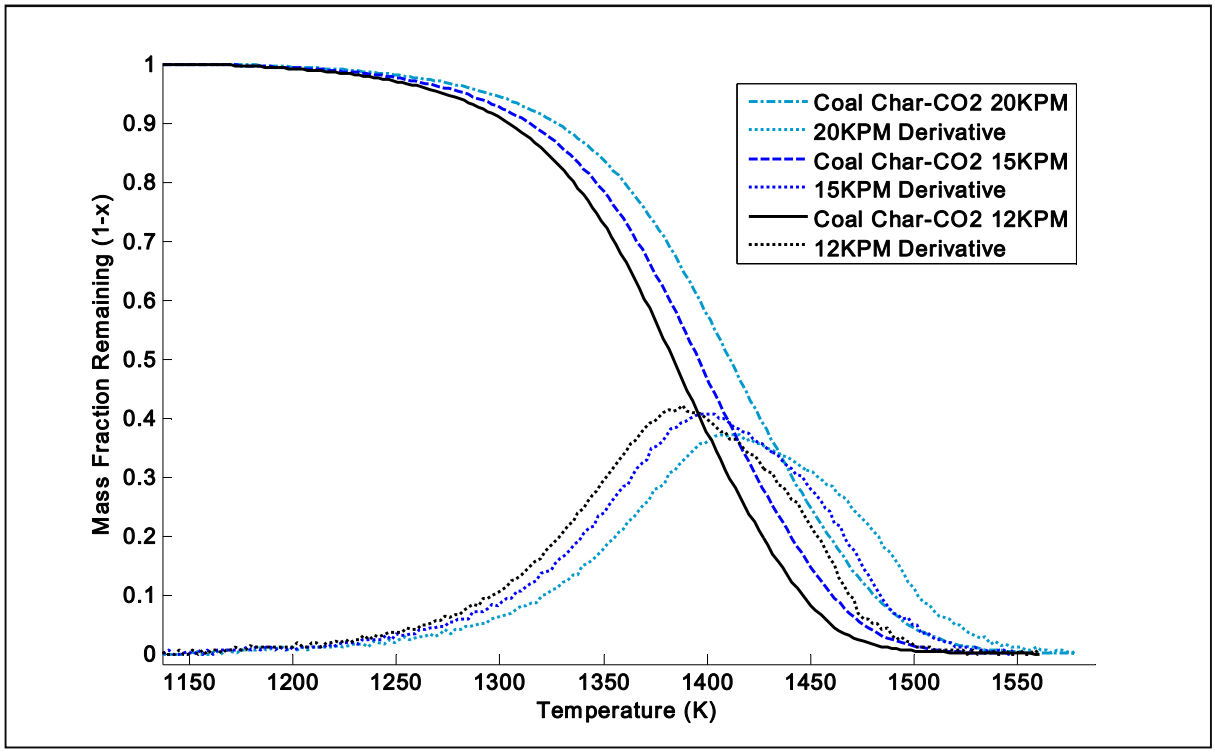

Figure 5.7: Normalised Coal Char Decomposition in CO2 and Derivatives

The derivative data are also shown to be able to readily determine whether one or multiple reactions are occurring, so as to anticipate the likely results produced by the algorithm. Upon examination of Figure 5.7, it can be seen that the derivatives do not indicate a single pronounced peak (as seen in single reaction simulations in Chapter 4, Figure 4.16) but rather an initial rapid increase in decomposition approaching a maximum, which is then followed by a varying decline before reaching complete reaction. This observation suggests that, even though multiple distinct peaks cannot be observed, the occurrence of multiple reactions is likely.

5.4.3. Kinetics Determination

This data will be used in two separate kinetics determination techniques. The first technique is the well-known method of using the Arrhenius plot to determine the activation energy, and then using another linear fit to determine the pre-exponential factor. The appeal of this method is that it is supposedly quick and easy to use, and gives a fairly good approximation of the kinetic parameters. The shortfall however, as shown in the previous section based on char-O_2 reactivity (Sangtong-Ngam and Narasingha, 2008), is that the common use of this method is generally based on the assumption of a single reaction. This does not imply that the Arrhenius plot is limited to the determination of single reaction only; this method can be used to determine the kinetics of complex systems (Koch, 1977), but the application is very calculation intensive and may require a large amount of experimental data (i.e. many different heating rates for non-isothermal experiments and many different temperatures for isothermal experiments).

Arrhenius Plot

The random pore model expression was linearised to obtain the following form, which follows the generic form of the Arrhenius plot relation, ln(A) vs. 1/T.

$$\ln\left(\frac{dx/dt}{(1-x)}\right) = -\frac{E}{RT} + \ln\big(G(x)\big) \qquad \textbf{5-3}$$

Where

$$G(x) = A^{*}\sqrt{1-\varphi\ln(1-x)} \qquad \textbf{5-4}$$

It can be seen that a straight line plot of ln[(dx/dt)/(1-x)] vs. 1/T will yield a gradient that is equivalent to –E/R. Note too that the time differential is used and not the temperature differential; since temperature differential values are obtained from the experimental data, these must be manipulated to obtain the time differential value.

Then, once the activation energy is found, the value of G(x) can be determined by again using equation 5-3 over a range of conversion x, since all other terms are known. Equation 5-4 is then linearised:

$$G^{2}(x) = -A^{*2}\varphi\ln(1-x) + A^{*2} \qquad \textbf{5-5}$$

The gradient is the product of the structural factor and the square of the grouped pre-exponential factor. The y-intercept yields the square of the grouped pre-exponential factor. The square root of the y-intercept gives the pre-exponential factor A^{*} and the negative quotient of the gradient and the y-intercept gives the structural parameter.

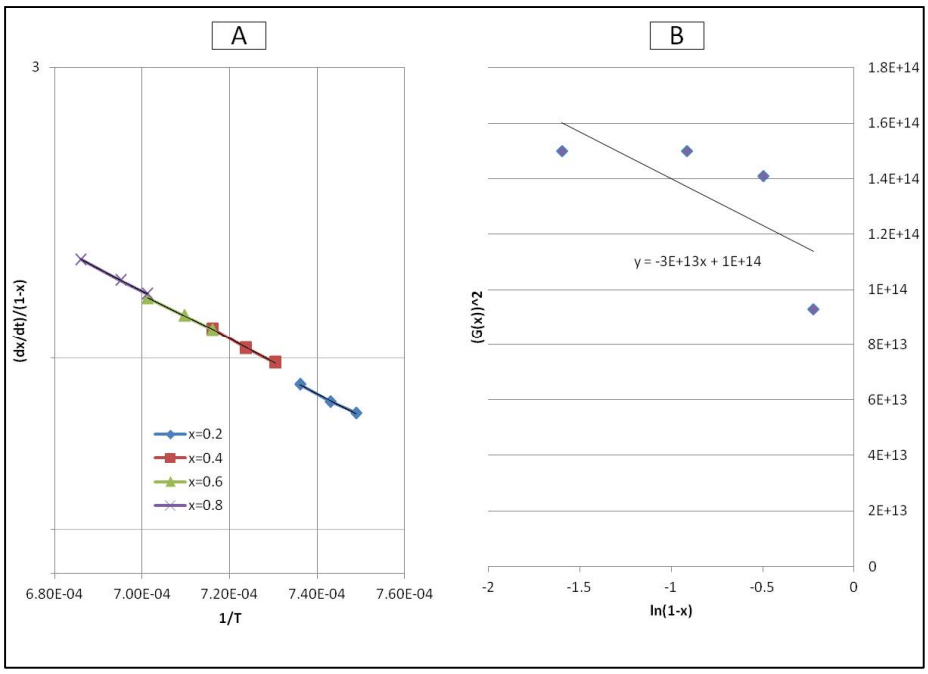

Figure 5.8: [A] Arrhenius Plot for E calculation for Coal Char-CO2 Reaction, [B] G(x) plot for A* and Ψ calculation

Like the char-O_2, the RPM produces a linear fit of the data when plotted on logarithmic axes, as seen in Figure 5.8 [A]; The correlation coefficients for the fitted straight lines were all

greater than R^2=0.99. This suggests that the RPM accurately represents the data. It must however be noted that although the fitted lines seem parallel, their gradients are in fact not equal. It can also be seen in Figure 5.8 [B] that the ln(1-x) vs. G(x) relationship is not linear; the best fit line was however used, according to the method, to determine the pre-exponential factor and structural parameter. The Arrhenius plots yield the following kinetics:

Table 5.4: Single Reaction Kinetics Determined by Arrhenius Plot

Variable	Value
Activation Energy ***E*** **(kJ/mol)**	254.45
Grouped Pre-exponential Factor **A ($s^{-1}.m^{-1}$)**	1E+07
Initial Mass Fraction $\mathbf{f_0}$	1
Structural parameter $\boldsymbol{\varphi}$	0.30

Ideally, each conversion line in Figure 5.8 should have equal gradients and so produce equal values of the activation energy. When this is not the case, researchers presumably use an average value, or use the activation energy value that provides the best fit for their specific reaction data. The former approach has been presented here. However, each individual activation energy determined from each gradient was used to fit the data (The values of activation energies determined were between 221kJ/mol and 294kJ/mol). Some values gave accurate fits (more accurate than using the average value), while some gave far less accurate fits.

This presents a problem with the technique: different users may produce different results from the same set of experimental data. The less user input required by a method, the higher the degree of consistency of the results. Unlike the Arrhenius-plot or other isoconversion methods, the DAEM-Based algorithm that has been developed here only needs the appropriate model to be chosen, and a conversion value to be calculated for the maximum reaction rate of that model. Thereafter, the algorithm uses the data to fully determine the kinetic triplet, even for multiple reactions, without user intervention. This automation reduces user input and improves consistency.

Figure 5.9 overleaf shows a comparison between the experimental data and the RPM reaction predicted using the kinetics given in Table 5.4.

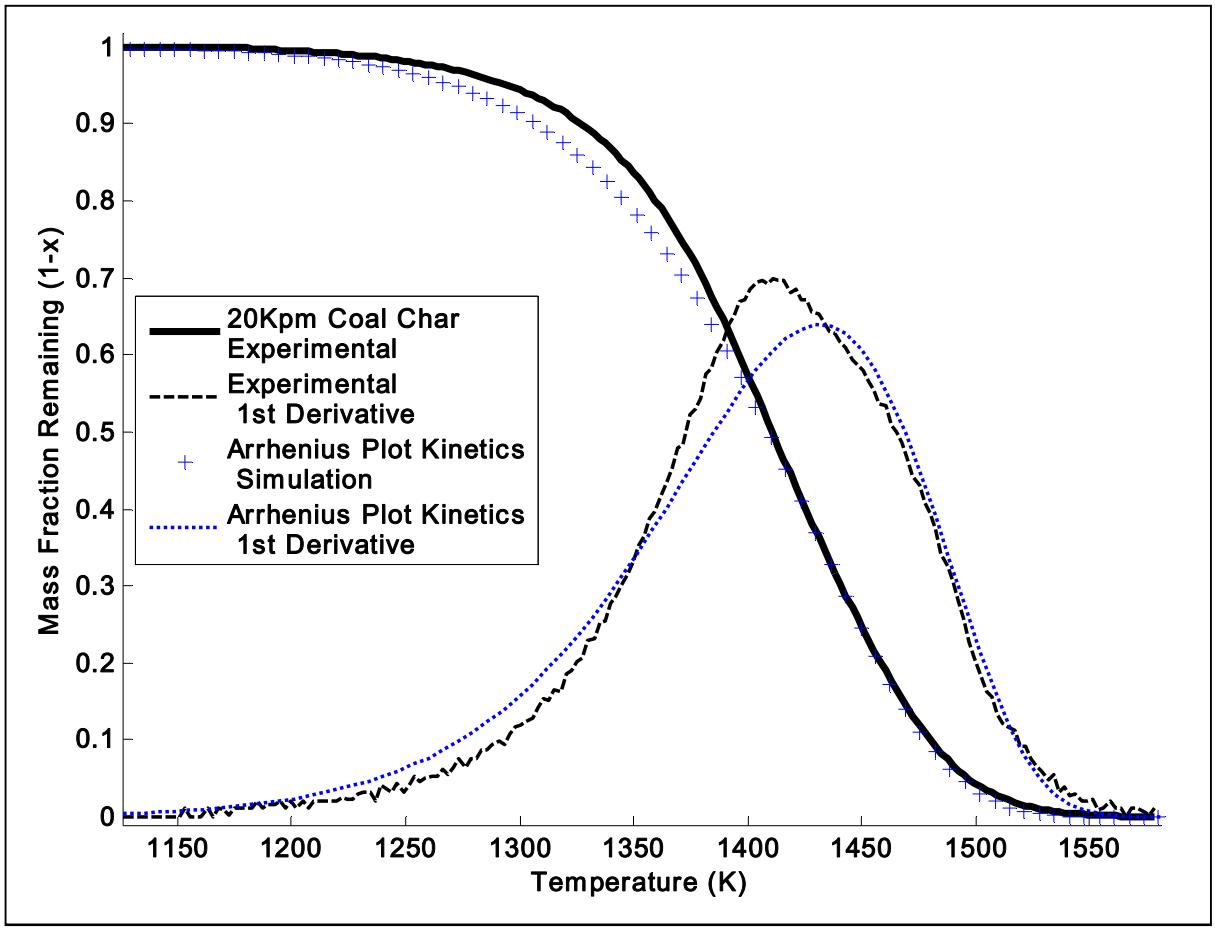

Figure 5.9: Single Reaction simulated using Arrhenius Plot Kinetics

The predicted reaction behaviour indicates a faster initial reactivity than observed during experimentation; consequently the simulated reaction terminates sooner (at a lower temperature) at the end of the conversion range. It is evident that the single reaction simulation is inaccurate over approximately the first half of the conversion range. The R-squared value over the first half of the range is 0.77, which implies an unsuitable fit. The second half of the range however shows a significantly better fit, with an overall R-squared value of 0.989. While this fit is reasonable, the inconsistent reliability of this method (when comparing the current results to those of the char-O_2 reactivity) has encouraged the development of more robust methods.

RPM-Modified DAEM-based Algorithm

The second kinetics determination technique is the DAEM-based algorithm developed in this research. The data handling and calculation will be done in the same way as was done for the char-O_2 data in section 0. Only two heating rates are required to determine the kinetics. The third heating rate is used to compare the simulation to experimental data, to assess the accuracy of the predicted reaction behaviour. Since three heating rates are available, the opportunity exists to use each of the possible combinations, and use the kinetics that yield the best-fit simulation. Again, all combinations were calculated to identify which combination would yield the best fit, and to determine whether the general approach suggested in section 0 (discussion of Figure 5.2) could be ratified. The plots of all possible combinations of the

coal char-CO_2 reactivity data are presented in Figure 5.10. The kinetic data is presented in Appendix B.

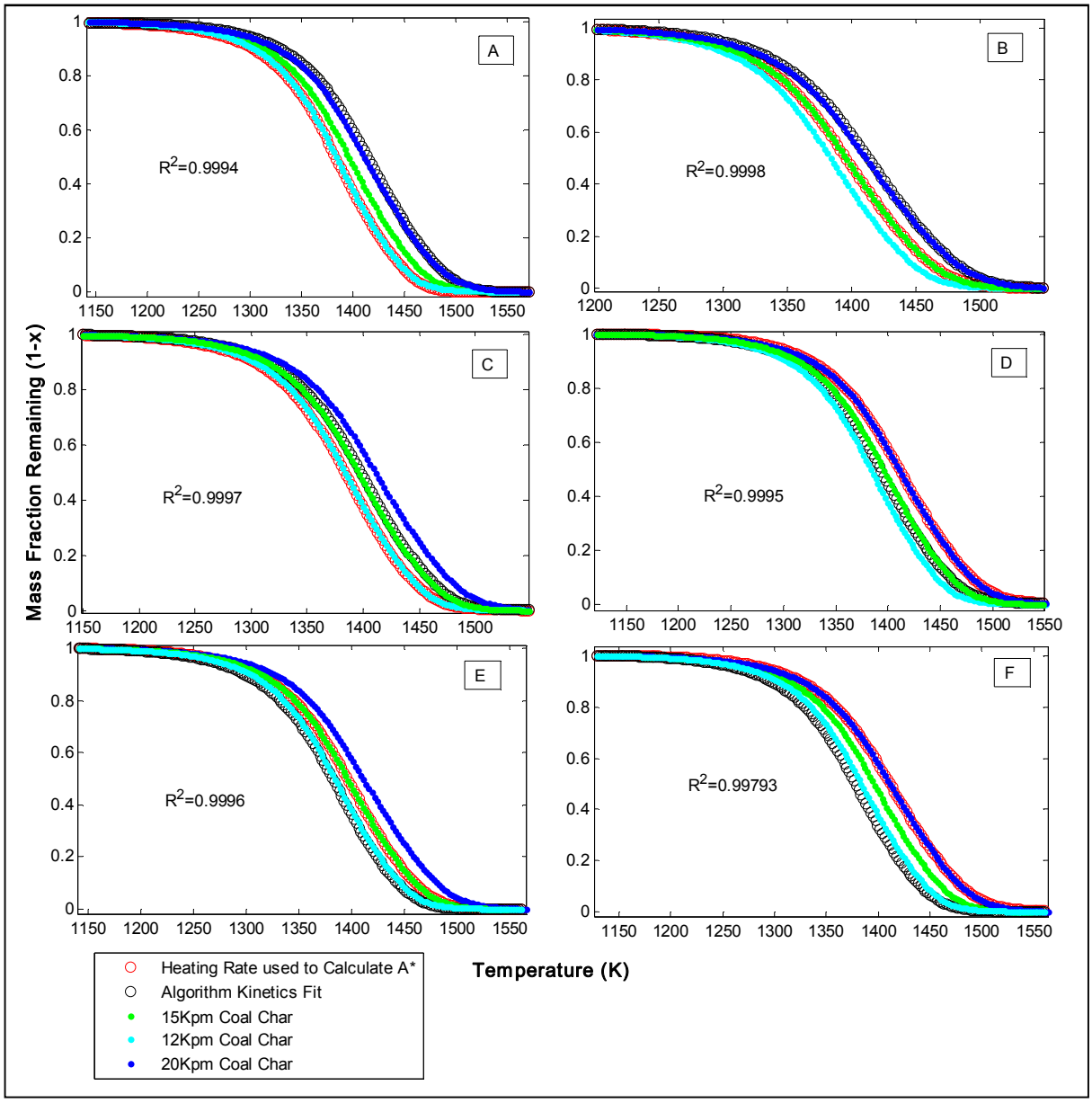

Figure 5.10: All combinations of kinetics determination and 3rd heating-rate reaction prediction for coal char-CO_2 data

As can be seen in Figure 5.10, all combinations of reaction data have resulted in precise fits. The range of R-squared values is 0.9979-0.9998. The same trend as observed in the previous section is observed here i.e. the best fits are achieved when the lower heating rate data are used to predict the higher heating rate, while the least accurate fits are obtained when trying to predict the lower heating rates with higher heating rate data. The best quality fit was obtained with the combination in Figure 5.10B, which is the same combination that produced the best fit for the previous data set in section 0. This is the combination in which the 12K/min and 15K/min data are used to predict the 20K/min reaction, with the 15K/min data being used in the calculation of A^*. The plot of the iterations conducted by the algorithm using this combination are presented in Figure 5.11.

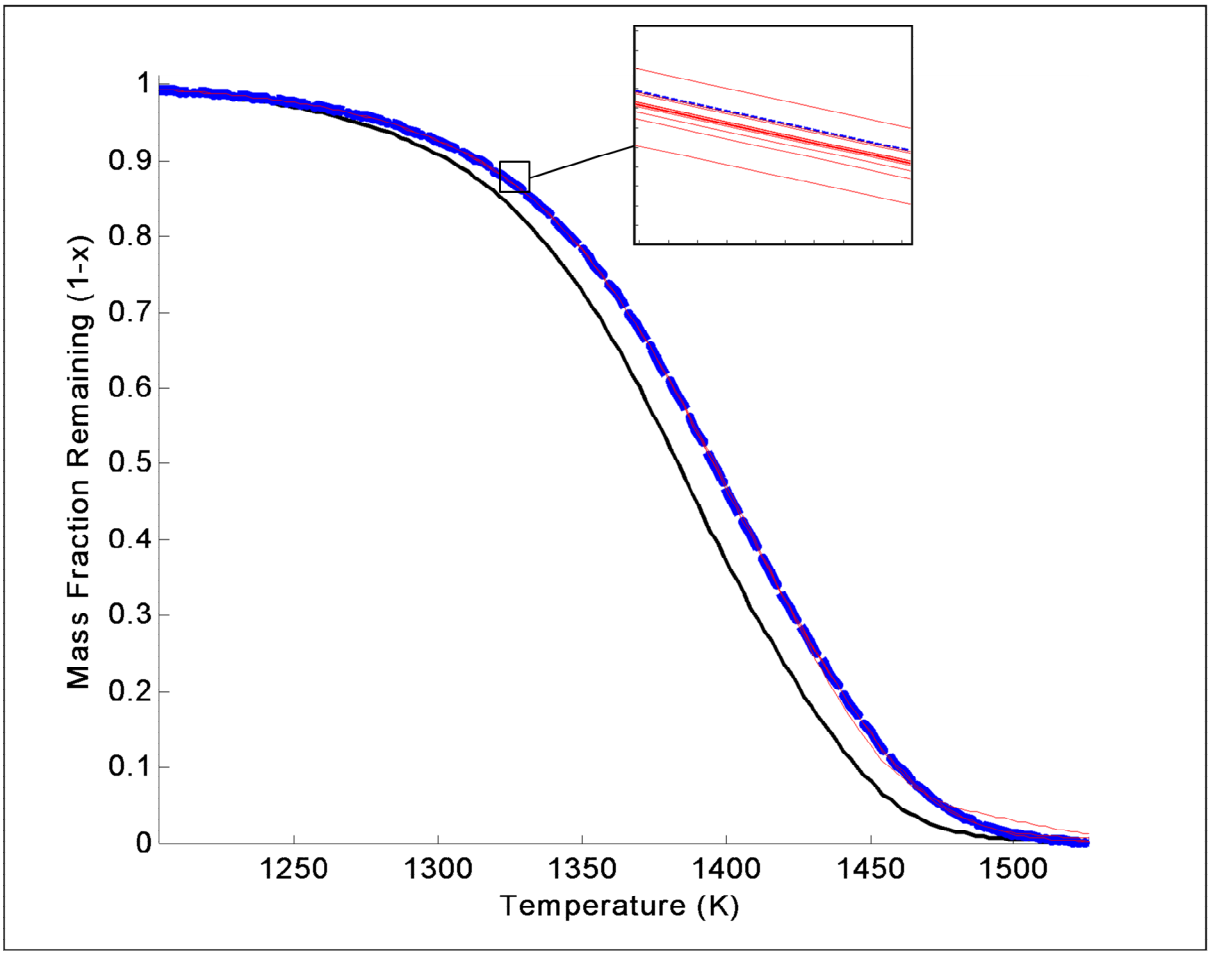

Figure 5.11: Curve Fitting by Algorithm to Determine Char-CO_2 Kinetics

As in Figure 5.3, Figure 5.11 shows the iterations done by the algorithm. Each red line represents a simulation using the two heating rates to determine the kinetic triplet (E, A^*, and f_0) with a proposed value of the characterisation parameter φ. The sum of squared errors (equation 4-14) is calculated between the experimental data and the iteration. This process is repeated until the sum of squared errors is minimised. The approach of fitting the experimental data with the curve produced directly by the model is a more accurate and robust approach than fitting a linearised manipulation of the model to data that has also been mathematically manipulated (Bhatia and Vartak, 1996). The reason for this, according to Bhatia and Vartak (1996) is mainly that straight line fits are very sensitive to experimental scatter, which is unavoidable in any experimental situation. The advantage of the algorithm developed in this research is that it enables one to fit the curve directly to the experimental data because the entire kinetic triplet is found in a single calculation set, which is unique among methods adopting an isoconversion approach.

Table 5.5 and Table 5.6 overleaf present the kinetic parameter values found by the algorithm.

Table 5.5: Coal-Char/CO_2 Multiple Reaction Kinetics Determined by DAEM-Based Algorithm

	Mass Fraction (f_0)	Activation Energy E (kJ/mol)	Grouped Pre-exponential Factor A^* ($s^{-1}.m^{-1}$)
Reaction 1	0.060	262.0	1.69E+07
Reaction 2	0.254	261.7	1.57E+07
Reaction 3	0.075	248.9	2.71E+06
Reaction 4	0.240	245.6	1.89E+06
Reaction 5	0.366	227.6	2.75E+05
Reaction 6	0.007	305.6	5.04E+07

Table 5.6: Summed/ Averaged Coal Char/CO_2 Kinetics Determined by DAEM-Based Algorithm

	Mass Fraction (f_0)	Activation Energy E (kJ/mol)	Grouped Pre-exponential Factor A^* ($s^{-1}.m^{-1}$)	Structural parameter φ
Reaction 1-2	0.313	261.8	1.60E+07	12.2
Reaction 3-4	0.315	246.4	2.08E+06	
Reaction 5	0.366	227.6	2.75E+05	

Table 5.5 presents the kinetics found by the algorithm. All non-zero mass-fraction results are presented. Reactions 1-2 and 3-4 both have similar activation energy and grouped pre-exponential factor values; they also occur at adjacent conversion values and can hence be combined and considered as single reactions. Reaction 6 does not correspond with reaction 5 in terms of kinetic parameter values and represents an almost negligible fraction of the reactive mass. For the simulation of other heating rates, this reaction should be included, but will not be discussed at length when comparing actual kinetic values.

For kinetic comparison, the summed and averaged reactions are given in Table 5.6. The kinetic parameter values found are of the order of those found for coal chars described by the RPM (Fermoso et al., 2010). Fermoso et al. (2010) found the activation energy of four of the five coals studies to lie within 256.6kJ/mol and 260.6kJ/mol. The structural parameter value found in the regression analysis is φ=12.2. This value is significantly higher than that found in the Arrhenius plot method, but is still of the order found in other detailed research of the parameter's value (Su and Perlmutter, 1985). These kinetic parameters were used to predict the reaction behaviour at 20K/min. The predicted data along with its derivative data are presented in Figure 5.12 and compared to the experimental data as well as the single reaction kinetics prediction.

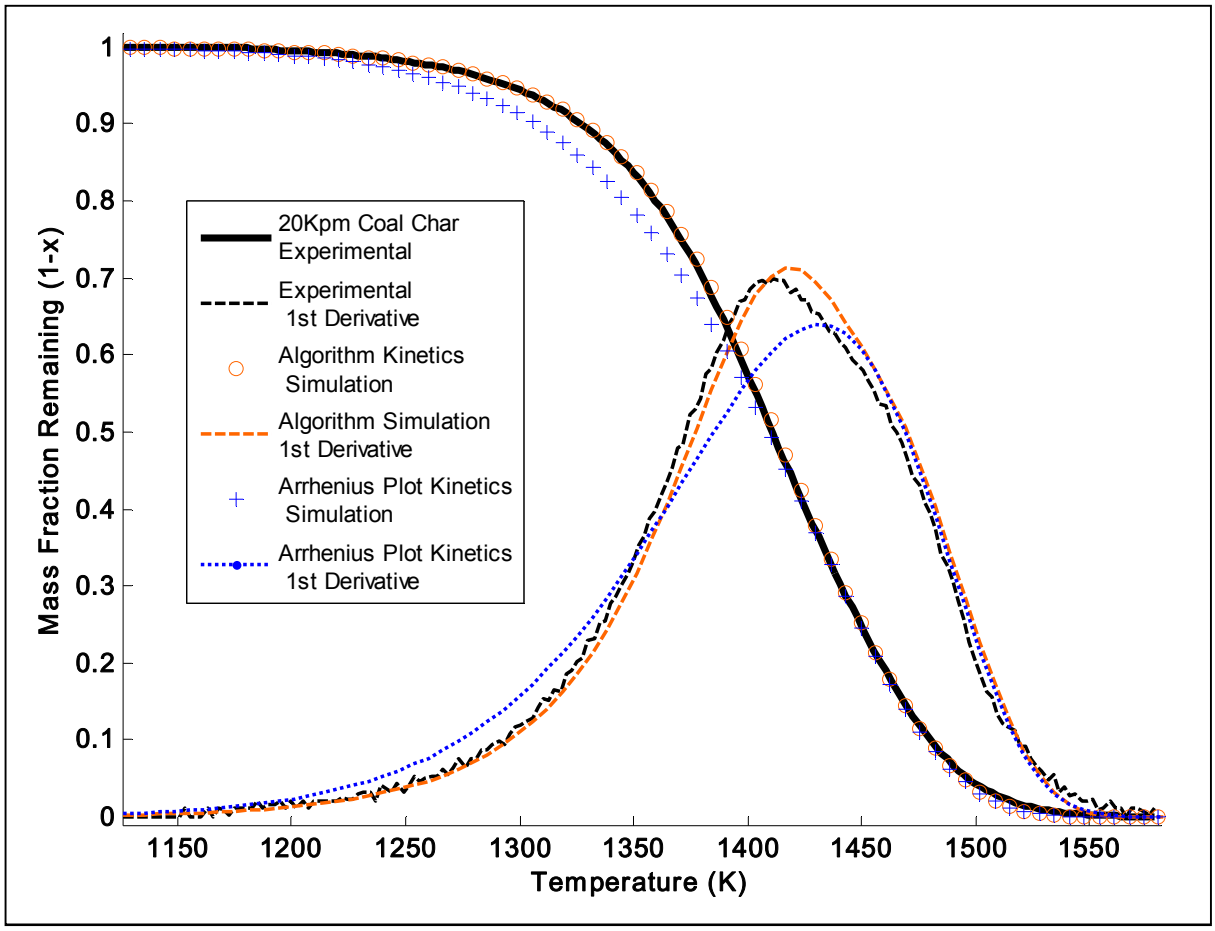

Figure 5.12: DAEM-based Algorithm Fit of 20Kpm Experimental Data Compared to Arrhenius Plot Fit

Figure 5.12 shows the fit of the random pore model prediction of the experimental data using the kinetics and structural parameter found by the algorithm. The fit is significantly more precise than that of the single reaction kinetics fit obtained using the Arrhenius plot, with a correlation coefficient value over the entire range of R^2=0.9998, which indicates a near perfect fit. It must be noted that this quality of fit was achieved without finding a unique structural parameter for each of the multiple reactions identified by the algorithm. An overall φ value produces a desirable quality of fit. Further affirmation of the quality of fit is given by the assessment of the derivative comparison. The multiple reaction simulation follows the experimental data derivative far more closely, deviating slightly at the maximum points. The sensitivity of the derivative is high, thus a good derivative correlation is clear indicator that the experimental behaviour has been accurately simulated. This is not the case for the single reaction simulation, which shows very little correlation with the experimental data derivative.

Again, the prediction of reaction behaviour at very high heating rates using the different kinetics results should be assessed. Figure 5.13 presents the plots of a 10^4K/min RPM reaction using the Arrhenius-plot derived single reaction kinetics and a 10^4K/min RPM reaction using the multiple reaction kinetics obtained from the DAEM-based algorithm.

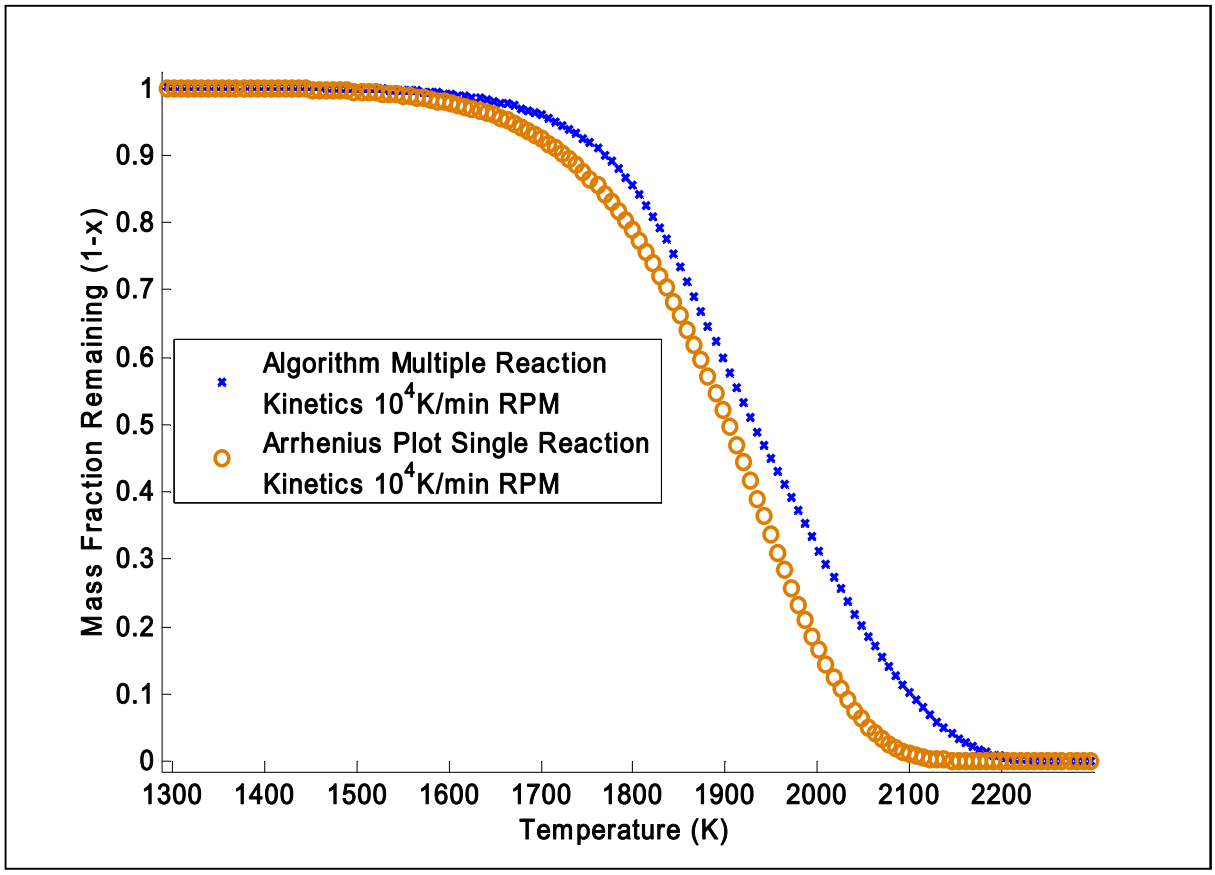

Figure 5.13: Comparison of coal char RPM reaction prediction at high heating rate using different kinetic parameter sets

As was observed in Figure 5.5, Figure 5.13 shows that the difference in reaction behaviour predictions produced using the two kinetic parameter sets increases with higher heating rates. At this high heating rate an appreciable difference in the temperature range in which the material reacts is observed. This result indicates that it may be beneficial to consider multiple reaction kinetics when attempting to predict high heating rate behaviour; this can be done using the DAEM-based algorithm developed in Chapter 4.

5.5. Further Algorithm Adaptation and Application: Isothermal Data Processing

Plain coal char was also reacted in CO_2 under isothermal conditions. (The full details of the sample preparation and experimental procedure are provided in Chapter 3) This was done to provide experimental data to determine the efficacy of the algorithm processing experimental isothermal data. The normalised isothermal data is presented in Figure 5.14. Temperatures of 1319K, 1349K and 1368K were used. The DTG data is also presented. These temperatures were chosen based on the predicted length of time in which the reactions would reach completion. This was done to accommodate the hold time limit of the experimental equipment being used. These temperatures are however of the order used in other research when investigating isothermal coal/char reactivity (Liu, 2004).

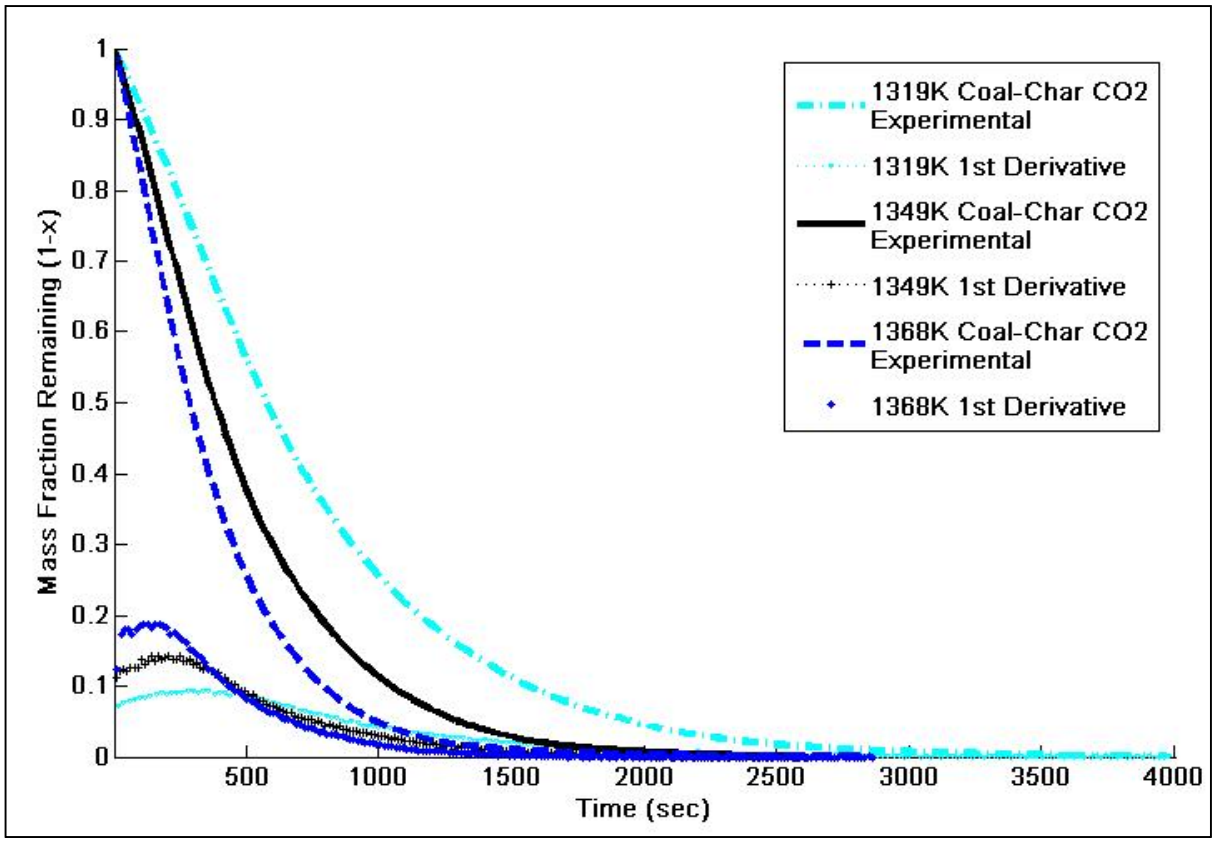

Figure 5.14: Normalised Isothermal Data of Coal in CO_2 at Various Temperatures

As expected, reactivity increases with temperature. This is evident in the different times taken to react under the various temperatures: At 1368K, the material reacts in the shortest time, followed by the reaction at 1349K, and lastly the reaction at 1319K. The steepness of the derivative data also shows this. It must be borne in mind that in the derivation of the algorithm, it was assumed that the initial time was always zero. The time at which the sample reaches the specified temperature was therefore taken as $t_0=0$ and time recorded proceeds from this point. Also, it can be seen that the initial lag-time data has been ignored i.e. the short period in which the instrument rapidly heats to the specified temperature.

The same methods used for the non-isothermal data was applied here. Since three datasets are available, all three combinations were used, with the best fit being presented. Unlike the

findings for non-isothermal data, it was found that the combination of the highest and lowest temperatures' data yielded kinetics that fitted the intermediate temperature's data with the best accuracy. The plot of the algorithm's iterations is given below in Figure 5.15.

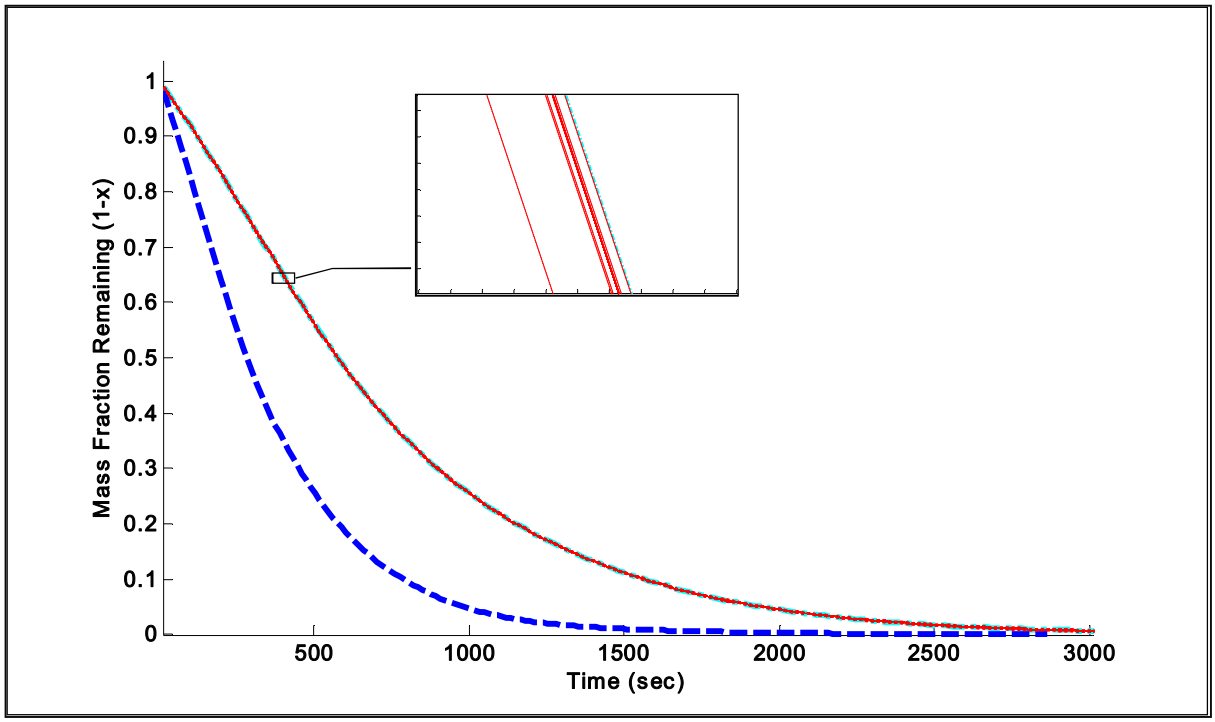

Figure 5.15: Algorithm Iterations to Determine Kinetics Overlaid on Experimental Isothermal Data

The algorithm again found multiple reactions, which is expected since the non-isothermal experiments and kinetic analysis also showed multiple reactions occurring. The kinetic parameter results are presented in Table 5.7. The value of the structural parameter determined during the regression analysis was found to be $\varphi=16.8$.

Table 5.7: Reaction Kinetics for Coal Char in CO_2 under Isothermal Conditions

	Mass Fraction (f_0)	Activation Energy E (kJ/mol)	Grouped Pre-exponential Factor A* ($s^{-1}.m^{-1}$)	Structural parameter φ
Reaction 1	<1%	202.58	1.78E+06	16.8
Reaction 2	<1%	220.34	4.42E+06	
Reaction 3	0.02	219.39	1.55E+06	
Reaction 4	0.39	210.59	2.46E+05	
Reaction 5	0.49	203.04	1.20E+05	
Reaction 6	0.10	107.586	4.25E+04	

Again, a number of the reactions found by the algorithm have almost negligible fractions mass allocated to them, but are important when aiming to predict the material's behaviour at different temperatures. In discussing the kinetic parameter values, the two largest reactions, reactions 4 and 5 are focussed upon. The values of activation energy and pre-exponential factors correspond well with those found by other researchers conducting similar research (Everson et al., 2008)

It is clear that the bulk of the material is reacting with lower activation energy than under non-isothermal conditions, but also with a smaller frequency factor, which implies slower reactivity. The structural parameter is also appreciably different, suggesting a difference in the structural changes during reaction.

It might be argued that since the same material is being reacted with the same gaseous reactant, the kinetics should be the same for both isothermal and non-isothermal conditions, this is however not necessarily the case (Ravindran et al., 1989; Lua and Su, 2006). Ravindran et. al. (1989) found, while studying the dehydration reaction kinetics of an inorganic compound, that isothermal and non-isothermal data yielded different sets of kinetic parameters, and even needed two different reaction models to be fitted to achieve precise fits. They attributed the difference in kinetics to the difference in impedance to the removal of product gases (water vapour) from the reaction interface. The impedance was explained to result from a possible recombination reaction occurring (in this case there is a possibility of the CO molecules reacting again to form CO_2 and carbon). It is stated that this is less likely to occur under non-isothermal conditions. Lua & Su (2006) found that while the same number of reaction stages was observed under both isothermal and non-isothermal conditions of the pyrolysis of a polyimide, the Arrhenius parameters were found to be inconsistent. They attribute this to the differences in the mathematical models applied to the data in determining the parameters.

Regardless of the differing kinetic results, the ultimate determination of the accuracy of the parameters produced is established by assessing the correlation between the predicted reaction behaviour and the measured experimental reaction behaviour (Lua and Su, 2006). Figure 5.16 presents a plot of the predicted mass loss at 1349K as compared to the experimental data obtained at 1349K.

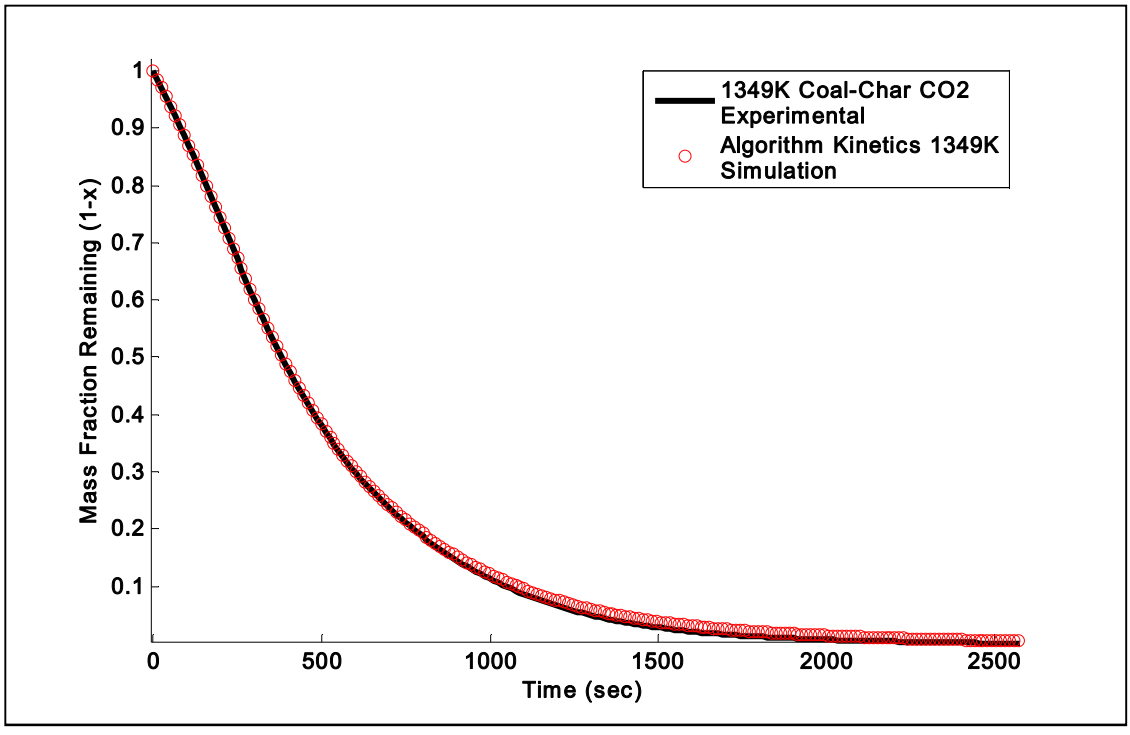

Figure 5.16: RPM prediction of coal char reactivity at 1349K compared to experimental data

The third heating rate, which was not used at all in the determination of the kinetics, was used as a comparison with the simulated data. The correlation coefficient for the fit in Figure 5.16 was found to be R^2=0.9994. This represents a near perfect fit. There is a slight under-prediction in reactivity in approximately the last 10% of the mass, but the result offers an appreciably accurate prediction of the material behaviour overall at this temperature.

In order to illustrate the need to determine isothermal and non-isothermal kinetics independently, Figure 5.17 and Figure 5.18 present attempts to fit isothermal data using kinetics determined using non-isothermal data, and vice versa.

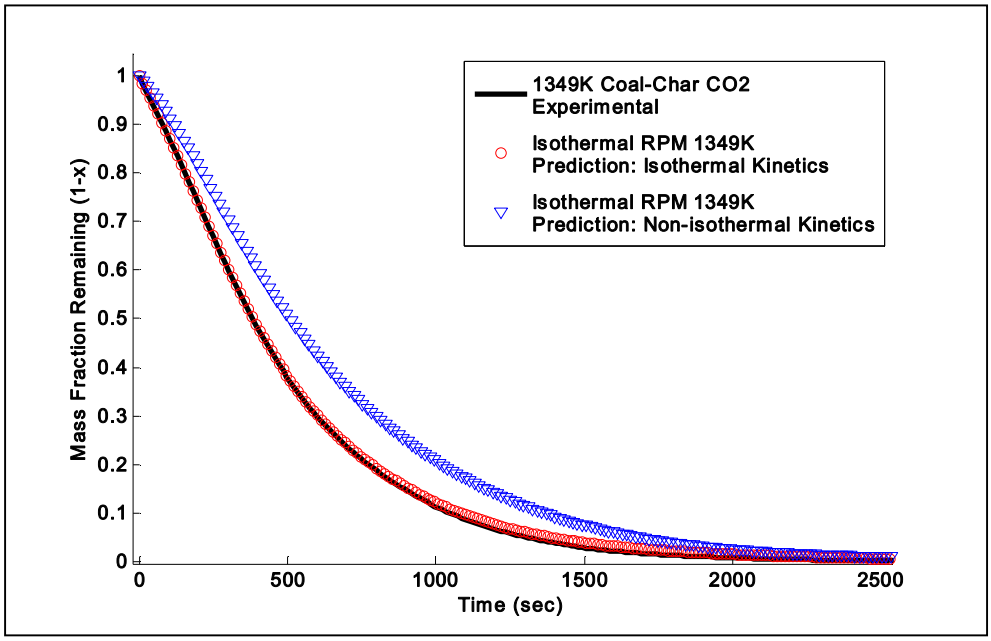

Figure 5.17: Comparison of isothermal RPM fits generated with kinetics derived from non-isothermal and isothermal datasets

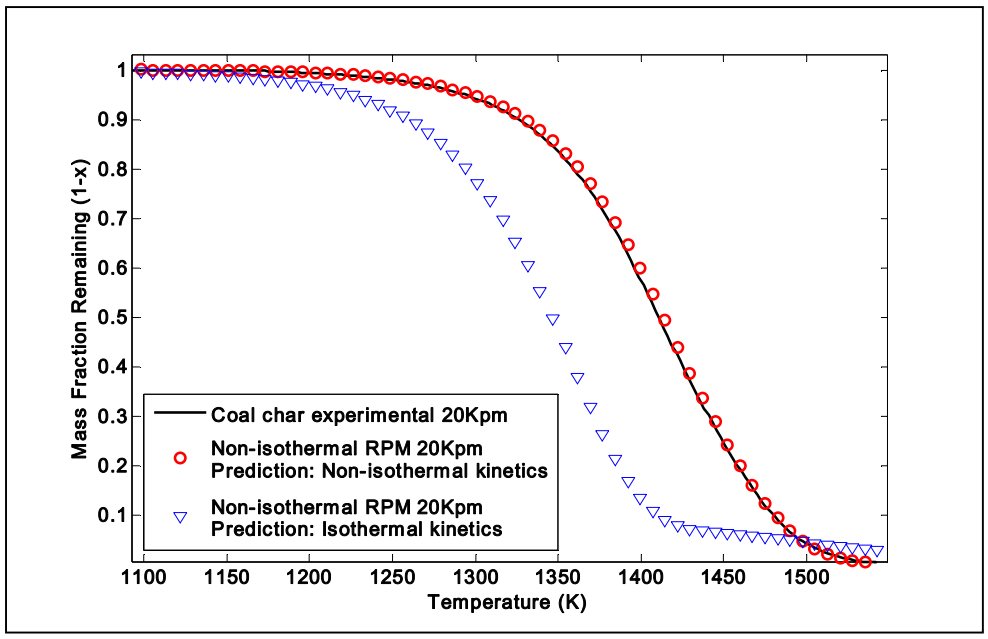

Figure 5.18: Comparison of non-isothermal RPM Fits generated with kinetics derived from non-isothermal and isothermal datasets

It is evident in Figure 5.17 and Figure 5.18 that kinetics determined using non-isothermal data is not necessarily applicable to isothermal reaction behaviour prediction, even when the material reacted is the same. The same can be said for kinetics derived from isothermal data for use in non-isothermal reaction behaviour predictions. As is evident when studying the reactivity of this sample, it is best to use the same heating regimes during experimentation to predict other reaction behaviour. The algorithm developed in chapter 4 is able to process and predict kinetics for both non-isothermal and isothermal data, which renders it a versatile as well as accurate kinetics determination method.

5.6. CO_2-Char Reactivity of a Coal-Biomass Blend

5.6.1. Plain Biomass

It has been established that the algorithm is capable of determining the reaction kinetics of experimental CO_2 reactivity data accurately and can now be used to determine and compare the effects of blending biomass and coal. The biomass being used is finely ground plain pinewood. The fresh pinewood was charred under the same conditions as the plain coal, and reacted in CO_2. The data presented in Figure 5.19 is the CO_2 reactivity data of the plain pinewood char at heating rates of 12, 15 and 20 Kelvin per minute. This data is again not representative of the ash content of the material, since the data has been normalised.

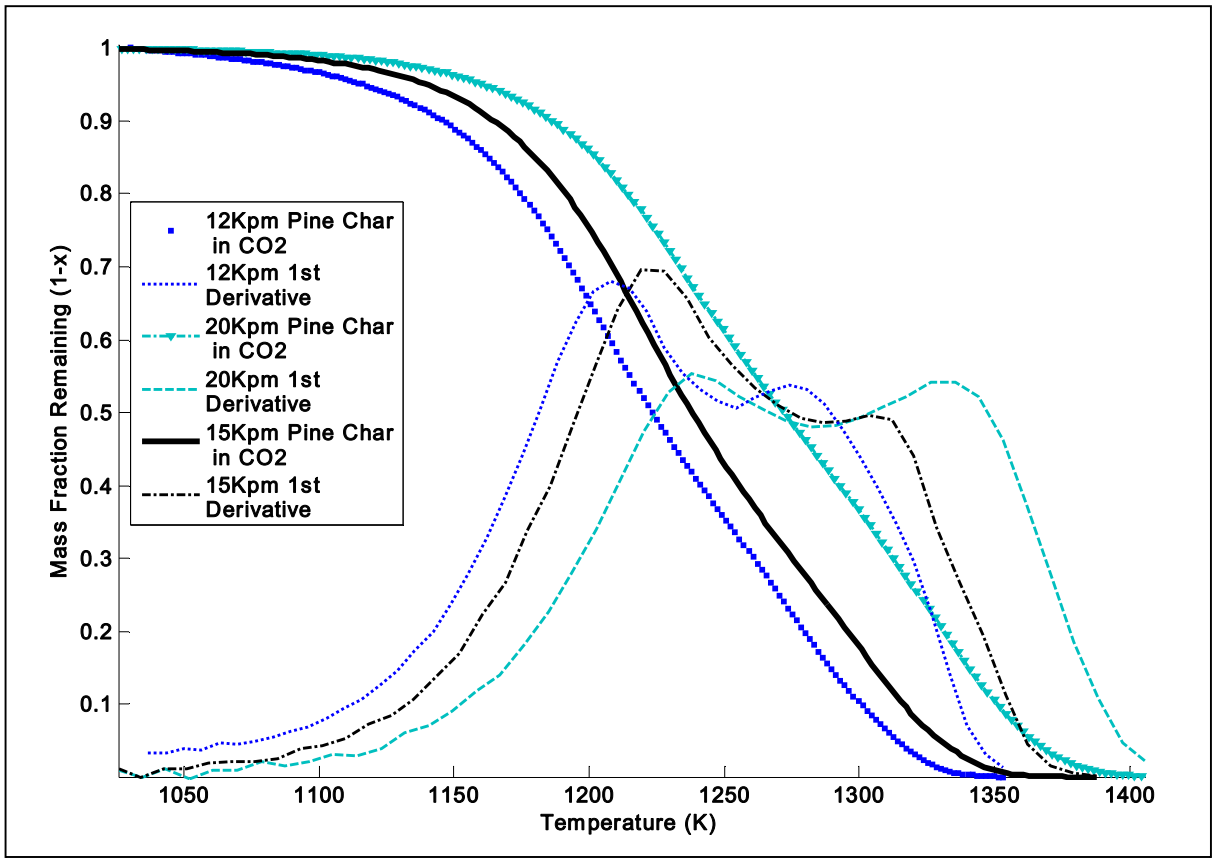

Figure 5.19: Experimental Data for Plain Pine Char in CO_2 at Various Heating Rates

The plain pine char seems to undergo a characteristic reaction with the CO_2, where the reactivity begins and reaction proceeds rapidly before slowing and terminating. From the assessment of the derivative data, it is evident that multiple reactions are occurring. The two

peaks indicate at least 2 distinct reactions are occurring with distinct kinetic parameters. This data was processed by the algorithm in the same way that the plain coal char data was processed.

All combinations of the three heating rate datasets were tested to determine which combination produced the most accurate kinetic parameter values and the most precise fit. The plots of the fits produced from all combinations are presented in Figure 5.20. The kinetic data is presented in Appendix B.

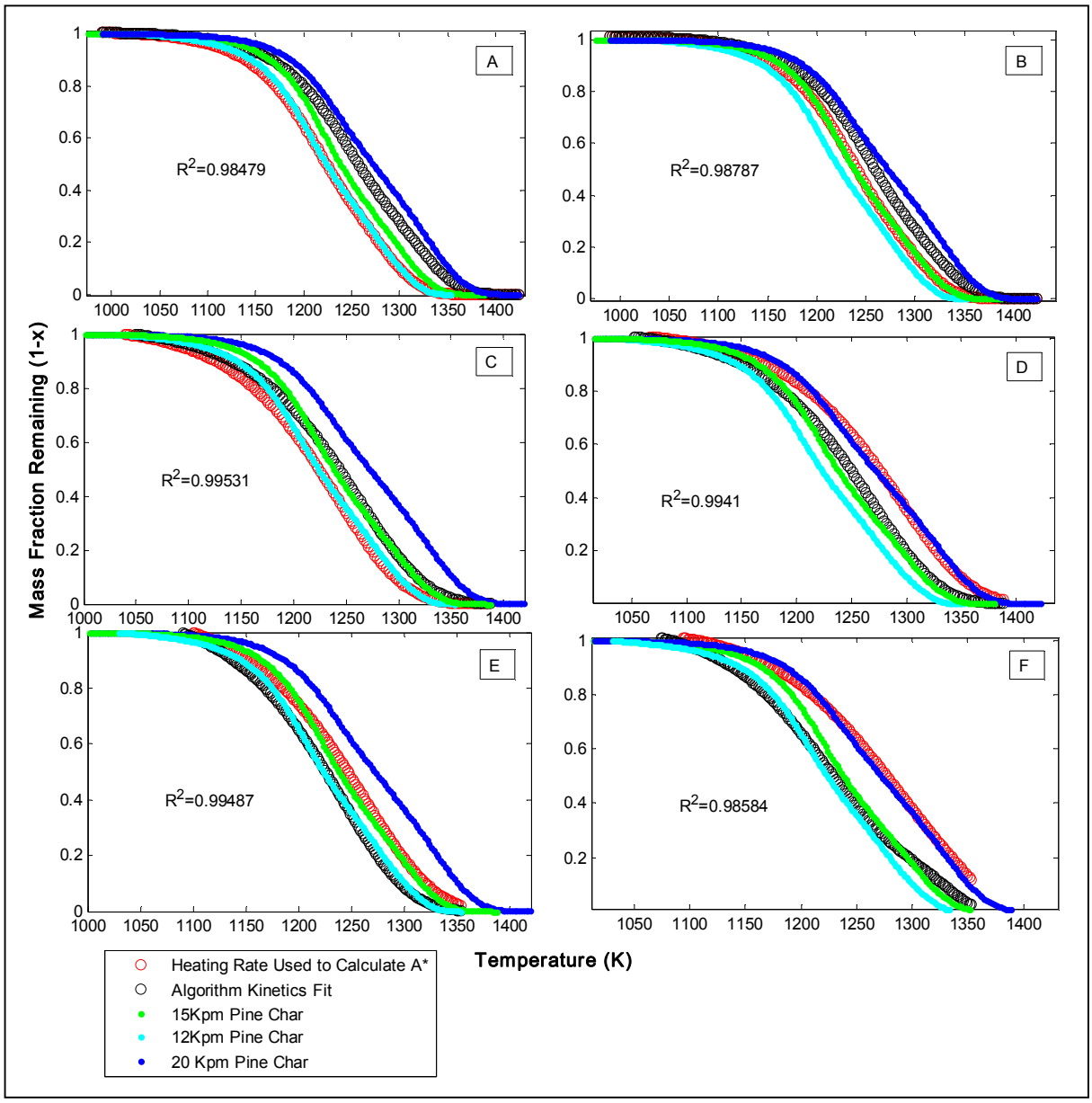

Figure 5.20: All combinations of kinetics determination and 3rd heating-rate reaction prediction for plain pine char-CO2 reactivity data

It is evident in Figure 5.20 that the RPM-modified algorithm was unable to accurately predict the reaction behaviour of plain pine char in CO_2. While all combinations predicted two distinct reactions, as observed from the experimental data, the fits do not correlate with the third independent heating rate data well. The R-squared values for the fits range from R2=0.984 to R2=0.995. It has been established, based on the sensitivity of this statistic that

a value below 0.99 can be regarded as an unsuitable fit. The best fits, unlike for the plain coal data, were achieved when using the highest and lowest heating rate data to predict the intermediate heating rate reaction. The best fit achieved is presented in Figure 5.20C. The deviation between the RPM based predictions and the actual experimental reaction behaviour can be attributed to the selection of reaction model. While the RPM is useful in describing materials that have high pore volume, low pore volume materials are better described by other models such as the shrinking core model (Khalil et al., 2009). Khalil et. al. (2009) found that experimental data from pine char reacting with CO_2 was predicted most accurately with the use of the shrinking core model, while other more porous chars, produced from coal did not correlate well with shrinking core model predictions.

However, given the reasonable fit achieved when predicting the intermediate heating rate, the kinetics found were used only as means of comparison with other kinetic parameter values. If the pine char reactivity were the primary focus, the algorithm would need to be re-written to accommodate the shrinking core model, so that more accurate kinetic parameters could be determined. The best fit identified in Figure 5.20C is presented in Figure 5.21. It is evident that a different model would better predict the behaviour of the plain pine char.

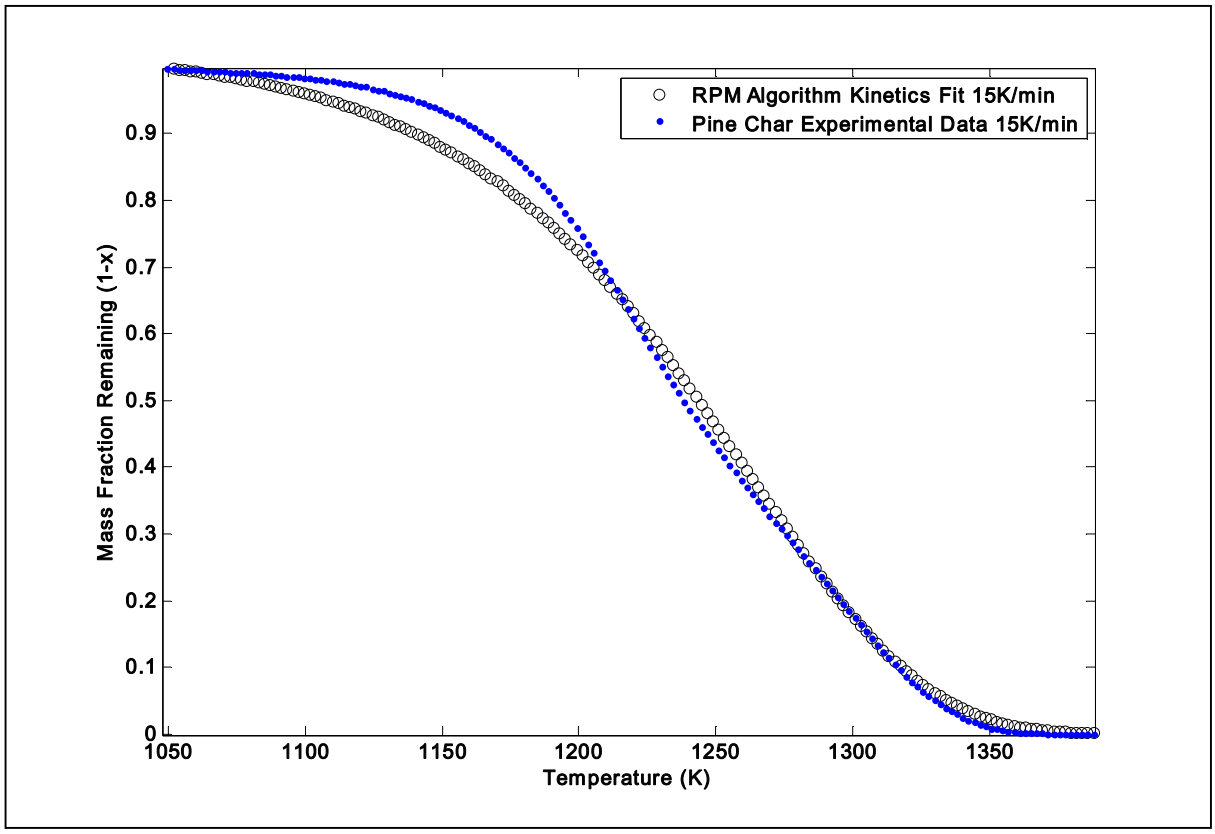

Figure 5.21: Best fit obtained for plain pine char data fitted with RPM algorithm derived kinetics

Table 5.8 presents the kinetic parameters determined by the RPM DAEM-based algorithm. The algorithm results confirm that two distinct reactions are occurring. It must be borne in mind that the algorithm is capable of finding accurate activation energy values independently of any reaction model. These values can hence be considered accurate; the inaccuracy of the kinetics found lies mainly in the value of the pre-exponential factor. Lower activation energy values and lower reaction temperature indicate that the plain pine char is more reactive than the plain coal char.

Table 5.8: Plain Pine Char Reaction Kinetics in CO_2

	Mass Fraction (f_0)	Activation Energy E (kJ/mol)	Grouped Pre-exponential Factor A^* ($s^{-1}.m^{-1}$)	Structural parameter φ
Reaction 1	0.27	115.53	9.25E+01	12.5
Reaction 2	0.73	124.57	1.46E+02	

The kinetics found correlate well with other kinetic parameter results obtained for pine char reactivity in CO_2 (Seo et al., 2010). It indicates that the plain pine char is appreciably more reactive than the plain coal char. This result supports the investigation into whether the blending of the two materials would be beneficial.

What must also be determined is whether they indeed interact and whether the coal char reactivity is catalysed by mixing it with the pine char. This material reacts completely at a much lower temperature than that of the plain coal char. If there is no interaction, one would expect to see the same behaviour observed in Figure 5.19 being exhibited by a portion of the blend's mass occurring at the same temperatures, followed by the remainder of the blend's mass reacting according to the mass-loss observed in Figure 5.14. That is, if no interaction exists between the materials, behaviour described by the additive rule (Fermoso et al., 2010) would be expected. If there is interaction, the material should react smoothly over a temperature range between that of the plain coal and the plain pine char.

5.6.2. Coal-Biomass Blend

The biomass used in this study was pinewood, and to determine the effects of blending, a relatively large mass fraction (50%) of the wood was used. This mass fraction is of the order used in other coal-biomass blending research (Bockelie et al., 2011) but is large compared to viable industrial scale blend fractions. Due to cost of transport and sourcing, it is unlikely that a fraction of this order would be viable commercially, but for the purposes of assessing the effects on reactivity, larger mass fractions are required.

The blend was charred under the same conditions as the plain coal, and treated under the same heating rates to ensure consistency and comparability of the two datasets. The proximate analysis of the coal-pinewood blend is provided overleaf in Figure 5.22 and Table 5.9.

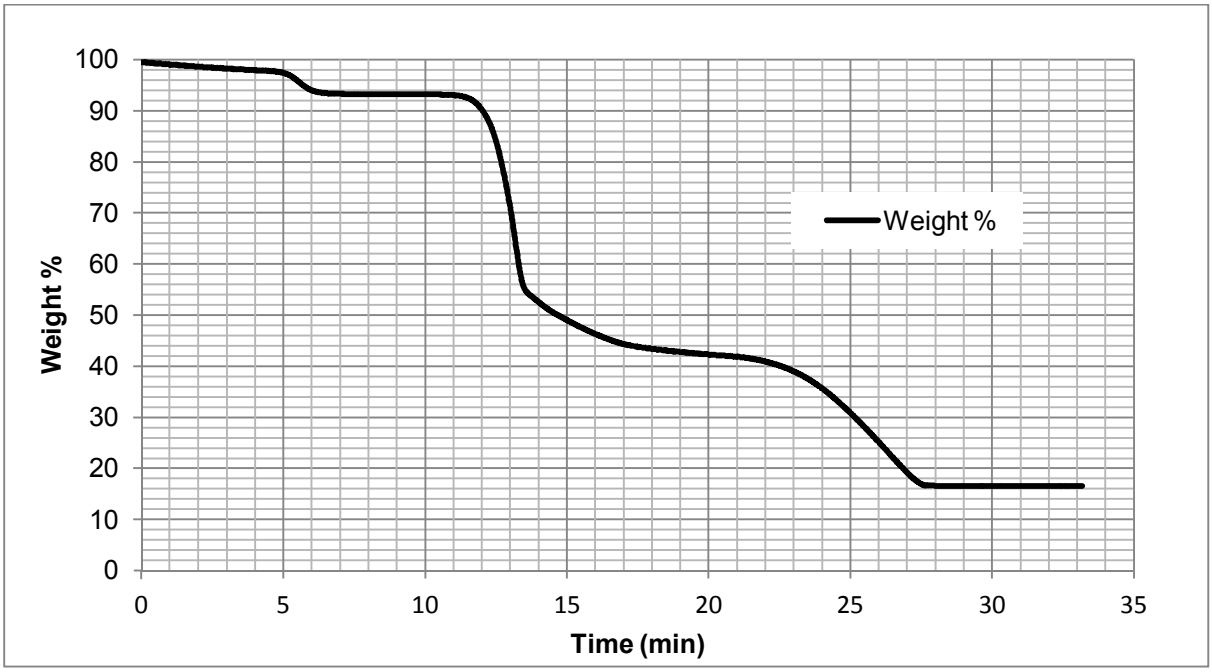

Figure 5.22: 50:50 Coal-Biomass Blend Proximate Analysis

Table 5.9: 50:50 Coal-Biomass Blend Composition

Component	Weight Percentage
moisture	6.23
Volatile matter	50.68
fixed carbon	25.93
Ash Content	17.16
total	**100**

Unlike the coal, the biomass has a significantly smaller ash fraction, as well as a small fixed carbon fraction. To concentrate the mineral content, it may be beneficial to dry the biomass before blending, although in industry, this would add cost and complexity to the process. For this reason, tests were done with raw biomass.

The thermo-gravimetric data produced for the material blend at heating rates of 12K/min, 15K/min and 20K/min are presented in Figure 5.23.

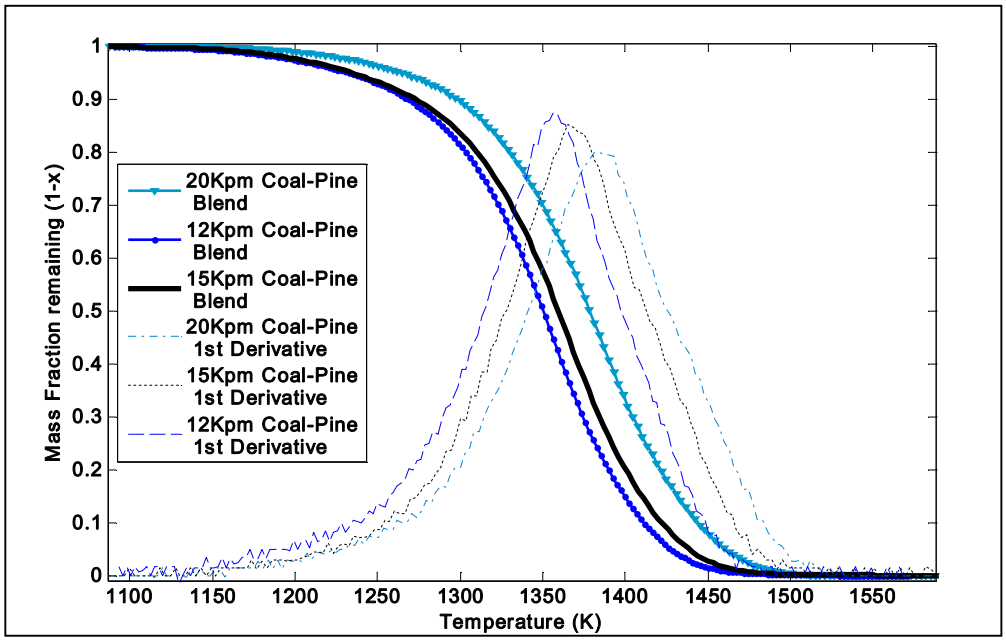

Figure 5.23: 50:50 Coal-Pine Non-isothermal Reaction in CO2 at Various Heating Rates

The steeper derivative thermo-gravimetric (DTG) data and the distinct peak suggest a more dominating reaction, but the change in curvature on the latter slope also suggests multiple reactions may be occurring.

Figure 5.24 presents a comparison between the coal-pine char blend reactivity and the plain coal reactivity at the same heating rate.

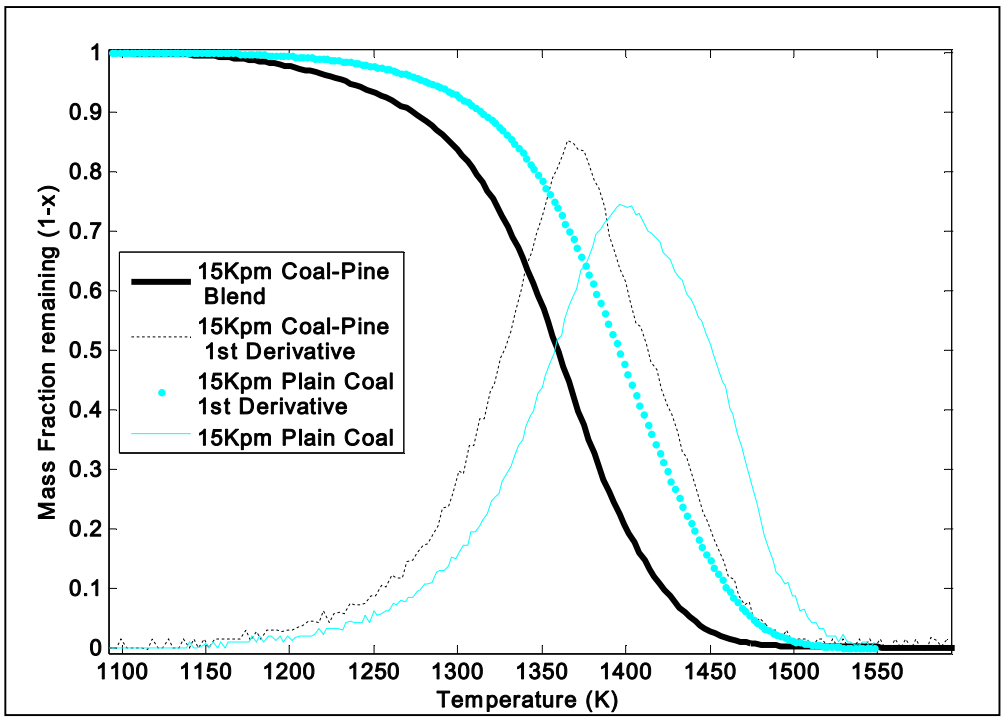

Figure 5.24: Comparison of 15Kpm Data for Plain Coal Char and Coal-Pine Blend Char

It can be seen immediately by examining the DTG data that the reactions occurring between the blend and the CO_2 are different to those of the plain coal. When comparing the two sets

of data directly, it can be seen that the blend reacts at a lower temperature than the plain coal (refer to Figure 5.24). This suggests that overall reactivity of the blend may be higher than that of the plain coal char.

The experimental data was again processed by the RPM DAEM-based algorithm. Since three heating rate datasets were available, each combination was processed and used to simulate data from the third heating rate. The predictions for all the combinations are presented in Figure 5.25. The kinetic data is presented in Appendix B.

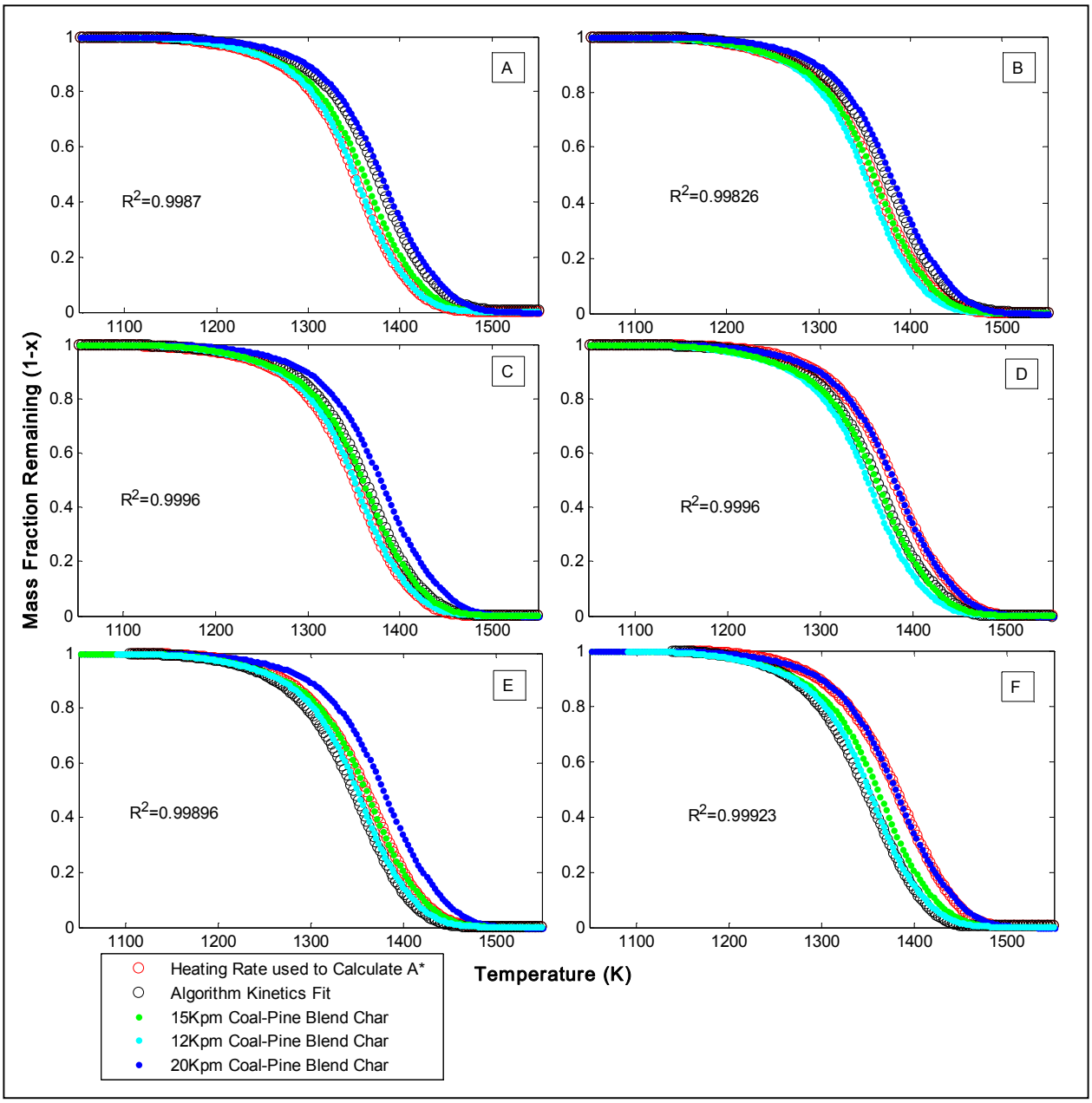

Figure 5.25: All combinations of kinetics determination and 3rd heating-rate reaction prediction for coal-pine blended char-CO_2 reactivity data

Figure 5.25 shows that the RPM DAEM-based algorithm is able to accurately predict the independent heating rate data. For all combinations, the fits correlate well with the experimental data, with the R-squared values ranging from 0.9983 to 0.9996. Unlike the plain coal char, it was found the most accurate fit was achieved by using the lowest and

highest heating rate data to predict the intermediate heating rate reaction. The fit, presented in Figure 5.25C was found to give a high correlation coefficient of R^2=0.9996. It is evident however that any combination would result in an accurate prediction, suggesting that the kinetics determined could be used to predict reaction behaviour under different non-isothermal conditions.

The comparison of the predicted 15K/min reaction and the experimental 15K/min reaction is presented in Figure 5.26. The DTG data also shows good correlation.

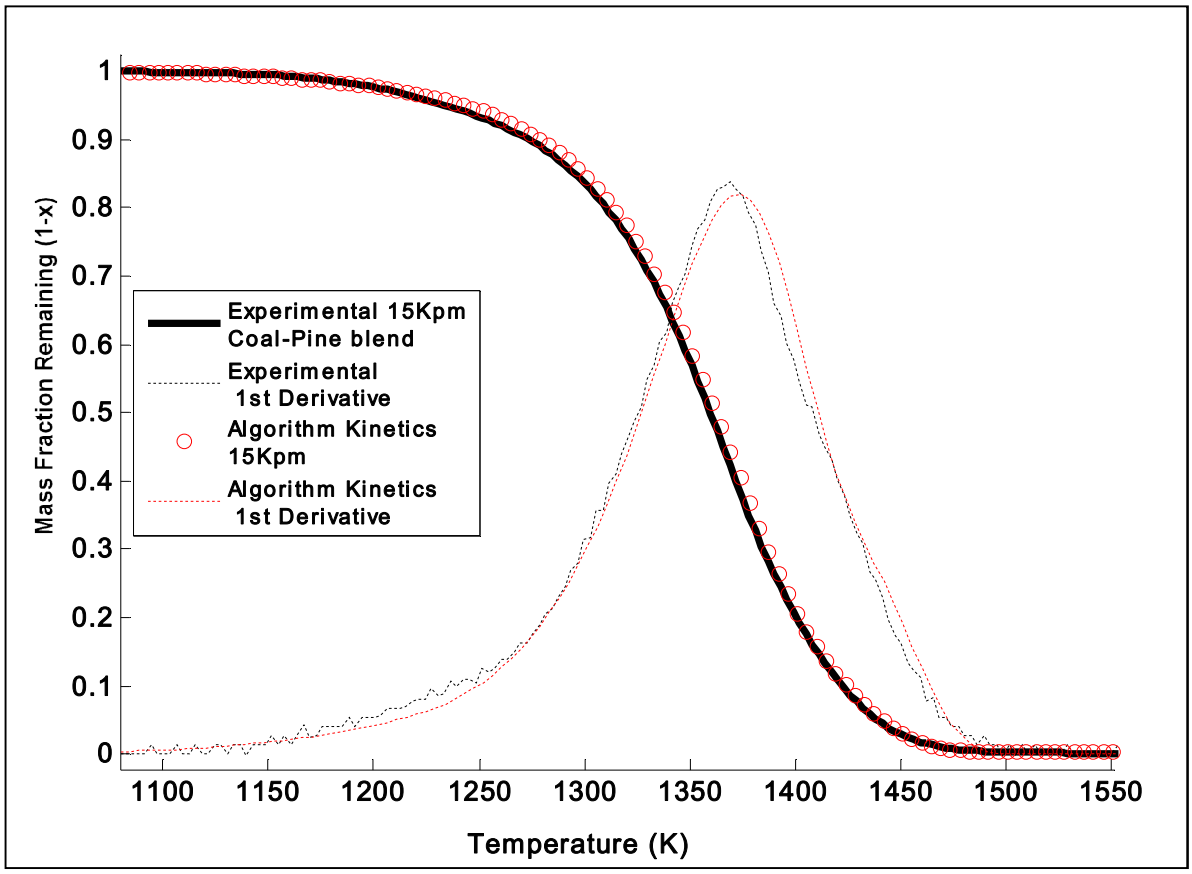

Figure 5.26: Simulated 15K/min Coal-Pine Char Blend in CO_2 Compared to Experimental Data

Despite the precise fit, it can be seen in Figure 5.26 that the multiple reaction prediction's initial reactivity deviates slightly from the experimental data. As explained by Gupta and Bhatia (2000), this is most likely due to differing initial reactivity of the sample, which is not captured by the original random pore model. An even more precise fit may be achieved by adapting the algorithm developed here to incorporate the modified random pore model which accounts both for the finiteness of the structural parameter φ as well as the inhibitory effect of functional groups and surface complexation on initial reactivity (Gupta and Bhatia, 2000). This would however present two more characterisation parameters to the equation which increased the complexity of calculation; or if the parameters are to be found experimentally, would increase the amount of experimental data required to be collected (e.g. mercury porosimetry and various adsorption measurements of the char would be needed). The quality of fit achieved here shows that just one characterisation parameter is sufficient in this instance.

The high correlation coefficient and good visual fit suggest that the kinetics found are indeed reliable and can be used for comparison. The kinetics determined by the algorithm are presented in Table 5.10. All non-zero mass-fraction results are presented. it can be seen that E and A^* values of reactions 4 and 5 are similar, and since they occur at adjacent conversion values and seem to straddle a conversion node, they may be averaged (weighted according to mass fraction) and considered to be one reaction. The first 3 reactions represent an almost negligible fraction of the total reacted mass, but are necessary to ensure good simulation of other heating rates. For the purposes of analysis and discussion, the kinetics presented in Table 5.11 will be used. The value of the structural parameter found during the regression analysis was φ=11.7.

Table 5.10: Coal-Pine Char CO_2 reactivity as determined by the DAEM-Based algorithm

	Mass Fraction (f_0)	Activation Energy E (kJ/mol)	Grouped Pre-exponential Factor A^* ($s^{-1}.m^{-1}$)
Reaction 1	0.003	305.6	1.00E-07
Reaction 2	0.009	158.3	1.69E+04
Reaction 3	0.002	181.9	1.31E+05
Reaction 4	0.104	240.6	3.22E+06
Reaction 5	0.567	239.6	2.78E+06
Reaction 6	0.315	259.1	6.59E+06

Table 5.11: Summed and Averaged Reaction Kinetics Found for Coal-Pine Blend Char Reactivity in CO_2

	Mass Fraction (f_0)	Activation Energy E (kJ/mol)	Grouped Pre-exponential Factor A^* ($s^{-1}.m^{-1}$)	Structural parameter φ
Reaction 4-5	0.671	239.8	2.85E+06	11.7
Reaction 6	0.315	259.1	6.59E+06	

The kinetics found and their corresponding mass fractions corroborate the initial assessment of the DTG data observed in Figure 5.23. A large fraction of the material is reacting in reaction 4-5, and the majority of the remaining material react last reaction; these explain the steepness of the DTG curve and the inflection on the latter slope.

In order to assess and compare the kinetics, one must first understand what the parameters represent. The activation energy is the minimum amount energy required to initiate a chemical reaction (Brown et al., 2009). This suggests that a lower activation energy value represents a reaction that occurs more readily, or that the reactants and conditions are more reactive than those with high activation energy. The pre-exponential factor is also referred to as the *frequency factor*. This parameter indicates the number of collisions of particles occurring both with a sufficient amount of energy to initiate a reaction as well as with the correct orientation to facilitate a reaction (Brown et al., 2009). This implies that a large frequency factor represents a higher degree of reactivity than that of a small frequency factor. Here, a grouped factor is reported, but it is grouped with terms that are assumed fairly

constant, and hence the value of the factor can be compared to determine reactivity differences. The mass fractions then identify the fraction of total reactive mass that is reacting with a particular set of kinetic parameters. This is important when simulating multiple reaction scenarios.

When comparing the kinetics of the plain coal char and that of the coal-biomass blend, the differences are not entirely self-evident. If the average E and A^* were taken, the blend would have less reactive kinetics. However, when assessing the mass fractions of each reaction, there is an indication that the blending of coal and biomass in this instance indeed improves reactivity. Table 5.12 presents the kinetic parameter sets founds for the plain coal char and for the coal-pine char blend. Table 5.12 presents the kinetic parameter values found in Table 5.11 for the coal-pine char reactivity and the values found in Table 5.6 for the plain coal reactivity.

Table 5.12: Comparison of Reaction Kinetics of plain coal char and coal-pine char blend

Coal-Pine Char Blend				Plain Coal Char			
f_0	E (kJ/mol)	$A^*(s^{-1}.m^{-1})$	φ	f_0	E (kJ/mol)	$A^*(s^{-1}.m^{-1})$	φ
0.315	259.1	6.59E+06	11.7	0.313	261.8	1.60E+07	12.2
0.671	239.8	2.85E+06		0.315	246.4	2.08E+06	
-	-	-		0.366	227.6	2.75E+05	

It can be seen in Table 5.12 that the blend's activation energy values range between 239.8kJ/mol and 259.1kJ/mol, with the frequency factors ranging between 2.85E+6 and 6.59E+6; the majority of the material (67%) reacts with the more reactive energy of 239.8kJ/mol. Both reactions occur with relatively high frequency factors. The plain coal char activation energy values range between 227.6kJ/mol and 261.6kJ/mol and the frequency factors range between 2.75E+6 and 1.6E+7. The plain coal char reacts in 3 almost equal fractions. The first fraction reacts with a high frequency factor, but also requires a high activation energy 261.6kJ.mol. This reaction can be compared to the 259.1kJ/mol reaction in the blend. The second coal mass fraction reacts with 246.4kJ/mol and an A^* value of 2.08E+6. This reaction can be compared to the main reaction occurring in the blend (E=239.8k/mol and A^*=2.85E+6). For this reaction it can be noted that twice the mass fraction reacts with activation energy of this magnitude ($E_{blend} < E_{coal}$) and the frequency factor of the blend is higher for this reaction than for the plain coal. A major difference between the reactivity of the two materials is the reaction occurring in the plain coal. While this occurs with a relatively lower activation energy which suggests higher reactivity, the frequency factor is significantly lower, indicating a slow reaction. The addition of the biomass seems to eliminate this reaction, possibly by affecting the char formation so that final third of the material reacts in the 239.8k/mol - 2.85E+6$s^{-1}.m^{-1}$ reaction.

What is also evident is that the structural parameter value has been reduced. While the plain coal char had a φ value of 12.2 and the plain pine char had a value of 12.5, the blend's structural parameter is found to be 11.7. According to Bhatia and Perlmutter (1980), a maximum in reaction surface area is achieved by two opposing forces: surface area growth due to pore expansion during reaction, and the progressive collapse of pores as they coalesce during reaction. It has been determined that for materials with φ<2, pore growth is negligible compared to pore coalescence, but for φ>2 maximum surface area due to pore growth occurs. While φ values for both the blend and the plain coal fall within the latter

segment, indicating that pore growth is prevalent, the structural parameter value for the blend is lower. This indicates that a structural change may have occurred as a result of the blending, resulting in a slightly increased occurrence of pore coalescence in the blended char particles. Other research has noted that the structural parameter can be correlated to CO_2 chemisorption and surface area data (Gil et al., 2010; Zhang et al., 2010). Gil et al. (2010), while studying the CO_2 reactivity of plastic waste noted an inverse relation between the CO_2 reaction surface area of the material and the magnitude of the structural parameter φ, where the range of all φ values was also found to be in the pore growth region of $\varphi>2$. While this has not been confirmed, the increased reactivity of the coal-biomass char blend may be attributed to surface area changes.

These findings correlate with that of other studies on coal and biomass char reactivity with CO_2 (Zhu et al., 2008; Song et al., 2011; Vamvuka et al., 2011). Vamvuka et al. (2011) attributed the observed degradation of materials starting at lower temperatures (increased reactivity) to the catalytic effect mineral content in the biomass. The actual structural effects are not discussed, but the observed increase in reactivity may be explained by possible structural changes observed here and in other research (Gil et al., 2010; Zhang et al., 2010). A difference between the observation in their findings and findings in this research is that Vamvuka et al. (2011) observed a clear change in the kinetic parameter values along with the shift in reaction temperature. This was not observed in the results in this research. However, this research differs in that multiple reactions are proposed and the shift in mass related to the different reactions indicates a change in kinetics.

While the kinetics have not shifted significantly in value, the fraction of mass reacting with more reactive kinetics has increased, with a decrease in the structural parameter. The decrease in the structural parameter value suggests structural changes that are believed to improve overall reactivity. The observation made, i.e. that the blended char reacts at a lower temperature and hence requires less energy input to reach completion, has therefore been corroborated.

5.7. Conclusions

A number of significant conclusions can be drawn from the results presented above.

The first is that the DAEM-based algorithm is a reliable and accurate method for determining the kinetics of thermo-gravimetric data, whether isothermal or non-isothermal data. The method has been shown to generate kinetics that result in significantly more accurate simulations of material behaviour than other more popular methods, mainly due to its ability to identify and simulate multiple reactions. An important observation is that while multiple reactions are processed, only one overall structural parameter value is required and calculated, which reduces calculation complexity. Unlike most other approaches that presuppose a single reaction, the DAEM-based algorithm is uniquely able to identify single as well as well multiple reaction scenarios and accurately predict reaction behaviour independent of the data used during the kinetics determination. This approach seems more reliable especially at rapid heating rates where the difference between single and multiple reaction system behaviour is significant.

The algorithm's sensitivity to how available reaction data is paired was assessed. It was found that if more than the minimum of two heating rate/temperature datasets are available,

and all combinations are processed, that the level of accuracy of the predictions can vary with how the data is paired. It was found that is generally best to use lower temperature/heating rate data to predict higher temperature/heating rate behaviour. It was also observed that determining reaction behaviour between the heating rate/temperature limits of the two datasets used produced very accurate, if not the most accurate predictions. The least accurate approach is to attempt to predict reaction behaviour at heating rates/temperatures lower than that of the data used.

Although the RPM DAEM-based algorithm was able to accurately predict plain coal char and coal-pine char blend behaviour accurately, plain pine char reactivity predictions were not entirely accurate. For further use of the RPM there are opportunities to achieve an even higher degree of accuracy, by incorporating additional parameters into the model. The level of accuracy of predictions observed in the coal and coal-pine reactivity results however negates the need for this. Where necessary, the algorithm can be re-written for different models as outlined in Chapter 4 to predict other reaction behaviour more accurately.

A note on ash or inert fraction in the material must be made. Although the ash fraction data was not included in the experimental data fed to the algorithm, the ash fraction is known directly from the experimental data. Not representing the ash does not alter the curvature of the experimental data nor does it change the temperatures at which the reactions occur, therefore the kinetics found from the 'ashless' data are still applicable to the material, which contains ash. The data is normalised for ease of calculation but once the algorithm has determined the kinetics accurately, the ash fraction can be included in the total mass fraction and predictions of the behaviour of the material including the ash content is possible.

When assessing the algorithm's capability to process isothermal and non isothermal data, it was noted that kinetics determined from isothermal data may not be applicable to non-isothermal reactions. Non-isothermal predictions using isothermal data derived kinetics did not correspond well with experimental non-isothermal data; the same is true for the converse scenario. While this assessment is not a basis for conclusively stating that kinetic parameters are not applicable from one scenario to another, it suggests that if possible, it is best to use a method that can process and predict reaction behaviour exclusively for either non-isothermal or isothermal reactions. The algorithm presented in this research is such a method.

With regard to the effects of biomass addition on reactivity, it is evident that the overall reactivity of the blend was higher than that of the plain coal char. This is observed when assessing the temperature range in which the two materials react; the blended char reacts within a lower temperature range, implying higher reactivity. If catalysis is defined strictly as a lowering of activation energy, it may be unfounded to conclude that the fresh pinewood grains mixed with the coal particles resulted in a catalysed reduction of the coal. However, if the total energy required to react the sample is assessed, less energy was required for the reaction to occur when the biomass-coal-char was being reduced, as compared to the plain coal char. Upon assessment of the structural parameters, it was evident that structural changes may have occurred which affected the reactivity of the coal-pine blend. As has been noted, it cannot be conclusively stated that biomass addition improves reactivity for all coal during CO_2 reactivity, further extensive research into the specific blends and mechanisms is required to definitively ascertain whether a true catalytic relationship exists between the biomass and the coal during CO_2 reactivity.

Chapter 6: Conclusions and Recommendations

The aim of this research was to assess the applicability and adaptability of the DAEM-based algorithm to various scenarios beyond its original development. The algorithm was modified to process CO_2 reactivity and under both isothermal and non-isothermal conditions, which follows a different reaction model to that specified in the original algorithm's development. Another aim was to use the algorithm to assess and compare the reactivity of plain coal and coal-biomass blends, using the developed algorithm. The hypotheses and objectives outlined in Chapter 3 are addressed here. Recommendations for further development of this research are also presented. (Note that the poster presented at the 2011 International Pittsburgh Coal Conference as well as the draft journal article prepared for publication is presented in Appendix D.)

6.1. Conclusions

6.1.1. Algorithm development

The first hypothesis states that the algorithm can be modified to process reactions adhering to models other than the first order model. The objective linked to this hypothesis was to confirm the model-independence of the algorithm in determining the activation energy, *E*. Another objective was to develop a method for modifying the algorithm. In Chapter 4, it was determined that the algorithm could indeed determine accurate *E* values, regardless of reaction model, which was also found in Saloojee (2011).

A method for modifying the original algorithm was also formulated in Chapter 4. It was found that as long as the expression for a reaction model could be integrated, it could be used in the algorithm. Two main steps are required to modify the algorithm to incorporate another reaction model. The conversion value that results in a maximum decomposition rate for the specified model must be found. This value is used in the determination of the pre-exponential factor *A*. Then, the integrated model expression must be incorporated when calculating the mass fraction value(s), f_0. The outcome is that the modified algorithm is able to process reaction data for any thermo-chemical process, then identify and predict single as well as multiple reaction behaviour in the process accurately, provided a suitable model was chosen.

The modification method developed can also be followed to modify the algorithm to process isothermal data. It was found that the algorithm could be successfully modified to process and predict isothermal reactions.

6.1.2. Algorithm application

The second hypothesis focuses specifically on accurately determining the behaviour of char-CO_2 reactions, under both isothermal and non-isothermal reactions, using the DAEM-based multiple-reaction approach and the incorporated RPM. Part of the adaptation of the algorithm

to incorporate the RPM was to be able to determine the structural parameter, φ. This was done successfully and used for the experimental data. A generic φ value was used for simulated data.

A series of tests were done and the following conclusions were drawn when testing this hypothesis:

- The algorithm successfully predicted the behaviour of coal char reactivity in CO_2 under isothermal and non-isothermal conditions. Arrhenius parameters found for simulated single reaction RPM data were found to be within 2% relative error, and within 6% for multiple reactions. For experimental data, fits produced using the algorithm derived kinetics consistently had correlation factors of R^2>0.99, indicating precise fits. The multiple reaction observation and accurate data fit using a multiple reaction approach for RPM reactions is a novelty in this field of research.

- When processing char-O_2 partial oxidation reactivity (Sangtong-Ngam and Narasingha, 2008), it was observed from the DTG data that a multiple reaction scenario was likely. The RPM DAEM-based algorithm which determined multiple reaction kinetics produced a more accurate prediction of the reaction behaviour than the single reaction kinetics (determined using Arrhenius plots). It was noted that the multiple reaction kinetic set still only used a single structural parameter, which reduced calculation complexity as well as the number of parameters used to fit the data.

- Using the kinetics found from the Arrhenius plots for both the char-O_2 and char CO_2 reactions and the kinetics found using the DAEM-based algorithm, high heating rate reactions were simulated. It was found that at high heating rates (10^4K/min), reaction behaviour simulated with single reaction kinetics differed appreciably from that of multiple reaction kinetics. It was determined that if multiple reactions are expected to occur, they should be accounted for whenever possible especially for RPM reactions; the algorithm developed here is capable of processing single and multiple reaction systems.

- When comparing the kinetics found for isothermal and non-isothermal reactions of the same material reacting in the same CO_2 atmosphere, it was found that the kinetics found were different. Kinetics determined from one set could not be used to accurately predict the behaviour of the other. It was determined that it is best to use a method that able to independently process and predict behaviour for either system. The modified DAEM-based algorithm is a method that is capable of this.

6.1.3. Biomass

The third hypothesis states that the blending of coal with a suitable biomass would improve the overall reactivity with CO_2. This hypothesis was tested by preparing coal biomass blends and reacting them in CO_2 under the same conditions as the plain coal. The developed algorithm was then used to determine the kinetics and structural parameters and compare them to that of the plain coal. Before the kinetic parameter values were assessed, it was evident that the blended char produced had reacted over a lower temperature compared to the plain coal, which indicated improved reactivity.

Assessment of the kinetics indicated that while the overall range of activation energy had not reduced significantly, the amount of material reacting with the more reactive kinetics within the multiple reaction system had increased after addition of the biomass sample. When assessing the structural parameter, it was determined that the addition of biomass reduced the value of this parameter. This indicates that biomass addition may influence reactivity by means of affecting pore structure during pyrolysis, or during the CO_2 reaction. The structural change, as well the shift in mass fraction and lowered temperature range of reaction all serve to confirm this hypothesis, for this particular sample.

6.2. Recommendations

Opportunities to further the research conducted lie in each phase of the investigation presented here.

The algorithm can be adapted and rewritten for other reaction sub-models such for the shrinking core model, or grain model, for both isothermal and non-isothermal data. An opportunity in the algorithm development phase also lies in developing a more user-friendly graphic user interface (GUI) which would facilitate the processing of different datasets by many different users, without the need to rewrite all the necessary code.

The relationship between isothermal and non-isothermal kinetic data can also be further investigated using the algorithm, to determine the applicability of one set to other heat-treatment regimes.

With regard to assessing the quality of fit, the correlation coefficient could be modified so that it is more sensitive. One could compare the proposed fit to a first-order fit, instead of to the mean of the curve. This would result in a more sensitive factor, which could be analysed more closely.

The algorithm can be used to determine the kinetic parameter values of more coal and biomass blends. Using various coal samples sourced from different mining regions within South Africa, as well as the use of different biomass species and various blend percentages of these materials would help to garner a more detailed understanding of the effects of blending these materials during CO_2 reactivity. These materials could also undergo steam gasification (which is more in line with current industrial practice) and the algorithm could be modified to incorporate a suitable reaction model for this process and be used to determine the kinetics. Further study of the actual mechanisms responsible for the change in reactivity following biomass addition would also be beneficial.

Chapter 7: References

Bhatia, S.K., Perlmutter, D.D., 1980. A random pore model for fluid-solid reactions: I. Isothermal, kinetic control. AIChE Journal 26, 379-386.

Bhatia, S.K., Vartak, B.J., 1996. Reaction of microporous solids: the discrete random pore model. Carbon 34, 1383–1391.

Bockelie, M., Davis, K., Fry, A., Sarofim, A., Claxton, C., Whitty, K., 2011. Enhanced Methane Production By Co-Gasification of Potassium-Rich Biomass and Coal, in: International Pittsburgh Coal Conference. pp. 1-20.

Braun, R.L., Burnham, a. K., 1987. Analysis of chemical reaction kinetics using a distribution of activation energies and simpler models. Energy & Fuels 1, 153-161.

Brink, J., Marx, S., Waanders, F., 2011. Sustainability And Environment Integrated Btl Process As Potential Solution, in: International Pittsburgh Coal Conference. pp. 2-8.

Brown, T., LeMay, H., Bursten, B., 2009. Chemistry: The Central Science, Internatio. ed. Pearson Prentice Hall.

Draper, N.R. (University of W., Smith, H. (Mount S.S. of M., 1981. Applied Regression Analysis, 2nd ed. John Wiley & Sons Inc., New York, USA.

Everson, R., Neomagus, H., Kaitano, R., Falcon, R., Ducann, V., 2008. Properties of high ash coal-char particles derived from inertinite-rich coal: II. Gasification kinetics with carbon dioxide. Fuel 87, 3403-3408.

Everson, R., Neomagus, H., Kasaini, H., Njapha, D., 2006. Reaction kinetics of pulverized coal-chars derived from inertinite-rich coal discards: Gasification with carbon dioxide and steam. Fuel 85, 1076-1082.

Everson, R.C., Neomagus, H.W.J.P., Njapha, D., 2006. Kinetic analysis of non-isothermal thermogravimetric analyser results using a new method for the evaluation of the temperature integral and multi-heating rates. Fuel 85, 418-422.

Farmer, J., Turk, B., Gupta, R., Trembly, J., 2011. Determination of the Effect of Coal / Biomass-Derived Syngas Contaminants on the Performance of Fischer-Tropsch and Water- Gas-Shift Catalysts, in: International Pittsburgh Coal Conference.

Feng, B., Bhatia, S.K., 2002. On the validity of thermogravimetric determination of carbon gasification kinetics. Chemical Engineering Science 57, 2907-2920.

Fermoso, J., Gil, M.V., Pevida, C., Pis, J.J., Rubiera, F., 2010. Kinetic models comparison for non-isothermal steam gasification of coal–biomass blend chars. Chemical Engineering Journal 161, 276-284.

Gil, M.V., Fermoso, J., Pevida, C., Pis, J.J., Rubiera, F., 2010. Intrinsic char reactivity of plastic waste (PET) during CO_2 gasification. Fuel Processing Technology 91, 1776-1781.

GraphPad Software Inc, 1999. How Good is the Fit [WWW Document]. URL http://graphpad.com/curvefit/goodness_of_fit.htm

Gupta, J., Bhatia, S.K., 2000. A modified discrete random pore model allowing for different initial surface reactivity. Carbon 38, 47-58.

Hla, S.S., Roberts, D.G., Harris, D.J., 2011. Using Fundamental Data to Model Entrained Flow Gasification : Impacts of Coal Type on Gasifier Performance, in: International Pittsburgh Coal Conference.

Instruments, T., 2010. Comprehensive Thermal Analysis Brochure.

Irfan, M.F., Usman, M.R., Kusakabe, K., 2011. Coal gasification in CO_2 atmosphere and its kinetics since 1948: A brief review. Energy 36, 12-40.

Joseph, K., 2000. Kinetics of thermal decomposition of Th(C2O4)2·6H2O. Journal of Nuclear Materials 281, 129-139.

Khalil, R., Ja, S., Grønli, M.G., Hustad, J., 2009. CO 2 Gasification of Biomass Chars: A Kinetic Study. Science 94-100.

Kirtania, K., 2011. Pyrolysis and Gasification Reactivity of Brown Coal-Algae Blends, in: International Pittsburgh Coal Conference.

Kirubakaran, V., Sivaramakrishnan, V., Nalini, R., Sekar, T., Premalatha, M., Subramanian, P., 2009. A review on gasification of biomass. Renewable and Sustainable Energy Reviews 13, 179-186.

Koch, E., 1977. Non-Isothermal Reaction Analysis. Academic Press Inc. (London) Ltd., London, (UK).

Koga, N., 1994. A review of the mutual dependence of Arrhenius parameters evaluated by the thermoanalytical study of solid-state reactions: The kinetic compensation effect. Thermochimica acta 244.

Kumar, A., Jones, D.D., Hanna, M. a., 2009. Thermochemical Biomass Gasification: A Review of the Current Status of the Technology. Energies 2, 556-581.

Liu, H., 2004. Effect of pyrolysis time on the gasification reactivity of char with CO_2 at elevated temperatures. Fuel 83, 1055-1061.

Lua, A.C., Su, J., 2006. Isothermal and non-isothermal pyrolysis kinetics of Kapton® polyimide. Polymer Degradation and Stability 91, 144-153.

Means, N.C., 2011. NETL ' s FY11 In-house Research: Advanced Gasification Program, in: International Pittsburgh Coal Conference.

Miles, T.R., Miles, T.R.J., Baxter, L.L., Jenkins, B.M., Oden, L.L., 1993. Alkali Slagging Problems with Biomass Fuels, in: First Biomass Conference of the Americas: Energy, Environment, Agriculture, and Industry, Volume 1.

Miura, K., 1995. A New and Simple Method to Estimate f(E) and k0(E) in the Distributed Activation Energy Model from Three Sets of Experimental Data. Energy & Fuels 9, 302-307.

Miura, K., Maki, T., 1998. A Simple Method for Estimating f (E) and k_0 (E) in the Distributed Activation Energy Model. Energy & Fuels 12, 864-869.

Navarro, M.V., Aranda, a., Garcia, T., Murillo, R., Mastral, a. M., 2008. Application of the distributed activation energy model to blends devolatilisation. Chemical Engineering Journal 142, 87-94.

Pitt, G.J., 1962. The Kinetics of the Evolution of Volatile Products From Coal. Fuel 41, 264-274.

Please, C., McGuiness, M.J., McElwain, D.L.S., 2003. Approximations to the distributed activation energy model for the pyrolysis of coal. Combustion and Flame 133, 107-117.

Ravindran, P., Rangarajan, J., Sundaram, A.K., 1989. Kinetics of dehydration reactions-A comparison between isothermal and non-isothermal studies. Thermochimica Acta 147, 331-345.

Sadhukhan, A.K., Gupta, P., Saha, R.K., 2010. Modelling of combustion characteristics of high ash coal char particles at high pressure: Shrinking reactive core model. Fuel 89, 162-169.

Saloojee, F., 2011. Kinetics of pyrolysis and combustion of a south african coal using the distributed activation energy model. MSc Dissertation, University of the Witwatersrand, Johannesburg, RSA.

Sangtong-Ngam, K., Narasingha, M.H., 2008. Kinetic Study of Thai-lignite Char Gasification Using the Random Pore Model. Thammasat Int. J. Sc. Tech. 13, 16-26.

Scott, S., Dennis, J., Davidson, J., Hayhurst, a, 2006. An algorithm for determining the kinetics of devolatilisation of complex solid fuels from thermogravimetric experiments. Chemical Engineering Science 61, 2339-2348.

Seo, D.K., Lee, S.K., Kang, M.W., Hwang, J., Yu, T.-U., 2010. Gasification reactivity of biomass chars with CO2. Biomass and Bioenergy 34, 1946-1953.

Serra, R., 1998. A new method for the kinetic study of thermoanalytical data: The non-parametric kinetics method. Thermochimica Acta 316, 37-45.

Sipila, K., 1993. New power-production technologies: Various options for biomass and cogeneration. Bioresource technology 46, 5-12.

Song, H., Boggs, C., Akunuri, N., Turk, B., Gupta, R., Trembly, J., 2011. Catalytic CO_2 Char Gasification for Commercial Materials Production Center for Energy Technology CO_2 Utilization Vs . CO_2 Emissions, in: International Pittsburgh Coal Conference.

Starink, M., 2003. The determination of activation energy from linear heating rate experiments: a comparison of the accuracy of isoconversion methods. Thermochimica Acta 404, 163-176.

Su, J.L., Perlmutter, D., 1985. Effect of pore structure on char oxidation kinetics. AIChE journal 31, 973–981.

Vamvuka, D., Karouki, E., Sfakiotakis, S., 2011. Gasification of waste biomass chars by carbon dioxide via thermogravimetry. Part I: Effect of mineral matter. Fuel 90, 1120-1127.

Vyazovkin, S., 1997. Advanced isoconversional method. Journal of Thermal Analysis and Calorimetry 49, 1493-1499.

World Coal Institute (WCI), n.d. The Coal Resource: a comprehensive overview of coal, Energy. London.

Zhang, Y., Hara, S., Kajitani, S., Ashizawa, M., 2010. Modeling of catalytic gasification kinetics of coal char and carbon. Fuel 89, 152-157.

Zhu, W., Song, W., Lin, W., 2008. Catalytic gasification of char from co-pyrolysis of coal and biomass. Fuel Processing Technology 89, 890-896.

Chapter 8: Appendices

Appendix A: TGA Sequences

The detailed sequences programmed into the TGA control sequences are given below. The proximate analysis sequence is given first.

TA Instruments Thermal Analysis -- DSC-TGA Standard

Method Log:
1: Select Gas: 1
2: Mass flow 70.0 mL/min
3: Equilibrate at 25.00°C
4: Isothermal for 4.00 min
5: Ramp 80.00°C/min to 110.00°C
6: Isothermal for 4.00 min
7: Ramp 80.00°C/min to 700.00°C
8: Isothermal for 4.00 min

The sequence up to this point just establishes a baseline measure for the mass at ambient temperature. It then heats rapidly up to the point at which moisture can be driven out of the material and is held there. Then the material is heated again and held to eliminate volatile matter. This is done under “gas 1”, which is ultra high purity Nitrogen.

9: Select Gas: 2
10: Mass flow 70.0 mL/min
11: Ramp 80.00°C/min to 1000.00°C
12: Isothermal for 8.00 min

The remaining fixed carbon and ash are then reacted in “gas 2” which is dry air.

13: Select Gas: 1
14: Mass flow 70.0 mL/min
15: Isothermal for 1.00 min
16: End of method

The inert carrier is again selected to purge the furnace of any remaining combustion by-product, and the run is ended.

The next sequence produces the char and reacts the char in Carbon Dioxide.

TA Instruments Thermal Analysis -- DSC-TGA Standard

Method Log:
1: Select Gas: 1
2: Mass flow 70.0 mL/min
3: Ramp 20.00°C/min to 1250.00°C
4: Mark end of cycle 1
5: Data storage: Off
6: Select Gas: 1
7: Mass flow 40.0 mL/min
8: Air cool: On

9: Air cool: On
10: Air cool: Off
11: Equilibrate at 700.00°C
12: Air cool: Off
13: Isothermal for 15.00 min

Up to this point, the material is being treated in an inert atmosphere (nitrogen). It is slowly heated and then slightly cooled and held to ensure that all volatile matter is removed. The heating rate was limited by the safe operating threshold for the equipment; the maximum heating rate when heating above 1000°C is 25K/min. a 20% safety margin was observed, and the 20K/min rate was used. Once this is done, the CO_2 reactivity can commence.

14: Select Gas: 1
15: Mass flow 5.0 mL/min
16: External event: On
17: Isothermal for 1.00 min
18: Data storage: On

The CO_2 was fed to the furnace environment and was hence controlled by the "external event" command. The gas flow cannot be zero, hence gas 1 was set to 5ml/min. The CO_2 flowrate was set externally to 60ml/min. The data strorage only commences after a minute, after the external flowrate of CO_2 has stabilised.

19: Ramp 20.00°C/min to 1350.00°C
20: Isothermal for 1.00 min
21: Data storage: Off
22: Mark end of cycle 2
23: External event: Off
24: Select Gas: 1
25: Mass flow 60.0 mL/min
26: Isothermal for 1.00 min
27: End of method

The temperature is then ramped at the desired heating rate (20K/min≡20°C/min shown here) to the desired temperature (observed temperature at which the reaction reached completion). The isothermal command is used to ensure that the unti reaches the specified temperature and does not heat passed the specified temperature, since it is close to the upper limit of safe operation of the unit (1500°C). The reactive gas is shut off, the inert gas is then increased to purge the furnace area and the run is ended.

This sequence was used for all non-isothermal experiments; only the heating rate in step 19 was altered.

The final sequence is the isothermal sequence.

Method Log:
1: Select Gas: 1
2: Mass flow 70.0 mL/min
3: Ramp 20.00°C/min to 1250.00°C
4: Mark end of cycle 1
5: Data storage: Off
6: Select Gas: 1
7: Mass flow 40.0 mL/min
8: Air cool: On
9: Air cool: On

10: Air cool: Off
11: Equilibrate at 700.00°C
12: Air cool: Off
13: Isothermal for 15.00 min
14: Select Gas: 1
15: Mass flow 5.0 mL/min
16: External event: On
17: Isothermal for 1.00 min
18: Data storage: On

The sequence up to this point is identical to the non-isothermal sequence, since the aim was to produce the char in the same way for all experiments.

19: Jump to 1050.00°C
20: Isothermal for 70.00 min
21: Data storage: Off
22: Mark end of cycle 2
23: External event: Off

Instead of a temperature ramp, the unit was set to jump to the required temperature as quickly as possible, and maintain the temperature for the desired time (the observed time in which the reaction reached completion).

24: Select Gas: 1
25: Mass flow 60.0 mL/min
26: Isothermal for 0.50 min
27: End of method

Again the reactive gas is shut off, the inert gas is then increased to purge the furnace area and the run is ended.

Appendix B: Kinetics Determined for all Dataset combinations

The tables, Table A1, Table A2, Table A3 and Table A4 present all the kinetic parameter sets determined by the algorithm. Each set is produced by using a particular combination of heating rate data for each set of experimental data captured for the various materials and conditions used in the research.

Table A1: Data for all combinations of char-O_2 data

Heating Rate Data Used (Heating Rate Data used to calculate A*)	Heating Rate Data Predicted	Initial Mass Fraction (f0)	Activation Energy E (kJ/mol)	Grouped Pre-Exponential Factor A* (s-1.m-1)	Candidate Reaction no.	Structural Factor	R-Squared
2Kpm		0.00	45.61	1.39E+01	2	18.918	0.99846
(5Kpm)	10Kpm	0.02	104.21	4.18E+05	5		
		0.19	125.72	3.57E+06	27		
		0.52	149.95	7.89E+07	47		
		0.16	151.85	9.58E+07	48		
		0.10	310.62	9.32E+18	50		
2Kpm		0.01	305.57	1.00E-07	1	13.323	0.99814
(10Kpm)	5Kpm	0.00	72.89	3.67E+03	2		
		0.01	104.80	9.28E+05	3		
		0.05	120.18	3.09E+06	13		
		0.42	146.39	7.59E+07	40		
		0.06	156.72	3.17E+08	45		
		0.04	159.89	4.94E+08	46		
		0.41	175.73	4.39E+09	49		
5Kpm		0.01	45.19	1.28E+01	2	16.841	0.98881
(2Kpm)	10Kpm	0.01	107.23	5.09E+05	7		
		0.01	107.25	4.49E+05	8		
		0.19	125.00	3.49E+06	25		
		0.33	143.60	3.55E+07	44		
		0.11	146.52	5.41E+07	45		
		0.30	162.38	4.70E+08	49		
		0.03	300.22	1.80E+18	50		
5kpm		0.01	305.57	1.00E-07	1	9.9366	0.96854
(10Kpm)	2Kpm	0.00	106.32	2.45E+06	2		
		0.01	99.24	3.24E+05	3		
		0.01	122.82	5.79E+06	11		
		0.05	124.76	7.51E+06	12		
		0.32	159.89	9.24E+08	35		
		0.26	171.75	3.76E+09	45		
		0.08	177.15	8.38E+09	46		
		0.26	189.14	3.86E+10	49		
10Kpm		0.00	305.57	1.00E-07	1	10.233	0.98645
(5Kpm)	2Kpm	0.02	99.78	2.48E+05	4		
		0.01	108.13	8.90E+05	5		
		0.19	138.57	4.57E+07	22		
		0.06	163.83	1.20E+09	43		
		0.51	165.93	1.59E+09	44		
		0.20	199.75	1.93E+11	50		
10Kpm		0.01	305.57	1.00E-07	1	25.563	0.98571
(2Kpm)	5Kpm	0.01	70.70	2.42E+03	2		
		0.01	114.65	1.88E+06	8		
		0.00	116.99	2.08E+06	11		
		0.02	118.98	2.73E+06	12		
		0.04	136.30	2.36E+07	28		
		0.18	137.59	2.83E+07	29		
		0.03	147.70	8.74E+07	42		
		0.49	160.89	5.62E+08	47		
		0.20	203.90	3.74E+11	50		

Table A2: Data for all combinations of char-CO_2 data

Heating Rate Data Used (Heating Rate Data used to calculate A*)	Heating Rate Data Predicted	Initial Mass Fraction (f0)	Activation Energy E (kJ/mol)	Grouped Pre-Exponential Factor A* (s-1.m-1)	Candidate Reaction no.	Strucutral Factor	R-Squared
12kpm		0.06	261.96	1.69E+07	33	12.221	0.9998
(15Kpm)	20Kpm	0.25	261.70	1.57E+07	34		
		0.07	248.91	2.71E+06	45		
		0.24	245.64	1.89E+06	46		
		0.37	227.61	2.75E+05	49		
		0.01	305.57	5.04E+07	50		
12kpm		0.14	261.92	1.60E+07	34	16.026	0.9995
(20Kpm)	15Kpm	0.13	260.08	1.29E+07	35		
		0.17	239.86	1.23E+06	45		
		0.03	236.06	8.23E+05	46		
		0.51	211.02	6.66E+04	49		
		0.02	305.57	5.04E+07	50		
15kpm		0.00	273.44	7.91E+08	3	14.127	0.9994
(12Kpm)	20Kpm	0.08	260.15	1.30E+07	35		
		0.23	259.53	1.17E+07	36		
		0.13	251.35	3.59E+06	44		
		0.55	227.45	2.73E+05	49		
15Kpm		0.29	259.95	1.28E+07	35	14.097	0.99793
(20Kpm)	12Kpm	0.31	223.60	2.61E+05	47		
		0.36	199.23	2.49E+04	49		
		0.04	149.71	2.25E+02	50		
20Kpm		0.28	254.73	6.90E+06	38	15.989	0.9997
(12Kpm)	15Kpm	0.03	252.87	5.54E+06	39		
		0.67	210.81	6.56E+04	49		
		0.01	387.92	4.19E+10	50		
20Kpm		0.31	259.97	1.28E+07	35	10.679	0.9996
(15Kpm)	12Kpm	0.44	223.62	2.62E+05	47		
		0.25	199.25	2.49E+04	49		

Table A3: Data for all combinations of pine-char data

Heating Rate Data Used (Heating Rate Data used to calculate A*)	Heating Rate Data Predicted	Initial Mass Fraction (f0)	Activation Energy E (kJ/mol)	Grouped Pre-Exponential Factor A* (s-1.m-1)	Candidate Reaction no.	Strucutral Factor	R-Squared
12kpm		0.42	189.63	2.33E+05	33	11.835	0.98787
(15Kpm)	20Kpm	0.60	169.46	1.10E+04	49		
12kpm		0.10	118.11	1.17E+02	41	13.172	0.9941
(20Kpm)	15Kpm	0.06	121.37	1.49E+02	42		
		0.86	126.03	1.66E+02	49		
15kpm		0.24	182.22	1.27E+05	31	11.908	0.98479
(12Kpm)	20Kpm	0.14	184.75	1.53E+05	32		
		0.62	168.36	9.96E+03	49		
15Kpm		0.24	182.22	1.27E+05	31	21.455	0.98584
(20Kpm)	12Kpm	0.14	184.75	1.53E+05	32		
		0.62	168.36	9.96E+03	49		
20Kpm		0.27	115.53	9.25E+01	41	12.549	0.99531
(12Kpm)	15Kpm	0.73	124.57	1.46E+02	49		
20Kpm	12Kpm	1.05	103.88	2.05E+01	49	13.005	0.99487
(15Kpm)							

Table A4: Data for all combinations of coal-pine blended char data

Heating Rate Data Used (Heating Rate Data used to calculate A*)	Heating Rate Data Predicted	Initial Mass Fraction (f0)	Activation Energy E (kJ/mol)	Grouped Pre-Exponential Factor A* (s-1.m-1)	Candidate Reaction no.	Structural Factor	R-Squared
12kpm (15Kpm)	20Kpm	0.01	610.95	6.41E+24	2	5.7263	0.99827
		0.01	800.00	1.87E+32	3		
		0.01	800.00	4.73E+31	4		
		0.00	800.00	1.80E+31	5		
		0.00	600.64	4.23E+22	6		
		0.01	400.18	5.63E+13	11		
		0.01	390.19	1.91E+13	12		
		0.11	303.26	1.47E+09	32		
		0.38	301.49	1.19E+09	33		
		0.12	296.91	3.69E+08	44		
		0.22	298.97	4.01E+08	45		
		0.12	307.13	4.17E+08	49		
		0.01	68.55	1.57E-01	50		
12kpm (20Kpm)	15Kpm	0.42	242.11	3.90E+06	39	11.319	0.9996
		0.23	240.99	3.33E+06	40		
		0.35	259.24	6.64E+06	49		
15kpm (12Kpm)	20Kpm	0.01	609.13	5.33E+24	2	6.9932	0.9987
		0.01	800.00	2.01E+32	3		
		0.00	800.00	5.25E+31	4		
		0.00	800.00	1.85E+31	5		
		0.00	600.60	4.22E+22	6		
		0.00	495.05	1.12E+18	7		
		0.01	399.99	5.53E+13	11		
		0.04	301.29	1.17E+09	33		
		0.45	301.59	1.14E+09	34		
		0.01	296.80	3.65E+08	44		
		0.30	298.88	3.97E+08	45		
		0.14	307.09	4.16E+08	49		
		0.01	71.75	2.10E-01	50		
15Kpm (20Kpm)	12Kpm	0.00	305.57	1.00E-07	1	16.867	0.99923
		0.28	209.97	1.90E+05	42		
		0.23	209.63	1.73E+05	43		
		0.48	233.35	7.33E+05	49		
20Kpm (12Kpm)	15Kpm	0.003	305.57	1.00E-07	1	11.704	0.9996
		0.009	158.31	1.69E+04	3		
		0.002	181.94	1.31E+05	4		
		0.104	240.62	3.22E+06	40		
		0.567	239.64	2.78E+06	41		
		0.315	259.14	6.59E+06	49		
20Kpm (15Kpm)	12Kpm	0.00	305.57	1.00E-07	1	12.013	0.99896
		0.13	209.97	1.90E+05	42		
		0.55	209.63	1.73E+05	43		
		0.31	233.35	7.33E+05	49		

Appendix C: Matlab Code

All the code used for data simulation and kinetics determination are presented and annotated here. The code is presented in the order used in Chapters 4 and 5.

The first simulation is that of first-order reactions. This is done using the *orates* function.

```
 function c=orates(f0,T0,E,PE,b,Tup,m)
%% Instructions
% f0 - mass fraction. Input as column vector. Last element is ash fraction
% E, PE - Activation energy and Pre-exp. factor. Input as row. should have
%       1 less element than f0.
%b - heating rate K/min
%T0, Tup - Min and Max temperature respectively
%m - number of simulation points within the temperature range.

%% Simulating Data
B=b/60;%K/sec
s=size(E');
nn=s(:,1);
T=linspace(T0,Tup,m);

for i=1:m
    for j=1:nn
        %B(j)=0.1*T(i)/60;
        %B(j)=B2100(T(i))/60;
        term1(j)=quad(@term,T0,T(i),[],[],E(j));
        chi2(i,j)=exp((-PE(j)/B)*(term1(j)));
        chi2(i,nn+1)=1;
        %chi2(1,1)=1;
    end
end

M=chi2*f0;
c=[T' M];
%% Plotting Data and Derivative

x=c(:,1);y=100.*c(:,2);
deriv=-diff(y)./diff(x);
x=x(2:length(x));

hold on
plot(T,M,'b.');
plot(x,deriv,'b')
 end
```

The section labelled “instructions” describes the required input. Another function is then needed to use this file to produce and process the data using the algorithm to determine the kinetics. This is called the scotteg2

```
function c = scotteg2(nrxns,rnTGA,nTGA,b1,b2,T0, Tf);
%% uses algorithm to determine f0 E & PE
%% Instructions
% nrxns - number of simulated reactions
% nTGA, rnTGA - number of simulated TGA and the reduced number TGA points,
%       included for anticipation for large datasets obtained from a TGA
% b1, b2 - Heating rates, specified in K/min
%T0, Tf - Initial and Final Temperature
```

```
%% Generating Data
f0=[1 0]'; PE=10^15; E=150;

B1=b1/60;%1st heating rate K/sec
B2=b2/60;%2nd heating rate K/sec
R=8.314; %j/molK

data1=orates(f0,T0,E,PE,B1*60,Tf,nTGA);
TT1=data1(:,1); x1=data1(:,2);

data2=orates(f0,T0,E,PE,B2*60,Tf,nTGA);
TT2=data2(:,1); x2=data2(:,2);


%% Generating T1 & T2 pairs for given number of rxns

X=linspace(0.99999999,f0(end)+0.0000001,nrxns)';

T1=interp1q(flipud(x1),flipud(TT1),X);
T2=interp1q(flipud(x2),flipud(TT2),X);

%% Generating TGA points with reduced number of points

Xtga=linspace(x1(1),x1(nTGA),rnTGA)';
Tr1=interp1(x1,TT1,Xtga,'spline');
Tr2=interp1(x2,TT2,Xtga,'spline');

%% Data Plots
hold on
plot(Tr1,Xtga,'g')
plot(Tr2,Xtga,'r')
plot(T1,X,'go')
plot(T2,X,'ro')

xlabel('Temperature K')
ylabel('Mass Fraction Remaining')

hold off

%% Feeding Data to the Algorithm
data3=funcscotteg2(T1,T2,B1,Tr1,Xtga,B1,B2,T0);
f0=data3(:,1);E=data3(:,2);PE=data3(:,3);
 c=[f0 E PE]
end
```

The conversion range is specified just below 1 and just above 0, to enable the integration of logarithmic terms, the complete conversion range would result in mathematical errors. The temperature range is also linearised. The actual algorithm is contained in the "*funcscotteg2*" function.

```
function c = funscotteg2(T1,T2,B,Tr,xx,B1,B2,T0);


warning off
options2=optimset('TolX',1e-6,'LevenbergMarquardt','off');

n=length(T1);
```

```
for i=1:n
   E(i)=fminbnd('AEerror2',0,800,options2,T1(i),T2(i),T0,B1,B2);
   PE(i)=Ai2(E(i),T1(i),T2(i),T0,B1,B2);
   PE(1)=0.0000001;
   chi_check20(i)=chi(E(i),PE(i),T1(i),T0,B,B2);
   chi_check100(i)=chi(E(i),PE(i),T2(i),T0,B,B2);
end
check=[chi_check20' chi_check100']

a=isfinite(PE');
PE=PE(a);
E=E(a);

q=length(Tr);

%% reduces no of data points in TGA set

npoints=q;
nn=length(E);

Tr1i=Tr;

for i=1:npoints
    for j=1:nn
        term1(j)=quad(@term,T0,Tr1i(i),[],[],E(j));
        chi1(i,j)=exp((-PE(j)/B)*(term1(j)));
        chi1(i,nn+1)=1;
         chi_1(i,j)=chi(E(j),PE(j),Tr1i(i),T0,B,B2);
        chi_1(i,nn+1)=1;
    end
end

options3=optimset('TolX',10);

f0=lsqnonneg(chi_1,xx)

E(n+1)=0;PE(n+1)=0;

c=[f0 E' PE'];

end
```

This function calls on a number of other functions but essentially takes the simulated (or experimental) data and uses the “least squares non-negative (lsqnonneg)” function to do the matrix inversion which produces the mass fraction vector with zero and non-zero elements, which correspond to “*E*” and “*PE*" vectors. The rows with non-zero “f0” elements are taken as triplet results.

The function *Aerror2* contains the integral equation for calculation of the activation energy *E* and uses the *expint* function to compute the exponential integrals.

```
function error = AEerror2(E,T1,T2,T0,B1,B2);
```

```
R=8.314; %j/molK

%terms in equation 13 Scott et. al.(2006)

first=T0*exp(-E*1000/(R*T0));

aa=E*1000/(R*T0);bb=exp(-aa)/aa;
second=(E*1000/R)*EXPINT(aa);
third=T1*exp(-E*1000/(R*T1));

cc=E*1000/(R*T1);dd=exp(-cc)/cc;
fourth=(E*1000/R)*EXPINT(cc);

fifth=first;
sixth=second;

seventh=T2*exp(-E*1000/(R*T2));

ee=E*1000/(R*T2);ff=exp(-ee)/ee;
eighth=(E*1000/R)*EXPINT(ee);

%LHS of EQ13
ls=(1/B1)*(first-second-third+fourth);

%RHS of EQ13
rs=(1/B2)*(fifth-sixth-seventh+eighth);

error = sqrt((1-rs/ls)^2);

end
```

Function *Ai2* calculates the value of the pre-exponential factor (*PE*) using the previously calculated '*E*' values for each candidate reaction.

```
function y = Ai2(E,T1,T2,T0,B1,B2);

R=8.314; %j/molK

%terms in equation 14 Scott et. al. (2006)

first=T0*exp(-E*1000/(R*T0));

aa=E*1000/(R*T0);bb=exp(-aa)/aa;
second=(E*1000/R)*EXPINT(aa);

third=T1*exp(-E*1000/(R*T1));

cc=E*1000/(R*T1);dd=exp(-cc)/cc;
fourth=(E*1000/R)*EXPINT(cc);

fifth=first;
sixth=second;

seventh=T2*exp(-E*1000/(R*T2));

ee=E*1000/(R*T2);ff=exp(-ee)/ee;
eighth=(E*1000/R)*EXPINT(ee);
```

```
%Here ln(chi) is specified as -1, hance the negative right hand side.
Ai=-B1/(first-second-third+fourth);
y=Ai;
end
```

The function *chi* is also called, and is used mainly as check to determine whether the elements of the chi matrix are indeed real and that the Ψ matrix does not contain any elements that are mathematical errors or not numbers.

```
function error = chi(E,PE,T1,T0,B1,B2);

A=PE;
R=8.314; %j/molK


%terms in equation 6

first=T0*exp(-E*1000/(R*T0));

aa=E*1000/(R*T0);bb=exp(-aa)/aa;
second=(E*1000/R)*EXPINT(aa);

third=T1*exp(-E*1000/(R*T1));

cc=E*1000/(R*T1);dd=exp(-cc)/cc;
fourth=(E*1000/R)*EXPINT(cc);

%RHS of EQ6
rhs=(A/B1)*(first-second-third+fourth);

error = exp(rhs);

end
```

The last function in this set is the *term* function, which merely holds the exponential term, and is called when using numerical integration functions such as *quad*.

```
function y=term(T,E)

y=exp(-E*1000./(8.314*T));

end
```

This set of functions is used to simulated and determine the kinetics of first-order reactions. The size of the *f0, E* and *PE* vectors determine the number of reactions simulated, so the same code can be used for single and multiple reaction simulations. The kinetics found can be compared to those specified, or used to re-plot the curves and compare them to the original curves.

This function set was then used to process shrinking core model simulations, only by editing the *scotteg2* function to call on a different data simulation file instead of orates. This was done to demonstrate the algorithm's ability to find activation energy values for reaction models other than first-order reactions.

The shrinking core simulation functions are presented below. The first function, *modelscm*, is a semi-analytical method for simulating the shrinking core reaction(s), and replaces the *orates* function. The structure and variables are mostly the same, all that has changed is the reaction model expression within the *for* loops.

```
function c=modelscm(f0,T0,E,PE,b,Tup,m);

%% Instructions
% f0 - mass fraction. Input as column vector. Last element is ash fraction
% E, PE - Activation energy and Pre-exp. factor. Input as row. should have
%       1 less element than f0.
%b - heating rate K/min
%T0, Tup - Min and Max temperature respectively
%m - number of simulation points within the temperature range.


B=b/60;%K/sec

s=size(E');
nn=s(:,1);

T=linspace(T0,Tup,m);

for i=1:m
    for j=1:nn
        term1(j)=quad(@term,T0,T(i),[],[],E(j));
        chi2(i,j)=exp((-PE(j)/B)*(term1(j)));
        chi2(i,nn+1)=1;
        chinew(i,j)=(1+(log(chi2(i,j))/(3*(f0(j).^(1/3))))).^3;
        chinew(i,nn+1)=1;
    end
end

M=chinew*f0;
I=find(M<=(f0(end)));
M(I)=f0(end);

c=[T' M]

plot(T,M,'k.');
x=c(:,1);y=100.*c(:,2);
deriv=-diff(y)./diff(x);
x=x(2:length(x));
plot(x,deriv,'b')
end
```

The alternative to the semi-analytical approach is to use an ODE solver to simulate the reaction. This was done using the *model13,* and *model* functions.

```
function rate = model13(t,s,B);

%% Instructions
% f0 - mass fraction. Input as column vector. Last element is ash fraction
% E1, A1 - Activation energy and Pre-exp. factor. Input as number.
%B - heating rate K/min
%t – Min/ start temperature
%s - number of simulation points within the temperature range.

M = s(1);
```

```
A1=10^10;
% A2=10^9;
E1=200;
% E2=120;
B;
T=t;
R=8.314; %j/molK

k1=1*(A1/B)*exp(-E1*1000/(R*T));
% k2=1*(A2/B)*exp(-E2*1000/(R*T));


rhs=-1*(k1*1*(M)^(2/3))-0*(k2*1*(M)^(2/3));

if (rhs>=0)
    rhs=0;
else
rhs = rhs;
end

rate=rhs;
end
```

This function just contains the shrinking core model expression. Then the *model* function, calls on the *model13* function to apply the ODE solver.

```
function c = model(tf,nTGA,B,T0);
%interpolates coats-redfern equation for the number of reactions required
%yields (T1 T2 X) data set

%Initial conditions
M0 = 1;

temp=linspace(T0,tf,nTGA)';
options=odeset('RelTol',1e-2);

 [t,state1] = ode45('model13',temp,M0,options,B);

%% collect the integration results
M1 = state1(:,1);

c=[t M1];

%% Plot Results

hold on
plot(t,M1,'b')
axis([280 tf 0 1])
xlabel('Temperature (K)');
ylabel('Mass Fraction Remaining (f0)');

x=c(:,1);y=100.*c(:,2);
deriv=-diff(y)./diff(x);
x=x(2:length(x));
plot(x,deriv,'b')


end
```

Here, the choice of ODE solver can be changed to determine which gives the smoothest resulting curve. In this example of the function, ODE45 is being used, one of several in-built solvers in the Matlab program. The difficulty with this method is the inability to easily simulate multiple reactions.

The focus then shifted to adapting the algorithm to both non-isothermal and isothermal random pore model simulation and reaction kinetics determination. The non-isothermal simulation-based code is presented first, followed by the isothermal simulation-based code. Then the code sets written for processing experimental data for both non-isothermal and isothermal conditions are presented.

The function written to simulate random pore model reactions is called *rpmodel*. It follows the form of the *orates* function. It was first used with the rest of the first-order model code and simply substituted the orate*s* function.

```
function c=rpmodel(f0,E,PE,b,T0,Tup,m)
global s0 L0 eps0 phi
%b=heating rate K/min
%T0, Tup= minimum, maximum plot temperature
%m=number of points on the curve
% sample input format in command window for multiple reactions
%rpmodel([0.5 0.5 0]', [100 150], [10^8 10^8], 20, 400, 1000, 1000)

%initial mass fraction

f=f0(1,:);
w=f0(2,:);

B=b/60;%K/sec
s0=10^4;    % "structural parameters for common porous solids"
L0=10^7;    % "structural parameters for common porous solids"
eps0=0.3;   % "structural parameters for common porous solids"
phi=(4*pi*(L0)*(1-eps0))/((s0)^2);

s=size(E');
nn=s(:,1);
T=linspace(T0,Tup,m);

for i=1:m
    for j=1:nn
        term1(j)=quad(@term,T0,T(i),[],[],E(j));
        chi2(i,j)=exp((PE(j)/B)*(term1(j
        chi2(i,nn+1)=1;
        chinew(i,j)=exp((1-(phi/2*(log(chi2(i,j))+2/phi))^2)/phi);
        chinew(i,nn+1)=1;
    end
end

fi=chinew*f0;

I=find(fi<=(f0(end)));
fi(I)=f0(end);

hold on
```

```
c=[T' fi];
%% Plots
%Fraction Remaining vs. Temperature
plot(T,fi,'b');

% First Derivative Plot
x=c(:,1);y=100.*c(:,2);
deriv=-diff(y)./diff(x);
x=x(2:length(x));
plot(x,deriv,'b.')

% Second Derivative Plot
deriv2=diff(deriv)./diff(x);
plot(x(1:size(deriv2)), deriv2, 'r.')

% Finding and Plotting X and Chi at Max Decomposition Rate
maxChiT=c(find(deriv==max(deriv))+1,:);
maxXT=[maxChiT(:,1) 1-maxChiT(:,2)];
plot( [maxChiT(1,1) maxChiT(1,1)], [-.05 max(deriv)], 'k', [T0 Tup],
[maxChiT(1,2) maxChiT(1,2)], 'k')
end
```

As seen in the sample input, this function is capable of simulating multiple reactions.

This function contains the calculation of the structural parameter φ (phi). The physical structural measurements were assumed to that of common porous solids (Bhatia and Perlmutter, 1980). The expression used to calculate the value is also found in Bhatia & Perlmutter (1980).

The second derivative plots and the identification of the maximum point of the first derivative were two approaches both coded to determine the conversion value at the maximum rate of decomposition, which was used in order to find an accurate pre-exponential factor value.

Before this value was determined, the first-order algorithm code was used, and an “integral method” similar to that used by Saloojee was used to determine the pre-exponential factor. The function written for this is *Anewrp2*.

```
function c = Anewrp2(f0,E,T1,B1,x);
% x=xmax => 0.64...<xmax< 0.66...  for RPM

%% Constants and Known Terms
T0=298.15;
R=8.314; %j/molK
b1=B1/60;

Tf=T1;

s0=10^4;    "structural parameters for common porous solids"
L0=10^7;    "structural parameters for common porous solids"
eps0=0.3;   "structural parameters for common porous solids"
phi=(4*pi*(L0)*(1-eps0))/((s0)^2);

%% Temperature integral according to Scott Eqn (6)
uo=(E*1000)/(R*T0);
uf=(E*1000)/(R*Tf);
```

```
first=T0*exp(-uo);

second=(E*1000/R)*expint(uo);

third=Tf*exp(-uf);

fourth=(E*1000/R)*expint(uf);

TI=(first-second-third+fourth);

%% dx/dt integrated between x0=0 and x
I =(2/phi)*(sqrt(1-phi*log(1-x)))-2/phi; %analytically integrated
expression of RPM

%% Calculation of A
A=(-b1*I)/TI;
c=[f0 E A]
end
```

This function used the activation energy found, and the corresponding heating rate, temperature and conversion to find the pre-exponential factor. This approach was unsuccessful, which led to the need to find the conversion value corresponding to the maximum decomposition rate for the random pore model. The graphical method seen above in the *rpmodel* function was used, but was not accurate enough. An analytical calculation of the conversion value at the maximum decomposition rate was then coded in the function, *dxdt2error*.

```
function error = dxdt2error(T,E,A,b)

%Command Window: T=fzero('dxdt2error',380,500,120,10^12,100)
%1st 2 parameters are the T range, then E, A, b
%Note: use E in units of kj/mol for term.m since conversion is in-built
%      Use e in units of J/mol for dxdt2 since Units of R are J/K.mol

%% Known Constants and Terms

T0=298.15;
B=b/60; %K/sec
e=E*1000; % in J/mol since R is J/K.mol
R=8.314;
s0=10^4;    % Bhatia n P "structural parameters for common porous solids"
L0=10^7;    % Bhatia n P "structural parameters for common porous solids"
eps0=0.3;   % Bhatia n P "structural parameters for common porous solids"
phi=(4*pi*(L0)*(1-eps0))/((s0)^2);

%% For Calculating 2nd Derivative
term1=quad(@term,T0,T,[],[],E);

chi2=exp((A/B)*(term1));  % working(2)

x=1-exp((1-(phi/2*(log(chi2)+2/phi))^2)/phi)  % this is x

% Mathcad Solution from Mathew
dxdt2=A^2*exp(-(2*e)/(R*T))*phi*(1-x)/(2*B^2)-(A^2*exp(-(2*e)/(R*T))*(1-
x)*(1-phi*log(1-x)))/B^2-(A*e*exp(-e/(R*T))*sqrt(1-phi*log(1-x))*(x-
1))/(B*R*T^2) % unsimplified dxdt2 from mathcad
```

```
dxdt2=dxdt2*100; % multiply by 100 since 'deriv' in rpmodel.m is multiplied
                   by 100. if dxdt2 is multiplied, it will lay over  2nd

%% Error function

% error=1/sqrt((dxdt2)^2); %for FMINBND
error=dxdt2; % for FZERO
end
```

A range of *E, B (heating rate)* and *A* values were used and the *fzero* function in Matlab was used to find the *x-value*. The value of x was recorded for each combination and the average value used as in the original algorithm. The *Ai2* function was used again, since it is still applicable, it was merely edited to include the new conversion value and is called *Ai3.* It can be seen that conversion, *x*, is now included as an input to the *Ai3* to be able to change the value from outside the function. The value use was however eventually hard-coded.

```
function y = Ai3(E,T1,T2,T0,B1,B2, x)
%NOTE: B1 must be input in K/sec when using it as a stand-alone


%% Constant Known terms
T0=T0;
R=8.314; %j/molK
global s0 L0 eps0 phi

%% terms in equation 13

first=T0*exp(-E*1000/(R*T0));

aa=E*1000/(R*T0);
bb=exp(-aa)/aa;

second=(E*1000/R)*expint(aa);

third=T1*exp(-E*1000/(R*T1));

cc=E*1000/(R*T1);
dd=exp(-cc)/cc;

fourth=(E*1000/R)*expint(cc);

% fifth=first;                                  %For calculation of A for B2
% sixth=second;                                 %For calculation of A for B2
% seventh=T2*exp(-E*1000/(R*T2));               %For calculation of A for B2
% ee=E*1000/(R*T2);ff=exp(-ee)/ee;              %For calculation of A for B2
% eighth=(E*1000/R)*EXPINT(ee);                 %For calculation of A for B2


%% Modified Expression based on Eqn 14 and Assumption that Chi=1-x

Ai= -0.8801*B1/(first-second-third+fourth); %** Value according to
sensitivity analysis

% Ai= -0.8797*B1/(first-second-seventh+eighth); %For calculation of A for
B2
```

```
y=Ai;
end
```

As can be seen, the code has been written to process either heating rate's data, the code in green must merely be "uncommented", since the green code is overlooked by the Matlab program. The coefficient of "*B1"* in the third-last effective line of the function shows the incorporation of the new *x-value* determined by the sensitivity analysis.

The problem was still that the *f0* value was being calculated according to the first-order model in the *funcscotteg2* function. The result of this was that the modified *x-value* was not sufficient in effectively calculating and identifying the correct kinetic triplet. The function had to be re-written in order to calculate the *f0* value according to the random pore model. This function was rewritten and called *funcrpm.* The *rpnewchi* function calls on the *funcrpm* function and hence specifies all the required input. *funcrpm* is where the matrix inversion is done used the least-squares-non-negative (*lsqnonneg)* function in Matlab. Both functions are presented below.

```
function c = funcrpm(T1,T2,B,Tr,xx,B1,B2,T0,x);

%% Constant Known terms and Settings
global phi

warning off

options2=optimset('TolX',1e-6,'LevenbergMarquardt','off');

n=length(T1);

%% Chi Check

for i=1:n
    E(i)=FMINBND('AEerror2',0,800,options2,T1(i),T2(i),T0,B1,B2);
    PE(i)=Ai3(E(i),T1(i),T2(i),T0,B1,B2,x(i));%added x into input for Ai3.m
    PE(1)=0.0000001;
    chi_check20(i)=chi(E(i),PE(i),T1(i),T0,B,B2);
    chi_check100(i)=chi(E(i),PE(i),T2(i),T0,B,B2);
end
check=[chi_check20' chi_check100']

a=isfinite(PE');
PE=PE(a);
E=E(a);

q=length(Tr);

%% reduces no of data points in TGA set

npoints=q;
nn=length(E);

Tr1i=Tr;
```

```
%% Calculation of F0 - Scott eq. 9
for i=1:npoints
    for j=1:nn
        term1(j)=quad(@term,T0,Tr1i(i),[],[],E(j));
        chi2(i,j)=exp((PE(j)/B)*(term1(j)));
        chi2(i,nn+1)=1;
        chirpm(i,j)=exp((1-(phi/2*(log(chi2(i,j))+2/phi))^2)/phi
        chirpm(i,nn+1)=1;
    end
end

%%
options3=optimset('TolX',10);


f0=lsqnonneg(chirpm,xx);

[length(f0) length(E') length(PE')];

E(n+1)=0;PE(n+1)=0;
E';

c=[f0 E' PE'];

end
```

The *rpnewchi* function then calls on RPM based functions presented above to simulate the reactions and then use the algorithm to process the simulated data and calculate the kinetic parameters used. The results can then be compared to the values initially specified.

```
function c = rpnewchi(nrxns,nTGA,rnTGA,m,b1,b2,T0,tf)
%uses scotts eg 2 to determine f0 E & EP
global triplet
format SHORT G %Best number display format for viewing answers

f0=[0.5 0.4 0.1]'; E=[135 120]; PE=[10^10 10^10];

B1=b1/60;%1st heating rate K/sec
B2=b2/60;%2nd heating rate K/sec

R=8.314; %j/molK


%% Generating TGA points
data1=rpmodel(f0,E,PE,b1,T0,tf,m); % First Heating rate
TT1=data1(:,1);
x1=data1(:,2);
data2=rpmodel(f0,E,PE,b2,T0,tf,m); % Second Heating rate
TT2=data2(:,1);
x2=data2(:,2);


%% reducing TGA points
% %lower heating rate
Tr1=linspace(TT1(1),TT1(length(TT1)),nTGA)';
Tr2=linspace(TT2(1),TT2(length(TT2)),nTGA)';
```

```
Xr1=interp1q(TT1,x1,Tr1);
Xr2=interp1q(TT2,x2,Tr2);

TT1=Tr1;
TT2=Tr2;
x1=Xr1;
x2=Xr2;
x1(length(x1))=x1(length(x1)-1);

X=linspace(0.99999999,f0(end)+0.0000001,nrxns)';
Xplot=linspace(1,0,nrxns)';
T1=interp1q(flipud(x1),flipud(TT1),X);
T2=interp1q(flipud(x2),flipud(TT2),X);


x=1-data1(:,2); %new line x for new Ai2 calc

%% Generating TGA points with reduced number of points

Xtga=x1;
Tr1=TT1;

%% Using Simulated Data to Calculate Triplet
data3=funcrpm(T1,T2,B1,Tr1,Xtga,B1,B2,T0,x);
f0=data3(:,1);E=data3(:,2);PE=data3(:,3);

l=length(f0)-1;
f0=f0(1:l); E=E(1:l); PE=PE(1:l);
c=[f0 E PE T1 T2 X];

%% MATLAB AUTOCODE PLOTS
% **Simulated Data Curves From rpmodel.m**

figure3 = figure(3);

% Create axes
axes1 = axes('Parent',figure3,'FontWeight','demi','FontSize',12);
% Uncomment the following line to preserve the Y-limits of the axes
% ylim(axes1,[0 1]);
hold(axes1,'all');

% Create multiple lines using matrix input to plot
plot1 = plot(TT1, x1, TT2,
x2,'Parent',axes1,'Marker','.','LineStyle','none');
set(plot1(1),'Color',[0 0 1],'DisplayName','Single RP model 50k/min');
set(plot1(2),'Color',[1 0 0],'DisplayName','Single RP model 100k/min');

% Create xlabel
xlabel('Temperature (K)','FontWeight','demi','FontSize',12);

% Create ylabel
ylabel('Mass Fraction Remaining (f)','FontWeight','demi','FontSize',12);

% Create legend
legend(axes1,'show');
```

```
% **STEM PLOTS FOR E, PE and f0**

% Create figure
figure2 = figure(2);

% Create axes
axes1 = axes('Parent',figure2,...
    'Position',[0.13 0.095663082437276 0.775 0.255591397849462],...
    'FontWeight','demi',...
    'FontSize',12);
hold(axes1,'all');

% Create stem
stem(Xplot,f0,'Parent',axes1);

% Create xlabel
xlabel('Fractional Conversion (x)','FontWeight','demi','FontSize',12);

% Create ylabel
ylabel('Mass Fraction (f0)','FontWeight','demi','FontSize',12);

% Create axes
axes2 = axes('Parent',figure2,...
    'Position',[0.13 0.725806451612903 0.775 0.247580645161291],...
    'FontWeight','demi',...
    'FontSize',12);
% Uncomment the following line to preserve the Y-limits of the axes
% ylim(axes2,[100 300]);
hold(axes2,'all');

% Create stem
stem(Xplot,E,'Parent',axes2);

% Create ylabel
ylabel({'Activation Energy','(kJ/mol)'},'FontWeight','demi','FontSize',12);

% Create axes
axes3 = axes('Parent',figure2,...
    'Position',[0.128613037447989 0.425412186379929 0.775
0.228709677419355],...
    'FontWeight','demi',...
    'FontSize',12);
% Uncomment the following line to preserve the X-limits of the axes
% xlim(axes3,[0 50]);
% Uncomment the following line to preserve the Y-limits of the axes
ylim(axes3,[PE(1,1)/10 2*PE(1,1)]);
hold(axes3,'all');

% Create stem
stem(Xplot,PE,'Parent',axes3);

% Create ylabel
ylabel(['Pre-Exponential',sprintf('\n'),' Factor A (1/sec)'],...
    'FontWeight','demi',...
    'FontSize',12);

%% Results
nonsp= find(c(:,1)>0.01);
E_found=[c(nonsp,1) c(nonsp,2)]
```

```
A_found=[c(nonsp,1) c(nonsp,3)]

triplet=[E_found A_found(:,2)]

end
```

Note that the code used for plot formatting was configured in the “plot tools” interface, and the auto-generated code (Matlab Autocode) was then used in the function. The last section of code, the results section, merely generates a condensed matrix of the non-spurious kinetics, based on the non-zero values of the mass fraction, *f0.*

The functions above were all rewritten for the isothermal case, for the Random pore model. The isothermal analog of *rpmodel* is *isotrpm*.

```
function c=isotrpm(f0,E,PE,T,t0,tup,m)
global s0 L0 eps0 phi
%b=heating rate K/min
%t0, tup= minimum, maximum plot time
%m=number of points on the curve
% sample input format in command window for multiple reactions
%isotrpm([0.5 0.5 0]', [100 150], [10^8 10^8], 1000, 0, 3000, 1000)
%initial mass fraction

R=8.314;
s0=10^4;    % Bhatia n P "structural parameters for common porous solids"
L0=10^7;    % Bhatia n P "structural parameters for common porous solids"
eps0=0.3;   % Bhatia n P "structural parameters for common porous solids"
phi=(4*pi*(L0)*(1-eps0))/((s0)^2);
s=size(E');
nn=s(:,1);

t=linspace(t0,tup,m);

for i=1:m
    for j=1:nn
        chinew(i,j)=exp((1-(phi*PE(j)*exp(-
1000*E(j)/(R*T))*t(i)/2+1)^2)/phi); % chinew with inert
        chinew(i,nn+1)=1;
    end
end

fi=chinew;
I=find(fi<=(f0(end)));
fi(I)=f0(end);

hold on

c=[t' fi];

%% Plots
%Fraction Remaining vs. Temperature
plot(t,fi,'b');

%First Derivative Plot
x=c(:,1);y=100.*c(:,2);
deriv=-diff(y)./diff(x);
x=x(2:length(x));
```

```
plot(x,deriv,'r.')

end
```

The same basic code structure exists except the *chinew* identity has changed to that of the isothermal expression. The curve and first derivative are again plotted.

The isothermal analogue of *Ai3* is *isotAi*.

```
function y = isotAi(E,t1,t2,t0,T1,T2)
%NOTE: B1 must be input in K/sec when using it as a stand-alone

%% Constant Known terms

R=8.314; %j/molK

%% Modified Expression based on Eqn 14

Ai=log(2.4819)/(exp(-E*1000/(R*T1))*t1); % BEST ANSWERS

%Best Answers Ln(chi) value derived from direct subs of E and A into
isotfuncrpm.m



y=Ai;
end
```

Since the isothermal expression does not contain the indeterminate temperature integral, the code is simplified into just one expression. The value used for conversion at the maximum decomposition rate was found by direct substitution of known parameters into the *isotfuncrpm* function. The conversion value was then back-calculated and was found to give accurate results thereafter; this value was therefore used.

```
function c = isotfuncrpm(t1,t2,Tr,xx,T1,T2,t0);

%% Constant Known terms and Settings
global phi

warning off

options2=optimset('TolX',1e-6,'LevenbergMarquardt','off');

R=8.314; %J/mol.K

n=length(t1);
%% Chi Check
[t1 t2];
for i=1:n
    E(i)=FMINBND('isotAEerror2',0,800,options2,t1(i),t2(i),t0,T1,T2);
    PE(i)=isotAi(E(i),t1(i),t2(i),t0,T1,T2);
    PE(1)=0.0000001;
%     chi_check20(i)=chi(E(i),PE(i),T1(i),T0,B,B2);
%     chi_check100(i)=chi(E(i),PE(i),T2(i),T0,B,B2);
end
```

```
% check=[chi_check20' chi_check100']

a=isfinite(PE');
PE=PE(a);
E=E(a);

q=length(Tr);

%% reduces no of data points in TGA set

npoints=q;
nn=length(E);

Tr1i=Tr;

%% Calculation of F0 - Scott eq. 9
for i=1:npoints
    for j=1:nn
%         PE(j)=10^10; % Hardcode for determining x for ln(chi)
%         E(j)=200; % Hardcode for determining x for ln(chi)
        isotchirpm(i,j)=exp((1-(phi*PE(j)*exp(-
1000*E(j)./(R*T1))*Tr(i)/2+1)^2)/phi); % this is the analogous expression
of 1-x... chi??   %Lines from rpmodel.m
        isotchirpm(i,nn+1)=1;
    end
end

%%
options3=optimset('TolX',10);


f0=lsqnonneg(isotchirpm,xx);

E(n+1)=0;PE(n+1)=0;
E';
[length(f0) length(E') length(PE')];
PE';
c=[f0 E' PE'];

end
```

The *AEerror2* function was also rewritten for isothermal data and is called *isotAEerror2*.

```
function error = isotAEerror2(E,t1,t2,t0,T1,T2)

R=8.314; %j/molK


%% LHS of EQ13
ls=exp(-(E*1000)/(R*T1))*t1;

%% RHS of EQ13
rs=exp(-(E*1000)/(R*T2))*t2;
%%
error = sqrt((1-rs/ls)^2);
```

```
end
```

The *isotfuncrpm* function is the isothermal analog of the *funcrpm* function. The isothermal version of the *chi* function was not written, since it is only used to confirm whether all elements in the *chi* matrix are real. For the isothermal case (and the non-isothermal) the code will not successfully complete the sequence if the elements are not real, which rendered the step redundant. Again, the function written to call on the functions presented above is *isotnewchi*, the isothermal analogue of *rpnewchi.*

```
function c = isotnewchi(nrxns,nTGA,rnTGA,T1,T2,t0,tf)
%isotnewchi(50,200,100,900,1000,0,150)

global triplet
format SHORT G %Best number display format for viewing answers

f0=[1 0]'; E=[200]; PE=[1*10^10];

R=8.314; %j/molK

%% Generating TGA points

% Change to isotrpm fn for IsoT runs
data1=isotrpm(f0,E,PE,T1,t0,tf,1000); % First Heating rate
TT1=data1(:,1);
x1=data1(:,2);
data2=isotrpm(f0,E,PE,T2,t0,tf,1000); % Second Heating rate
TT2=data2(:,1);
x2=data2(:,2);

%% reducing TGA points
% %lower Temp
Tr1=linspace(TT1(1),TT1(length(TT1)),nTGA)';
Tr2=linspace(TT2(1),TT2(length(TT2)),nTGA)';

Xr1=interp1q(TT1,x1,Tr1);
Xr2=interp1q(TT2,x2,Tr2);

TT1=Tr1;
TT2=Tr2;
x1=Xr1;
x2=Xr2;
x1(length(x1))=x1(length(x1)-1);

X=linspace(0.99999999,x1(end),nrxns)';
Xplot=X;
t1=interp1q(flipud(x1),flipud(TT1),X);
t2=interp1q(flipud(x2),flipud(TT2),X);


%% Generating TGA points with reduced number of points

Xtga=x1;
Tr1=TT1;

%% Using Simulated Data to Calculate Triplet
data3=isotfuncrpm(t1,t2,Tr1,Xtga,T1,T2,t0);
```

```
%isotfuncrpm(t1,t2,Tr,xx,T1,T2,t0,x);
f0=data3(:,1);E=data3(:,2);PE=data3(:,3);

l=length(f0)-1;
f0=f0(1:l); E=E(1:l); PE=PE(1:l);
c=[f0 E PE t1 t2 X];


%% MATLAB AUTOCODE PLOTS
% **Simulated Data Curves From rpmodel.m**

figure3 = figure(3);

x1=data1(:,1);
y=100.*data1(:,2);
deriv1=-diff(y)./diff(x1);
x1=x1(2:length(x1));

x2=data2(:,1);
y=100.*data2(:,2);
deriv2=-diff(y)./diff(x2);
x2=x2(2:length(x2));

% Create axes
axes1 = axes('Parent',figure3,'FontWeight','demi','FontSize',12);
% Uncomment the following line to preserve the Y-limits of the axes
% ylim(axes1,[0 1]);
hold(axes1,'all');

% Create multiple lines using matrix input to plot
plot1 = plot(data1(:,1), data1(:,2), data2(:,1),
data2(:,2),'Parent',axes1,'Marker','none','LineStyle','-', 'LineWidth',2);
plot2=plot(x1,deriv1,x2, deriv2,
'Parent',axes1,'Marker','o','MarkerSize',1.5,'LineStyle','none');
set(plot1(1),'Color',[0 0 1],'DisplayName','Single RP model 850K');
set(plot1(2),'Color',[1 0 0],'DisplayName','Single RP model 900K');
set(plot2(1),'Color',[0 0 1],'DisplayName','Single RP model 850K 1st
Derivative');
set(plot2(2),'Color',[1 0 0],'DisplayName','Single RP model 900K 1st
Derivative');

% Create xlabel
xlabel('Time (sec)','FontWeight','demi','FontSize',12);

% Create ylabel
ylabel('Mass Fraction Remaining (f)','FontWeight','demi','FontSize',12);

% Create legend
legend(axes1,'show');


% **STEM PLOTS FOR E, PE and f0**

% Create figure
figure2 = figure(2);

% Create axes
axes1 = axes('Parent',figure2,...
```

```
    'Position',[0.13 0.095663082437276 0.775 0.255591397849462],...
    'FontWeight','demi',...
    'FontSize',12);
hold(axes1,'all');

% Create stem
stem(Xplot,f0,'Parent',axes1);

% Create xlabel
xlabel('Fractional Conversion (x)','FontWeight','demi','FontSize',12);

% Create ylabel
ylabel('Mass Fraction (f0)','FontWeight','demi','FontSize',12);

% Create axes
axes2 = axes('Parent',figure2,...
    'Position',[0.13 0.725806451612903 0.775 0.247580645161291],...
    'FontWeight','demi',...
    'FontSize',12);
% Uncomment the following line to preserve the Y-limits of the axes
% ylim(axes2,[100 300]);
hold(axes2,'all');

% Create stem
stem(Xplot,E,'Parent',axes2);

% Create ylabel
ylabel({'Activation Energy','(kJ/mol)'},'FontWeight','demi','FontSize',12);

% Create axes
axes3 = axes('Parent',figure2,...
    'Position',[0.128613037447989 0.425412186379929 0.775
0.228709677419355],...
    'FontWeight','demi',...
    'FontSize',12);
% Uncomment the following line to preserve the X-limits of the axes
% xlim(axes3,[0 50]);
% Uncomment the following line to preserve the Y-limits of the axes
ylim(axes3,[10^9 2*10^10]);
hold(axes3,'all');

% Create stem
stem(Xplot,PE,'Parent',axes3);

% Create ylabel
ylabel(['Pre-Exponential',sprintf('\n'),' Factor A (1/sec)'],...
    'FontWeight','demi',...
    'FontSize',12);

%% Results
nonsp= find(c(:,1)>0.01);
E_found=[c(nonsp,1) c(nonsp,2)]
A_found=[c(nonsp,1) c(nonsp,3)]

triplet=[E_found A_found(:,2)]

end
```

The next set of code written to process the experimental data. The first set presented is for non-isothermal data.

Unlike simulated data, experimental data was be processed before being used. For plain coal, plain pine and coal-pine blend normalized data, the following steps were applied to reduce the number of data points to make the datasets more usable. *coalchar12* is being used as an example. The temperature (T) and conversion (X) vectors generated directly from the normalised TGA data usually have 2000-3000 elements, but only about 200 are needed for accurate results. The datasets are therefore reduced.

```
function c=coalchar12(n)

T=[830.66
830.76
830.86
830.96
......

1286.73
1286.83
1286.93
1287.03];


X=[1
1
1
1
1
........

0
0
0
0
0
];
T=T+273.15;
Tr=linspace(T(1),T(end),n)';
Xr=spline(T,X,Tr);

c=[Tr Xar];

% figure(2)
hold on
plot(Tr,Xr, 'g.')

legend('12kpm ashless')
x=c(:,1);y=100.*c(:,2);
deriv=-diff(y)./diff(x);
x=x(2:length(x));
plot(x,deriv,'g-')
end
```

The *linspace* and *spline* functions are used to linearise the temperature interval and interpolate the conversion values. The curves and derivatives are then plotted.

The *Ai3, rpmodel, term, AError2,* and *funcrpm* functions are unchanged from the simulated data functions, but the function that calls on these component functions is new. the new function proposes a value of the structural parameter and then uses the rpmodel to simulate a curve. The simulation is then compared to the experimental curve; this procedure is repeated with varying values of *φ* until the error between the simulation and the experimental curve is minimised. The two functions that conduct this calculation are *phicalc2* and *phierror2*. The third experimental curve is then plotted, and a simulation is generated with the heating rate corresponding to the third experimental curve. The correlation coefficient term (r-squared) is then calculated using the *rsquared* function. These are all called on by the *findphi* function, which is simply fed the three experimental curves and their heating rates, along with the number of proposed candidate reactions and experimental points. These four functions are presented below.

```
function d = phicalc2(data1, data2, nrxns,rnTGA,nTGA,b1,b2,nexp)

global kinetics triplet fit

options2=optimset('TolX',1e-6,'LevenbergMarquardt','off');

phi=fminbnd('phierror2',0.1,30,options2,data1,data2,nrxns,rnTGA,nTGA,b1,b2,
nexp);

d=phi;
end
```

This function uses the *fminbnd* function to find a minimum in the error value produced in the *phierror2* function. Once the error is minimised, it outputs the value of the structural parameter *phi.*

```
function error = phierror2(phi,data1,data2,nrxns,rnTGA,nTGA,b1,b2,nexp)


global kinetics triplet fitdata1

format SHORT G %Best number display format for viewing answers


B1=b1/60;%1st heating rate K/sec
B2=b2/60;%2nd heating rate K/sec

R=8.314; %j/molK

%% Generating TGA points

TT1=data1(:,1);
x1=data1(:,2);

TT2=data2(:,1);
x2=data2(:,2);

%% reducing TGA points
% %lower heating rate
Tr1=linspace(TT1(1),TT1(length(TT1)),nTGA)';
```

```
Tr2=linspace(TT2(1),TT2(length(TT2)),nTGA)';

Xr1=interp1q(TT1,x1,Tr1);
Xr2=interp1q(TT2,x2,Tr2);

TT1=Tr1;
TT2=Tr2;
x1=Xr1;
x2=Xr2;
x1(length(x1))=x1(length(x1)-1);

X=linspace(x1(1),x1(end),nrxns)';
% X=linspace(0.99999999,x1(end),nrxns)'; ***Original working line***

T1=interp1q(flipud(x1),flipud(TT1),X);
T2=interp1q(flipud(x2),flipud(TT2),X);

%% Generating TGA points with reduced number of points

Xtga=x2;
Tr1=TT2;

T0=Tr1(1);

%% Using Simulated Data to Calculate Triplet

data3=funcrpm(T1,T2,B2,Tr1,Xtga,B1,B2,T0,phi);

f0p=data3(:,1);Ep=data3(:,2);PEp=data3(:,3);

I=find(f0p>=(0.00));
k=find(f0p>=(0.05));

l=length(f0p)-1;

f0p=f0p(I);
Epp=Ep(I)';
PEpp=PEp(I)';
Epp(k)';
PEpp(k)';
Ep=Epp(1:(end-1));
PEp=PEpp(1:(end-1));
m=nexp;

ff=f0p(1:nrxns);
kinetics=[ff Ep' PEp' [1:1:nrxns]'];
nonsp= find(kinetics(:,1)>0.001);
E_found=[kinetics(nonsp,1) kinetics(nonsp,2)];
A_found=[kinetics(nonsp,1) kinetics(nonsp,3)];
triplet=[ E_found A_found(:,2) kinetics(nonsp,4)];

%% Sangtong-Ngam Method Sigma Curve Fit by Least Squares

;
Tup=Tr1(end);
fitdata1=rpmodel(f0p,Ep,PEp,b2,T0,Tup,m,phi);

TT1p=fitdata1(:,1);
```

```
x1p=fitdata1(:,2);
xexp=x2;
length(xexp);
length(x1p);
hold on
plot(TT1p,x1p,'r')

difference= (x1p-xexp).^2;
square=sqrt(difference/length(difference));

error=sum(square)

end
```

This function uses a basic error expression (Sangtong-Ngam and Narasingha, 2008) to represent the difference between the simulated curve produced with kinetics determined by the algorithm and the experimental data. This error is minimised in *phicalc2.*

```
function c=findphi(data1, data2, data3,b1,b2, b3,nrxns,m,ntga,rntga)

% findphi(coalchar12(200), coalchar15(200),
coalchar20(200),11.9,14.9,19.8,50,200,200,100)
% findphi(coalpine20(200),
coalpine12(200),coalpine152(200),20,12,14.8,50,200,200,100)
% rpmodel([triplet(:,1)', 0]', triplet(:,2)', triplet(:,3)', B, 298,
1600,200, phi)
format short g

global triplet fit phi

phi=phicalc2(data1,data2,nrxns,rntga,ntga,b1,b2,m)
expe=data3;
fit=rpmodel([(triplet(:,1))' 0]', triplet(:,2)', triplet(:,3)', b3,
expe(1,1), expe(200,1), m,phi);
plot(fit(:,1),fit(:,2),':','color', [0 0
0],'LineWidth',3.0,'MarkerSize',12.0);

rsqrd=rsquared(fit(:,2), expe(:,2));

createaxes(figure(2), data1,data2,data3);
triplet
c=rsqrd;
end
```

The *findphi* function is the function that could form the basis of the graphic user interface since it is here that that the experimental data, number of candidate reactions, and number of usable TGA points is specified. It then calls on all the relevant functions to produce a matrix of the kinetic triplet, the value of phi, and the plot of the experimental data and algorithm fits of the experimental data. It outputs the value of the correlation coefficient, calculated using the *rsquared* function.

```
function c=rsquared(fit, expe)
% "Coefficient of determination"
%compares 2 fits independently
expdash(1:length(expe),:)=mean(fit);
act_pred=sum((expe-fit).^2);
```

```
act_mean=sum((expe-expdash).^2);
rsqrd=1-(act_pred/act_mean);
c=rsqrd;
end
```

The same code set was used to process all the non-isothermal experimental data.

The same approach was taken for the isothermal data. The *isotAi*, *isotAError2 are isotrpm* unchanged. *isotfuncrpm* is replaced by *isotfuncrpmp* only because of the indexing for the now changing *phi* value, called *phii*. The same *rsquared* function is also used. Essentially the same files with the same purpose are written for isothermal cases and are called, *isotfindphi, isotphicalc* and *isotphierror*, corresponding to *findphi, phicalc2* and *phierror2*, respectively. These four functions are presented below. The first is *isotfuncrpm*.

```
function c = isotfuncrpmp(t1,t2,Tr,xx,T1,T2,t0,phii);

%% Constant Known terms and Settings

warning off

options2=optimset('TolX',1e-6,'LevenbergMarquardt','off');

R=8.314; %J/mol.K

n=length(t1);
%% Chi Check

for i=1:n
    E(i)=FMINBND('isotAEerror2',0,800,options2,t1(i),t2(i),t0,T1,T2);
    PE(i)=isotAi(E(i),t1(i),t2(i),t0,T1,T2); %added x into input for Ai2.m
    PE(1)=0.0000001;
%     chi_check20(i)=chi(E(i),PE(i),T1(i),T0,B,B2);
%     chi_check100(i)=chi(E(i),PE(i),T2(i),T0,B,B2);
end
% check=[chi_check20' chi_check100']

a=isfinite(PE');
PE=PE(a);
E=E(a);
E';

q=length(Tr);

%% reduces no of data points in TGA set

npoints=q;
nn=length(E);

Tr1i=Tr;

%% Calculation of F0 - Scott eq. 9
for i=1:npoints
    for j=1:nn
         %PE(j)=10^6; % Hardcode for troubleshooting. re-eval PE calc!!
         %E(j)=135; % Hardcode for troubleshooting. re-eval E calc!!
```

```
        isotchirpm(i,j)=exp((1-(phii*PE(j)*exp(-
1000*E(j)/(R*T1))*Tr1i(i)/2+1)^2)/phii);
        isotchirpm(i,nn+1)=1;
    end
end

%%
options3=optimset('TolX',10);


f0=lsqnonneg(isotchirpm,xx);

E(n+1)=0;PE(n+1)=0;
E';
[length(f0) length(E') length(PE')];
PE';
c=[f0 E' PE'];

end
```

The *isotphicalc* function is as follows:

```
function d = isotphicalc(data1, data2, nrxns,nTGA,rnTGA,T1,T2)

global phi

t0=data1(1,1);
tf=data2(end,1);

options2=optimset('TolX',1e-6,'LevenbergMarquardt','off');

phi=fminbnd('isotphierror',0.1,50,options2,data1, data2,
nrxns,nTGA,rnTGA,T1,T2,t0,tf);

d=phi;
phi

end
```

The *isotphierror* function is as follows:

```
function error = isotphierror(phii,data1, data2, nrxns, nTGA, rnTGA, T1,
T2,t0,tf)

global triplet kinetics t0 tf
format SHORT G %Best number display format for viewing answers

R=8.314; %j/molK

%% Generating TGA points

TT1=data1(:,1);
x1=data1(:,2);

TT2=data2(:,1);
x2=data2(:,2);
```

```
%% reducing TGA points
% %lower heating rate
Tr1=linspace(TT1(1),TT1(length(TT1)),nTGA)';
Tr2=linspace(TT2(1),TT2(length(TT2)),nTGA)';

Xr1=interp1q(TT1,x1,Tr1);
Xr2=interp1q(TT2,x2,Tr2);
% hold on
% plot(Tr2,Xr2,'ko')
% plot(Tr1,Xr1,'go')
TT1=Tr1;
TT2=Tr2;
x1=Xr1;
x2=Xr2;
x1(length(x1))=x1(length(x1)-1);

X=linspace(0.99999999,x1(end),nrxns)';

t1=interp1q(flipud(x1),flipud(TT1),X);
t2=interp1q(flipud(x2),flipud(TT2),X);

%% Generating TGA points with reduced number of points

Xtga=x1;
Tr1=TT1;
xexp=data1(:,2);
%% Using Simulated Data to Calculate Triplet
data3=isotfuncrpmp(t1,t2,Tr1,Xtga,T1,T2,t0,phii);
%isotfuncrpm(t1,t2,Tr,xx,T1,T2,t0,x);

f0p=data3(:,1);Ep=data3(:,2);PEp=data3(:,3);

I=find(f0p>=(0.00));
k=find(f0p>=(0.05));

l=length(f0p)-1;

f0p=f0p(I);
Epp=Ep(I)';
PEpp=PEp(I)';
Epp(k)';
PEpp(k)';
Ep=Epp(1:(end-1));
PEp=PEpp(1:(end-1));
m=nTGA;

ff=f0p(1:nrxns);
kinetics=[ff Ep' PEp' [1:1:nrxns]'];
nonsp= find(kinetics(:,1)>0.01);
E_found=[kinetics(nonsp,1) kinetics(nonsp,2)];
A_found=[kinetics(nonsp,1) kinetics(nonsp,3)];
triplet=[ E_found A_found(:,2) kinetics(nonsp,4)];

%% Fitting the Data
tf=Tr1(end);
fitdata1=isotrpmp(f0p,Ep,PEp,phii,T1,t0,tf,nTGA); % First Heating rate

TT1p=fitdata1(:,1);
x1p=fitdata1(:,2);
```

```
length(xexp);
length(x1p);
hold on
plot(TT1p,x1p,'r')

difference= (x1p-xexp).^2;
square=sqrt(difference/length(difference));

error=sum(square)


end
```

Appendix D: Presentations and Future Publications based on this Research

This appendix includes a poster presented at the 2011 International Pittsburgh Coal Conference (IPCC) as well as a draft journal article prepared for publication.

Determination of Kinetics of Char Gasification with Carbon Dioxide Using Thermogravimetry: Kinetics Determination Using Simulated TGA Data

Thinesh Vittee*, S. Kauchali, N. Wagner

School of Chemical and metallurgical Engineering, University of the Witwatersrand, 1 Jan Smuts Avenue, Braamfontein, Johannesburg, South Africa

*Contact: thinesh.vittee@students.wits.ac.za

1. Introduction

•The study of gasification of complex solid fuels to produce usable fuels and other products is an important field since gasification is accepted to be among the cleanest and most versatile solid fuel processing methods .

•Accurate kinetics determination of solid fuel gasification reactions are vital to ensuring accurate gasification system design and operation.

•Simulated data will be used to modify the Distributed Activation Energy Model (DAEM) based algorithm developed in Scott et. al. (2006) for use on reactions like the Boudouard reaction which, according to literature, adheres to the random pore reaction model (Irfan et al. 2011).

•The novelty of this method is that the activation energy determination is model-free, and the other parameters can be found with simple adjustments to the algorithm.

2. Theory

The algorithm used in this study is based on the Distributed Activation Energy Model (DAEM). The algorithm developed in Scott et. al. (2006) determines the kinetics from a series of thermogravimetric experiments conducted at different constant heating rates. The algorithm expression is as follows:

$$\frac{M(t)}{M_0} = w + \sum_{All\ reactions\ i} f_{i,0} \exp\left[-A_i \int_0^t \exp\left(\frac{-E_i}{RT}\right) dt\right]$$

Where:

$$\Psi(E,t) = \exp\left[-A(E)\int_0^t \exp\left(\frac{-E}{RT}\right)dt\right]$$

Or for experiments with constant heating rates:

$$\Psi(E,T) = \exp\left[-\frac{A}{B}\int_0^T \exp\left(\frac{-E}{RT}\right)dT\right]$$

The algorithm can be expressed in matrix form $\underline{M} = \underline{\Psi}\,\underline{f}$:

$$\frac{1}{M_0}\begin{bmatrix} M(t_0) \\ M(t_1) \\ M(t_2) \end{bmatrix} = \begin{bmatrix} \Psi_1(t_0) & \Psi_2(t_0) \cdots \Psi_n(t_0) & 1 \\ \Psi_1(t_1) & \Psi_2(t_1) \cdots \Psi_n(t_1) & 1 \\ \Psi_1(t_2) & \Psi_2(t_2) \cdots \Psi_n(t_2) & 1 \end{bmatrix} \times \begin{bmatrix} f_{1,0} \\ f_{2,0} \\ f_{3,0} \end{bmatrix}$$

Below is brief step-by-step guide of how the algorithm has been adapted and used. The guide is based on the original schematic found in Scott et. al. (2006)

Step 1
Collect Mass loss vs. Temperature data for at least 2 different constant heating rates (collect via experimentation or simulation)

Step 2
Choose *n* values of conversion. This is the number of equally spaced points over the range at which the activation energy and pre-exponential factor for each component *i* will be evaluated.

Step 3
Propose a reaction model (Or use the reaction model used for the simulation) and find the value of conversion *x* at which the reaction reaches a maximum rate of decomposition. Find the corresponding value for Ψ, from

$$\Psi_i(T) = 1 - x$$

Step 4
Using the expanded form of the equation

$$\Psi_i(B_1, T_1) = \Psi_i(B_2, T_2)$$

Find activation energy values for each component *i*. This is model independent.

Step 5
The value found in step 3 influences the value of the pre-exponential Factor. Using this value, and the known E_i the following can be solve for A_i

$$\ln \Psi_i = \left[T_0 exp\left(\frac{-E_i}{RT_0}\right) - \frac{E_i}{R}\int_{-E_i/RT_0}^{\infty} \frac{\exp(-u)}{u} du - T_1 exp\left(\frac{-E_i}{RT_1}\right) + \frac{E_i}{R}\int_{-E_i/RT_1}^{\infty} \frac{\exp(-u)}{u} du\right]$$

Step 6
Then, using the set of *n* reactions each with its own E and A value, find each reaction's mass fraction *f*, using matrix inversion in

$$\underline{M} = \underline{\Psi}\,\underline{f}$$

Non-zero mass fractions corresponding to E and A values found for each reaction indicate which values are to be used.

3. Results and Discussion

3.1. Data simulation method 1: ODE Solvers

Figure 1

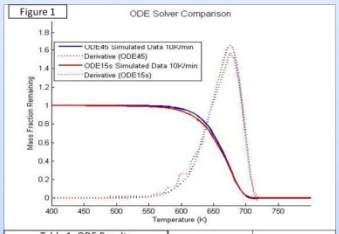

Table 1: ODE Results

Parameter	Activation Energy	Mass Fraction	Pre-exponential Factor
Specified Value	120kJ/mol	1	10^{10}
ODE45 *(%error)*	119.91kJ/mol *(0.075%)*	1.0034 *(0.34%)*	1.169×10^{10} *(16.9%)*
ODE15S *(%error)*	120.61kJ/mol *(0.5%)* 118.59kJ/mol *(spurious reaction)*	0.9995 *(0.05%)*	2.18×10^{10} *(118%)*

•Two ODE solvers were used to generate the mass loss curves in Figure 1, by solving the Random Pore Model expression (Irfan et. al., 2011), and after some manipulation is presented as:

$$\frac{dx}{dT} = -\frac{A'}{\beta} e^{-E/RT}(1-x)\sqrt{1-\varphi \ln(1-x)}$$

•The algorithm was applied as in Section 2 for both ODE solvers.
•The second solver, ODE15s inaccurately simulates two separate reactions, where one activation energy is specified. Multiple reactions can also been identified from the jagged curve of the derivative of the ODE15s simulation.
•ODE45 produces a smooth curve with relatively good results.
•The results also allude to the robustness of the algorithm, where fair accuracy can be achieved, even with poor data.

3.2. Data simulation method 2: Analytical Solution

Figure 2

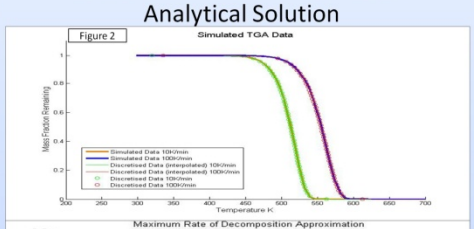

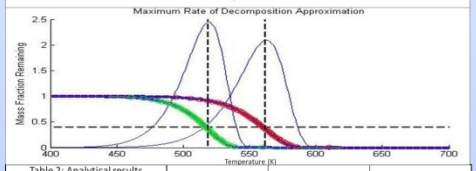

Table 2: Analytical results

Parameter	Specified Value	Algorithm Value	% Relative Error
Activation Energy (E)	120kJ/mol	120.0399 kJ/mol	*0.03%*
Mass fraction (f_0)	1 (unitless)	1.0031 (unitless)	*0.31%*
Pre-Exponential Factor (A')	10^{10}sec^{-1}	1.097×10^{10}sec^{-1}	*9.7%*

•Figure 2 presents the curves generated by solving the Random Pore Model (see Left in Section 3.1.) analytically and simulating a 10k/min regime. The value of *x* required in Step 3 (Section 2) was determined graphically by estimating where dx/dT=max, where x≈0.387.

•From the error analysis in Table 2, the analytical simulation results in a more accurate *E* value. The mass fraction, and more importantly the pre-exponential, *A* have now been found with acceptable accuracy. Only 1 set of kinetics was found.

•Hence, the DAEM-based algorithm has been used to accurately determine the kinetics of a simulated char-CO2 reaction. The determination of *E* was reaction-model-independent and the other parameters were found after a simple modification of the algorithm.

4. Conclusion

The DAEM- based algorithm developed by Scott et. al. (2006) has been successfully modified to accurately determine the kinetics of reactions following the Random Pore Model. The algorithm is model-free when determining activation energy *E* and must be altered to accurately determine the pre-exponential factor and mass fraction *A* and *f*.

References

Irfan, M.F., Usman, M.R. & Kusakabe, K. 2011, "Coal gasification in CO2 atmosphere and its kinetics since 1948: A brief review", *Energy*, vol. 36, no. 1, pp. 12-40.

Scott, S.A., Dennis, J.S., Davidson, J.F. & Hayhurst, A.N. 2006a, "An algorithm for determining the kinetics of devolatilisation of complex solid fuels from thermogravimetric experiments", *Chemical Engineering Science*, vol. 61, no. 8, pp. 2339-2348.

Acknowledgements

Coal and Carbon Research Group – University of the Witwatersrand, School of Chemical and Metallurgical Engineering

Partial Funding by: Sasol Corporate Graduate Services

Figure A1: Snapshot of the poster presented at the 2011 IPCC